An Experimental and Theoretical Study of CO2 Hydrate Formation Systems

Tzirakis, Fragkiskos

Publication date:
2016

Document Version
Publisher's PDF, also known as Version of record

An Experimental and Theoretical Study of CO_2 Hydrate Formation Systems

Fragkiskos Tzirakis

Supervisors: Georgios Kontogeorgis (CERE, Kemiteknik, DTU)
Christophe Coquelet (MINES ParisTech, CTP)
Co-supervisors: Nicolas von Solms (CERE, Kemiteknik, DTU)
Paolo Stringari (MINES ParisTech, CTP)

August 2016

CERE
Center for Energy Resources Engineering

Prolegomenon

At first, the author would like to express his gratitude to his parents, his brother and our Father in Heaven for his existence and providence during his life. In Appendix E the summary of his PhD study is shown.

Secondly, the author would like to thank his main supervisor Georgios Kontogeorgis for giving him the chance to work on this project and his support and Nicolas von Solms for his fruitful comments especially at the early stages of this PhD.

A big gratitude is owned to the warm welcome and support of Christophe Coquelet, Paolo Stringari and Alain Valtz during his experimental work (of 7 months) in Fontainebleau, France. The hydrate equilibrium data were measured at the Centre Thermodynamic of Processes of MINES ParisTech (France) as part of a collaborative project funded by the Danish Technical Research Council (FTP project: CO_2 hydrates - Challenges and possibilities, Project nr. 50868). The author wish to thank also Ing. Alain Valtz for his technical assistance and fruitful discussion during his stay in France.

In addition, warm thanks belong to his collegues, Alay, Martin and Xiaodong, for their guidance and discussion of the modeling part of this work.

Thirdly, his colleagues and friends in Denmark: Alay, Andre, Amalia, Alsu, Anders, Arne, Artem, Bjorn, Peter, Carolina, Georgia, Igor, Fahrdad, Jozsef, Martin, Mehrdad, Teresa, Xiaodong, Bjorn, Peter, Michael, Andrea, Andrea, Christos, Diego, Tina, Nathan, Krishna, Karin, Michael, Michael, Michael, Jessica, Fabrizio, Ewa, Veronica, Platon, f.Paul, Mørten, Jakob, Lazarus, Erakle, Frederik, Inger, Inger, Nina, Shi, Hans, Louise, Louise, Alessandra, Pantelis, Pantelis, Francesca, Ioanna, Eleni, Dejan, Emilian, Kostas, Anna, Panos, Pinelopi, Klaus, Martin, Giulia, Demi, Kiki, Manos, Marina, Nomiki.

…and in France, Stefano, Martha, Anne, Jie, Marine, Jamal, Lydia, f.Panayiotis, Jocelyne, Hervé.

ὁ Θεὸς ἀγάπη ἐστί, καὶ ὁ μένων ἐν τῇ ἀγάπῃ ἐν τῷ Θεῷ μένει καὶ ὁ Θεὸς ἐν αὐτῷ.[a]

Α΄ Ἰωάν. 4, 16

[a] *God is love, and the one that stays in His love, God stays in him.*

A John 4, 16

Synopsis in English

Hydrate crystallization can become equally important carbon capture method provided that this technology undergoes further research. Toward this objective, this study tries to shed light on a quite new topic of research: hydrate promotion. Hydrate promotion implies the production of hydrate at lower pressures (and thus lower adjunctive capital/operational costs) by the use of special chemicals (promoters).

At first, extensive literature review has shown that both experimental data and modeling in this subject are imperative. Therefore, experimental data were produced and published (see Appendix E) using as promoters tetra-n-butyl ammonium salts of bromide, fluoride and cyclopentane in collaboration with MINESParisTech in France. These chemicals are well known for their reduction capabilities of hydrate formation pressure. The results are in good accordance with the literature. Moreover, the simultaneous combination of these chemicals achieved greater pressure reduction than if they were used separately. Then, experimental uncertainties were measured (for pressure/temperature transducers and gas chromatograph) and calculated (for the inserted quantities of water and chemicals). The uncertainties were at an acceptable level for all cases. A further evaluation of the experimental data, regarding their consistency, included the use of Clapeyron equation. It was shown that the results of this work and many of the systems from literature are quite satisfactory. Finally, the well-known van der Waals-Platteeuw hydrate model coupled with CPA EoS was used against experimental data as it was developed in CERE, DTU. The model predicted very satisfactory the CP results of this work and also other CO_2+cyclolkane hydrate results from literature. This model´s consistency lies inter alia on the ground that fluid phases were modeled only with CPA EoS while correlations are utilized in current publications for the aqueous phase and an EoS for the hydrate phase.

Synopsis på Dansk

Hydrate krystallisering kan blive en vigtig kulstofopsamling metode, forudsat at denne teknologi undergår yderligere forskning. Med henblik på dette mål, forsøger denne undersøgelse at kaste lys over en helt nyt emne for forskning: hydrat forfremmelse.Hydrate forfremmelse indebærer produktion af hydrat ved lavere tryk (og dermed lavere supplerende driftsomkostninger) ved brug af specielle kemikalier (promotore).

I første omgang har et omfattende litteraturstudie vist at både eksperimentelle data og modellering i dette emne er bydende nødvendigt. Derfor, er forsøgsdata blevet udarbejdet og offentliggjort med tetra-n-butyl ammoniumsalte af bromid, fluorid og cyclopentan som promotorer, i samarbejde med MINESParisTech i Frankrig. Disse kemikalier er kendt for der evne til at reducere trykket for hydratdannelse. Resultaterne er i god overensstemmelse med litteraturen. Det blev det desuden fundet at med en kobination af disse kemikaler opnås en større trykreduktion end ved anvendelse enkeltvis. Efterfølgende er eksperimentelle usikkerheder blevet målt (for tryk / temperatur- transducere og gaskromatograf) og beregnet (for de brugte mængder vand og kemikalier). Usikkerhederne var på et acceptabelt niveau for alle tilfælde. En yderligere evaluering af de eksperimentelle data, med hensyn til konsistens, omfattede brugen af Clapeyron ligningen. Det blev vist, at resultaterne af dette arbejde og mange af systemerne fra litteraturen er ganske tilfredsstillende.

Endelig blev den velkendte van der Waals-Platteeuw hydrat model kombineret med CPA EoS, som den blev udviklet i CERE, DTU, og sammenlignet med de eksperimentelle data. Modellen forudsagde meget tilfredsstillende CP resultaterne af dette arbejde og også andre CO_2 + cycloalkane hydrat resultater fra litteraturen. Denne model's konsistens skyldes bl.a. at flydende fase bliver modelleret kun med CPA EoS, hvorimod korrelationer benyttes for den vandige fase og EoS for hydrat fase i nuværende publikationer.

Σύνοψις

Ἡ κρυσταλλοποίησης διὰ ὑδριτῶν βαθμηδόν δύναται περικυδὴς μέθοδος εἶναι δέσμευσης τοῦ διοξειδίου τοῦ ἄνθρακος ὑπό τήν αἵρεσιν ὅτι ἡ τεχνικὴ αὕτη ὑπόκειται εἰς περαιτέραν ἔρευναν. Πρὸς τοῦτον τὸν στόχον, ἡ διατριβὴ αὕτη πραγματεύεται περί τινος νέου θέματος ὅ καλείται ὑδριτικὴ προώθησις. Ὡς ὑδριτικὴ προώθησις συνιέναι δεῖ τὴν παραγωγὴν ὑδριτῶν εἰς ἥττονας πιέσεις καὶ τοιουτοτρόπως μείονας παρεπόμενας λειτουργικὰς ἐξόδους διὰ τῆς χρήσεως εἰδικῶν χημικῶν ουσιῶν: τῶν προωθητῶν.

Ἐν ἀρχή, ἅμα τῇ τῆς ὑπαρχούσης βιβλιογραφίας διεξοδικῇ ἐρεύνῃ πρόδηλον ἐγένετο ὅτι πειραματικὰ δεδομένα τε καὶ ἀλγοριθμοποίησις ἐλλείπῃ. Κατὰ συνέπειαν, νέα πειραματικὰ δεδομένα παρηγάγοντο καὶ ἐδημοσιεύθησαν διὰ τῆς χρήσεως τέτρα-ν-βουτυλαμμωνιακῶν ἁλάτων τε κυκλοπεντανίου συνεργείᾳ τῆς ἐν Κυανῇ Πηγῇ ἐν Φραγκίᾳ Ἐθνικῆς Σχολῆς Μεταλλειολόγων. Τοιαῦται οὐσίαι γνώριμαι εἰσὶ πρὸς τὰς δυνατότητας μείωσης σχηματισμοῦ ὑδριτῶν. Τὰ ἀποτελέσματα συνάδουσιν καλῶς τῇ ὑπαρχούσῃ βιβλιογραφίᾳ. Ἔτι δε ὁ κατ' ἄμφω συνδυασμός τῶν προωθητῶν ἐπήνεγκεν μειζοτέραν πτῶσιν πιέσεως ὡς ἄν μονόθεν χρησιμοποιοῖντο. Κατόπιν, πειραματικαί διακυμάνσεις ἐμετρήθησαν τοῖς μετρηταῖς πιέσεως τε καὶ θερμοκρασίας καὶ ὑπολογίσθησαν τοῖς εἰσαχθείσασι μεγέθεσι ὑδάτων καὶ χημικῶν ουσιῶν. Ἐν πάσει περιπτώσει καλαὶ αἱ διακυμάνσεις παρεγένοντο. Ἐπὶ τῷ διεξοδικώτερον τῶν πειραματικῶν δεδομένων ἀνάλυσις περιέκλειε συνεπείᾳ χάριν τὴν χρήσιν τῆς τοῦ Κλαπέϋρου ἐξισώσεως. Ὅπερ συνεγάγετο ὅτι τὰ τῆς ἐργασίας ταύτης ἀποτελέσματα καλὰ λίαν. Ἐν τέλει, ὁ περιώνυμος ἀλγόριθμος ὑδριτῶν τοῦ Βᾶλου-Πλαττέϋβ ἐλειτουργήθῃ παρ' ἁρμοσθείς τῇ καταστατικῇ ἐξισώσει *κυβικός-τε-σχέσις* (CPA) ὁ καὶ ἐν τῷ τμήματι χημικῶν μηχανικῶν Γετῶν ἐσκευάσθη. Ὁ ἀλγόριθμος πρόοιδεν εὖ μάλα τὰ τοῦ κυκλο-πεντανίου ἀποτελέσματα τε καὶ ἑτέρων συστημάτων διοξειδίου τοῦ ἄνθρακος σύν κυκλοαλκανίοις. Ἡ γε τοῦ ἀλγορίθμου συνέπεια ἔγκειται ἐν ἀλλήλοισι ἐπὶ τῇ βάσει ὅτι αἱ ὑγραὶ φάσεις ἀλγοριθμοποιήθησαν τῇ *κυβικός-τε-σχέσει* ἡνίκα συγκαιρινοῖς δημοσιεύσεσιν ἐδείκνυον πολυώνυμαι ἐξισώσεις μεν τῇ ὑδατικῇ φάσει, τινές δε καταστατικαὶ ἐξισώσεις τῇ ὑδριτικῇ φάσει.

List of Abbreviations

CC6	cyclohexane
CC7	cycloheptane
CC8	cyclooctane
CP	cyclopentane
CPA	Cubic-Plus-Association equation of state
DTAC	dodecyl trimethyl ammonium chloride
EC	equilibrium cell
EoS	equation of state
GC	gas chromatograph
mCC6	methyl-cyclohexane
mCP	methyl-cyclopentane
SAFT	statistical associating fluid theory
SDS	sodium dodecyl sulfate
SRK	Soave-Redlich-Kwong equation of state
rpm	rounds per minute
TBAB	tetra-n-butyl ammonium bromide
TBAC	tetra-n-butyl ammonium chloride
TBAF	tetra-n-butyl ammonium fluoride
$TBANO_3$	tetra-n-butyl ammonium nitrate
TBPB	tetra-n-butyl phosphonium bromide
THF	tetrahydrofuran

List of Symbols

α_0	pure component parameter of CPA/SRK EoS	[Pa·m^6·mol^{-2}]
b	pure component parameter of CPA/SRK EoS	[m^3· mol^{-1}]
$c1$	pure component parameter of CPA/SRK EoS	[-]
$C(T)$	Langmuir constant	[-]
$f(T,P,y)$	fugacity	[-]
$g(V_m)$	radial distribution function in CPA	[-]
ΔH	(apparent) dissociation enthalpy	[kJ·mol^{-1}]
k_B	Boltzmann constant	[J·K^{-1}]
k_{ij}	interaction parameter in CPA EoS	[-]
n	quantity of gas inserted in equilibrium cell	[mol]
P	hydrate equilibrium pressure	[MPa]
P_R	reference hydrate dissociation pressure	[MPa]
R^2	coefficient of determination	[-]
R_m	radius of cavity type m	[m]
r	linear distance from centre of the cell	[m]
T	hydrate equilibrium temperature	[K]
$u(T)$	temperature error	[K]

$u(P)$	pressure error	[Bar]
$U(T)$	standard temperature uncertainty	[K]
$U(P)$	standard pressure uncertainty	[Bar]
$U(y)$	standard uncertainty of gas in gas mixture cylinder	[mol%]
$U(n)$	standard uncertainty of gas molar composition in EC	[mol%]
$u_{cal.}(y)$	calibration error of gas in gas mixture cylinder	[mol%]
w	spherical core cell potential	[m]
x	liquid phase composition	[mol%]
Y	water-free composition	[mol%]
y	vapour phase mole fraction	[mol%]
Z	compressibility factor	[-]
Z_m	coordination number for the guest molecule	[-]

Greek letters

β	is refered to empty hydrate lattice (meta-stable β-phase)
β^{AiBj}	association volume
γ	symmetric activity coefficient
Δ^{AiBj}	association strength in CPA EoS
ε	characteristic energy (is refered to cell potential)
ε^{AiBj}	association energy
θ	fractional occupancy
v	number of cavities
φ	fugacity coefficient
κ	binary interaction parameter
μ	chemical potential
ρ	gas density
ω	acentric factor

Superscripts or subscripts

cal.	calibration
H	hydrate phase
m	cavity type
ij	components *i* and *j*
diss.	dissociation
rep.	repeatability
w	liquid or ice rich phase
0	reference state (273.15 K and 1 atm)
*	pure phase

List of Tables

List of Figures

Table of Contents

1

Introduction

Μεγίστη πρᾶξίς ἐστιν ἡ ἀπραξία.

Ἅγ. Γρηγόριος ὁ Θεολόγος (329 – 390 μ.Χ.)[b]

[b] *Greatest action is inaction.*

St. Gregory the Theologian (329 – 390 AD)

1.1 CO_2 capture via gas hydrate crystallization

Climate change is and will become further an issue of major international concern. The most significant geopolitical consequences include human migrations due to starvation, which is apparent many years now in sub-Saharan Africa. It has been very vividly shown in the late decades that carbon dioxide is an important contributor to climate change[1,2]. In this context, the technology of carbon capture and storage (CCS) has received increasing heed over the last decades as a potential method of limiting atmospheric emissions of carbon dioxide (CO_2)[3,4] from flue gas of power and process plants.

Carbon capture techniques are categorized based on which point of the process CO_2 is captured. In that sense, the approaches are post-combustion capture from power plant flue gases using amine-based solvents such as Monoethanolamine (MEA) and ammonia; pre-combustion capture (also via chemical solvents) from the synthesis gas produced in an integrated coal gasification combined cycle (IGCC) power plant; and oxy-combustion capture, in which high-purity oxygen gas rather than air is utilized for combustion in a pulverized coal (PC) power plant to produce a flue gas with a high CO_2 concentration of which is suitable for capture without a post-combustion chemical process[5]. The approaches are shown in Figure 1.1.

In a pulverized power plant, which emits low CO_2 emissions, various types of techniques are currently under investigation. They are differentiated based on liquid solvents (e.g. Monoethanolamine (MEA)) or dry regenerable solvents (e.g. activated coal, Na-, K-, Ca-carbonates) and membrane separation. Membrane material can be zeolites, polymers, silica, ceramic or enzyme-based. In addition, metal organic frameworks (MOF) can be used either or sorbents or membranes. They are constituted by a metal ion (Mg, Zn) and an organic ligand. Finally, cryogenic separation or hydrate crystallization is possible solutions. In cryogenic separation, the refrigerants used are CH_4, C_2H_6, C_3H_8, C_4H_{10} and mixtures of them[5].

Gas hydrate crystallization is to be used as a post-combustion capture process[6-8] in oil and gas industry. The scope of this method is to capture CO_2 from flue gas by means of hydrates and then the release of CO_2 so that CO_2 is purely concentrated in one stream.

This technology is still immature and requires high pressure for the hydrates to form. High pressure is linked with high operational costs[9,10]. Therefore, organic and inorganic chemicals (promoters) are tested recently which reduce the hydrate formation pressure[11-15]. The chemicals used in this study are tetra-n-butyl ammonium salts and cyclopentane. The experimental results were produced in MINESParisTech in Fontainebleau (March – October 2014).

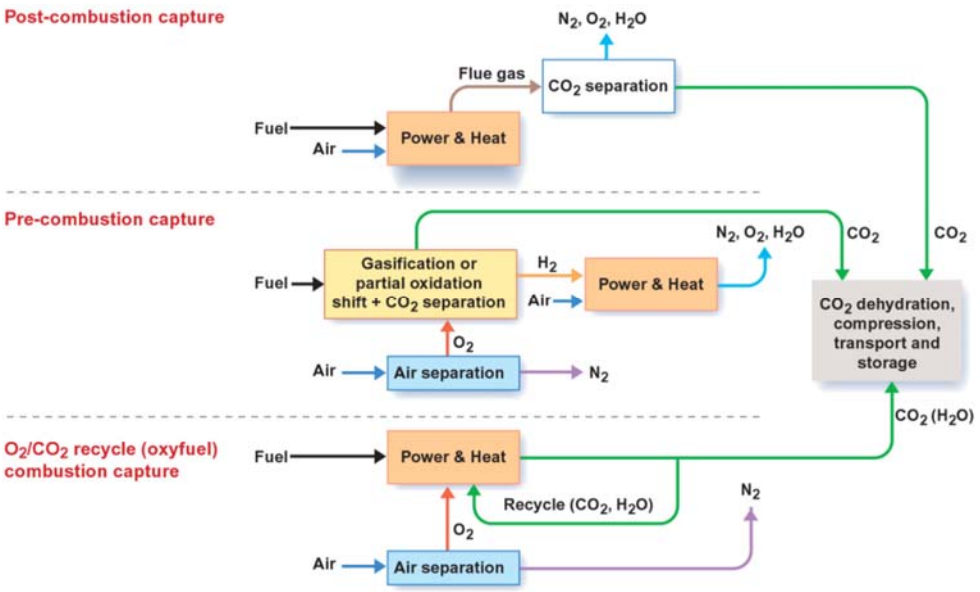

Figure 1.1 Carbon capture methods[16].

1.1.1 Gas hydrate promotion

Promoters are chemicals that shift the hydrate equilibrium line to higher temperatures and lower pressures. In this study, the focus was on tetrabutyl derivatives of ammonium salts and on an organic and hydrophobic compound; cyclopentane (CP).

In general, the polyhydrates of peralkylammonium salts, which are included in ionic clathrate hydrates according to G. Jeffrey's classification[17], are inclusion compounds that exhibit both hydrophilic and hydrophobic hydration. Depending on the charge, an anion replaces one or several water molecules in the water host lattice to form hydrogen bonds (hydrophilic hydration). A cation is also incorporated into cavities of the water-anion framework displacing water molecule with nitrogen atom, so that distances between the

cation atoms and water framework atoms are no less than a sum of their van der Waals radii (hydrophobic hydration). An interesting feature of these compounds is that within a narrow range of concentrations, the same salt may form several ionic clathrate hydrates with different structures, albeit with similar stoichiometry and thermal stability[18]. Cyclopentane forms in general s(II) structure which is one the three main hydrate structures.

1.2 Scope of the project

The purpose of this project is to develop a solid experimental and theoretical framework for better comprehending and addressing the problems of CO_2 hydrates in oil and gas industry and for enhancing the utilization of hydrate crystallization as a CO_2 capture technology. To achieve this goal, new experimental data were produced targeting on pressure-temperature (*PT*) measurements which can reveal profoundly the impact and usefulness of various potential hydrate promoters. To familiarize oneself with this topic, a proper model for the experimental data has been used based on van der Waals and Platteeuw hydrate model[19]. The model was previously developed in CERE, DTU and successfully used in modeling gas hydrate data[20-23]. This model describes only the solid hydrate phase and is typically combined with Cubic-Plus-Association equation of state (CPA EoS) and an activity coefficient model for the description of co-existing fluid phases. The solid phase is treated as a solid solution of hydrate formers in a crystalline host lattice.

1.3 Thesis structure

The chapters of this thesis are described below.

Chapter 2: Theory on hydrate promotion

- Hydrate theory
- Hydrate measuring techniques
- Critically Reviewed PT diagrams for CO_2+promoter systems

Chapter 3: Experimental methodology

- Calibration of instruments
- Measuring procedure
- Hydrate equilibrium results

Chapter 4: Experimental uncertainties and consistency analysis of results

- Hydrate equipment and random uncertainties
- Molar composition uncertainties
- Consistency analysis of results

Chapter 5: Thermodynamic modeling

- The van der Waals-Platteeuw Hydrate Model
- Cubic-Plus-Association (CPA)
- Modeling Results

Chapter 6: Conclusions – Future work

- Conclusions, process design aspects and future work

2

Theory on hydrate promotion

Ὅτε δὲ ὑψώσει ἡ ψυχή τήν θεωρίαν αὐτῆς ἄνω, καὶ ἁπλώσει τὰς ἐννοίας αὐτῆς ἐν τοῖς ἐπουρανίοις, καὶ ἐπιθυμήσει ἅπερ τοῖς ὀφθαλμοῖς τοῦ σώματος οὐχ' ὁρώνται, καὶ ἡ σάρξ οὐκ ἐξουσιάζει αυτῶν, τότε ἐν τῇ πίστει συνίστανται πάντα.

Ἀββᾶς Ἰσαὰκ ὁ Σύρος (630 – 699 μ.Χ.)[c]

[c] *When the soul ascends in her theory above and spreads out her meanings in (what exist in) heaven and lures those that by the eyes of body cannot be seen, and flesh doesn't rule them, then faith constitutes everything.*

Abbas Isaac the Syrian (630 – 699 AD)

2.1 Hydrate Structures

Natural gas hydrates are crystalline solids composed of water and gas. The gas molecules (guests) are captured in water cavities (host) that consists of hydrogen-bonded water molecules. Gas molecules which typically form hydrates are methane, ethane, propane and carbon dioxide. The research efforts on natural gas hydrates can be categorized into three historical phases[24]:

- The first period covers from their discovery (1810) until today and is interested on gas hydrates chemistry and research.
- The second period, continuing from 1934 until the present, predominantly refers to man-made gas hydrates as a hitch to the natural gas industry.
- The third period, from the mid-1960s until the present, enlightens hydrate aspect as a potential energy source, in situ in both the deep oceans and permafrost regions as well as in extraterrestrial environments.

In present, the concern on hydrates is growing more the last years due to environmental concerns. The growth in hydrate-related articles follows historically exponential growth from the 1930s and in general the research on hydrates started in early 1800s[24].

All common natural gas hydrates belong to the three crystal structures, cubic structure I s(I), cubic structure II s(II), or hexagonal structure H s(H) shown in Figure 2.1. The major contrast to ice is that ice forms as a pure component, while hydrates will not form without guests of the proper size.

The structure s(I) is formed with guest molecules of which diameters are among 4.2Å and 6Å, such as methane, ethane, carbon dioxide, and hydrogen sulfide. N_2 and small molecules including H_2 (for d<4.2Å) form s(II) as single guests. Larger single guest molecules (6Å<d<7Å) such as propane or iso-butane will form s(II). For molecules typically 7Å<d<9Å such as iso-pentane, neohexane (2, 2-dimethylbutane) or cyclooctane can form s(H) when accompanied by smaller molecules such as CH_4, H_2S, or N_2[24].

In CO_2+N_2 gas mixture, carbon dioxide is only captured in large cages of s(I) structure[25,26]. Methane is captured either in small or large cavities of s(I) structure due to their small size[25]. The Table 2.1 shows these common structures.

Table 2.1 Gas hydrate main structures and main physical description[24].

Structure	Cavity type			Guest molecule diameter (Å)	No. of cavities in unit cell (small/ medium/ large)	No. of H_2O molecules in cavity (small/ medium/ large)
	small	Medium	large			
s(I)	5^{12}	-	$5^{12}6^2$	4.2 – 6	2/-/6	20/-/24
s(II)	5^{12}	-	$5^{12}6^4$	6 – 7 or < 4.2	16/-/8	20/-/28
s(H)	5^{12}	$4^35^66^3$	$5^{12}6^8$	7 – 9	3/2/1	20/20/36

The next Figure 2.1 shows the diversity of the most common cavities.

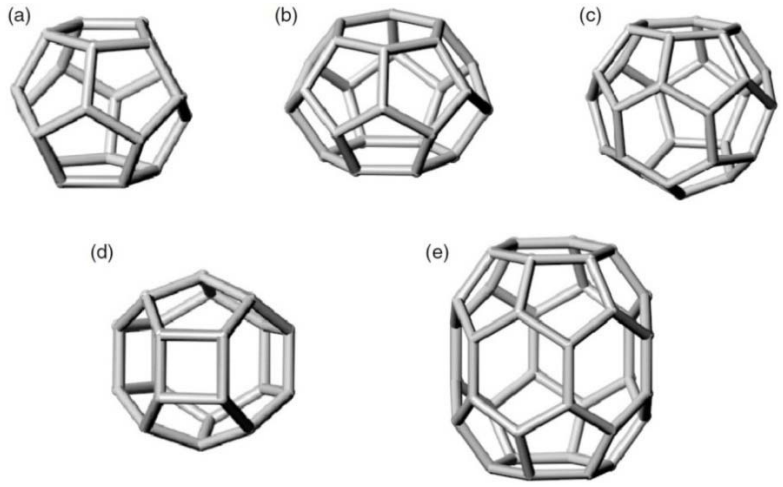

Figure 2.1 Gas Hydrate main structures: (a) pentagonal dodecahedron (5^{12}), (b) tetrakaidecahedron ($5^{12}6^2$), (c) hexakaidecahedron ($5^{12}6^4$), (d) irregular dodecahedron ($4^35^66^3$) and (e) icosahedron ($5^{12}6^8$)[24].

The 5^{12} cavity in a gas clathrate hydrate denotes pentagonal dodecahedron (12-sided cavity) because it has 12 pentagonal faces with equal edge lengths and, thus, equal angles. Similarly, the $5^{12}6^2$ cavity represents tetrakaidecahedron (14-sided cavity)

because of the 12 pentagonal and 2 hexagonal faces. The hexakaidecahedral cavity (16-hedron) is denoted $5^{12}6^4$ due to the 12 pentagonal faces and the 4 hexagonal faces. The irregular dodecahedron cavity ($4^35^66^3$) has 3 square faces, 6 pentagonal faces and 3 hexagonal faces. The largest icosahedron cavity ($5^{12}6^8$) has 12 pentagonal faces and 6 hexagonal faces and a hexagonal face each at the cavity crown and foot[24].

Less common clathrate hydrates exist that are formed by compounds other than natural gas guests (such as Jeffrey's structures III–VII, structure T, complex layer structures) and high pressure hydrate phases. Clathrate hydrate crystals are composed of cage structures formed by water molecules, and each of these cages can encapsulate a gas molecule. The structures consist of several types of cages, depending on the encaged gas molecules[24]. Clathrate hydrates encaging gas molecules (gas hydrates) are stable only under high pressure and low temperature. An exception is tetra-n-butylammonium bromide (TBAB) which forms a semiclathrate hydrate crystal with water molecules even at atmospheric pressure. Such a hydrate is called a semi-clathrate hydrate crystal because a part of the cage structure is broken in order to encapsulate the large tetra-n-butylammonium molecule. In TBAB semi-clathrate hydrate, the Br^- anion forms cage structures with water and the tetra-n-butylammonium cation occupies four cages[27] as shown in Figure 2.2.

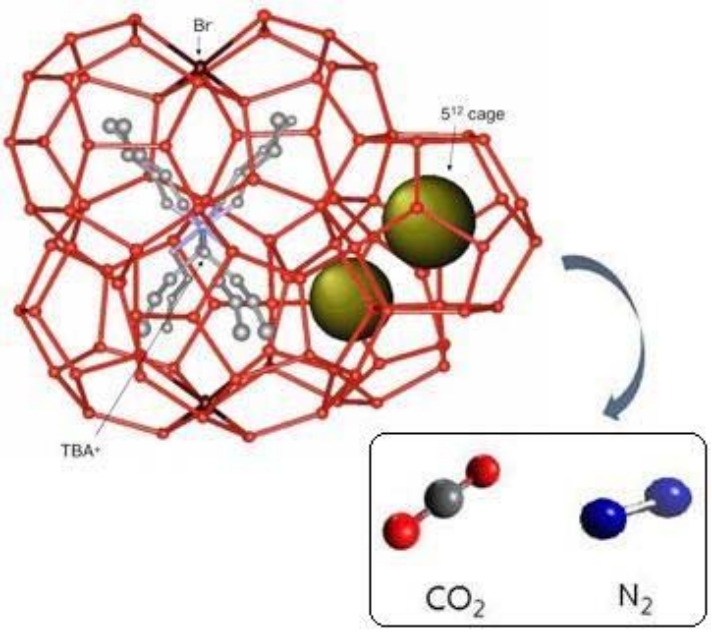

Figure 2.2 Semi-clathrate structure of TBAB[28].

2.1.1 The "Memory Effect" Phenomenon

There has been a consensus among hydrate researchers that hydrates retain a "memory" of their structure when melted at moderate temperatures. Consequently, hydrate forms more easily from gas and water obtained by melting hydrate, than from fresh water with no previous hydrate history. Conversely, if the hydrate system is heated sufficiently above the hydrate formation temperature at a given pressure, the "memory effect" disappears. The time for a hydrate cell to appear in the aqueous solution is called induction time. In Table 2.2, observations of this phenomenon are denoted.

Table 2.2 Experimental Observations on the ''Memory Effect'' Phenomenon[24].

Observations	Literature
Hydrates form more readily from melted hydrate	Makogon[29]
Thermal history of water affects hydrate induction times, that is, time of hot/warm water higher than thawed ice or hydrate	Vysniauskas and Bishnoi[30] Lederhos[31], Parent and Bishnoi[32], Takeya *et al.*[33], Ohmura *et al.*[34]
Successive cooling curves show decreased metastability from the vapor–liquid–hydrate line	Schroeter *et al.*[35]
Induction period is eliminated by re-forming hydrate on an ice surface preexposed to xenon	Moudrakovski *et al.*[36]
Induction times decrease when hydrate is reformed from hydrate decomposed for 1 h compared to 12 h	Lee *et al.*[37]
Hydrate morphology depends on the dissociation conditions before reformation. A rough surface forms from hydrates decomposed for ≥24 h, while a smooth surface forms from hydrates decomposed for only 30 min	Servio and Englezos[38]

2.1.2 Phase diagram

A general axiom in thermodynamics is called Gibbs phase rule. The phase rule is shown in Eq. 2.1:

$$F = 2 + C - Z \tag{2.1}$$

where F are the degrees of freedom, C are the number of components, and Z are the number of phases in thermodynamic equilibrium between each other. For example, a single component existing as a vapor and a liquid has one degree of freedom. If the pressure is specified, then there are zero degrees of freedom—the temperature is fixed. In gas hydrates, two components are at least present (binary systems). From Eq. 2.1, if N = 2 and for two phases e.g. a system of water and a gas, the degree of freedom, F, becomes equal to two and, thus, the hydrate area can be presented in a 2-D diagram of *P,T* as shown in Figure 2.3.

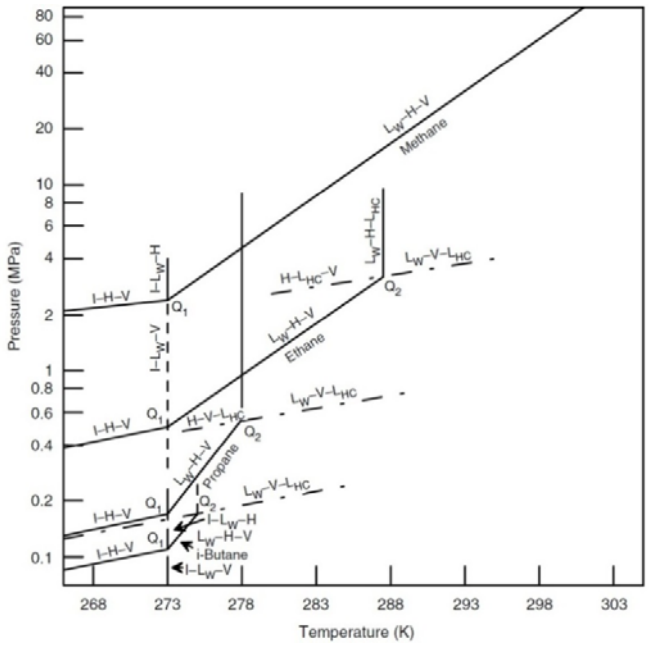

Figure 2.3 Hydrate loci for several NG components. The designations are: $L_w \equiv H_2O$, V ≡ vapor, I ≡ ice, H ≡ hydrate, and L_{HC} ≡ non aqueous liquid[24].

The intersection of four three-phase loci is called quadruple point. There are two quadruple points (Q_1, Q_2) which are denoted by the equilibrium phases. The hydrate

region is bounded by three lines: I–H–V at conditions below Q1, line L_W–H–V between Q_1 and Q_2, and line L_W–H–L_{HC} at conditions higher than Q_2. An upper quadruple point, Q_2, is often considered as the maximum temperature of hydrate formation because line L_W–H–L_{HC} is almost vertical. Note that N_2 and CH_4 do not have Q_2. This is because N_2 and CH_4 have critical temperatures at 191 and 126 K respectively, which are far lower to the quadruple point Q_1 and, thus, the intersection of the vapor pressure line with the L_W–H–V line above 273 K is occluded[24].

The experimental results of this work include a quaternary system of three phases, so the available degrees of freedom are three which are the gas composition, aqueous solution composition and the pressure. If these are fixed, an invariant hydrate equilibrium point is obtained for every different temperature value. In that sense, by changing pressure of the system, a new temperature equilibrium point is attained.

2.2 Gas hydrates usage

2.2.1 Energy supply from gas hydrate reservoirs

Gas hydrates reserves in the earth can be implemented as a (natural) gas supply to cover the increasing energy gap of the world economy. The estimated amount of in situ gas reserves is approximately 1016 m^3 for methane hydrate[39]. In addition, several estimations show that there are worldwide more organic carbon reserves as methane hydrates than all other forms of fossil fuels[40]. It is currently believed that if only 1% of the estimated methane hydrate reserves are recovered, it will be sufficient for the US to satisfy its energy demands for the next eight decades[41]. Although there is no commercial scale plant for exploiting gas hydrate reserves, it is still regarded as a promising approach of which harvest should begin in the next 15 years, mainly due to the rapid depletion of conventional natural gas reservoirs[42].

2.2.2. Hydrates for gas storage

Several studies indicate that the gas hydrate structures can become potential storage media for various gases[3,43,44]. Gas hydrate technology for storage and transportation has the advantage of safety for the given processes, as well as much lower process volumes compared to conventional storage methods like liquefaction. Detailed economic studies

show that the capital cost for natural gas transportation with hydrate technology is 48% lower than that for the conventional liquefied natural gas (LNG) technique, mainly due to lower investment in infrastructure and equipment[45]. However, LNG-type gas transportation is currently preferred for distant markets or transportation of natural gases produced from huge gas fields because of expensive capital investment[45]. On the contrary, there are reports proposing that gas hydrates are economically more cost effective for storage and transportation of standard gas (gas streams of small quantity, especially those far from the pipeline) compared to the LNG method[46-48].

2.2.3 Gas hydrates applications in separation processes

The capture of CO_2 and sequestration (CCS) has become an important area of research for treating CO_2 emissions[49]. CO_2 separation is the most expensive step of the CCS process[50,51]. The effort is to develop energy efficient and environmental friendly technologies to capture the CO_2 produced in large scale power-plants, where mostly CO_2 and N_2 in the flue gas is typically contained[52]. One novel approach to separate CO_2 from combustion flue gas is via gas hydrate crystallization techniques[50-52]. When hydrate crystals are formed from a binary mixture of these gases, the different attraction between CO_2 and other gases in the hydrate cages will enrich the hydrate phase in CO_2 and the gas phase in other gases. The hydrate phase is then dissociated by depressurization and/or heating and thus CO_2 is retrieved[52]. According to experimental results[9], CO_2 selectivity in the hydrate phase is at least four times higher than that in the gas phase. For efficient design of such processes, reliable phase equilibrium data are required.

Methane (CH_4) is a gas with 21 times greater impact on global warming than that of CO_2 and it contributes to 18% of the total global greenhouse effects[53]. This component is the major constituent of natural gas and its reserves in the form of hydrates in the earth. Therefore, methane separation from emitted industrial gas streams has heeded significant attention in the last few decades. Recently, novel separation processes using gas hydrate formation phenomena have been proposed in the literature[45,47-49].

Economic studies for such processes would focus mainly on the price of the promoters needed to reduce the pressure and increase the temperature of the separation steps

because the design of other required equipment is generally simple. It seems that the industry will be interested in such investments whenever the environmental regulations are rigid and when the natural gas reserves tend to reach their half-lives.

Gas hydrate can also be used to remove acid gases during gas processing. When reservoir content high quantities of acid gases (CO_2, H_2S), a pre-treatment can be to reduce the concentration of acid gases by using gas hydrates while the pressure is very high. Then the concentration of acid gases is reduced before utilization of amines. Other uses of hydrates include the field of oil and gas separation, desalination process, food engineering, biotechnology and separation of ionic liquids.

2.3 Hydrate measurements

2.3.1 Hydrate dissociation methods

The hydrate dissociation is a reversible process which can be defined as the point of temperature and pressure where the last hydrate crystal melts. There are experimental procedures for measuring hydrate dissociation conditions as in Table 2.3 are shown.

Table 2.3 Hydrate dissociation procedures[24].

Method	Experimental procedure	Hydrate formation	Hydrate dissociation
Isothermal	Constant temperature	Temperature increase	Visual observation of hydrate crystal disappearance
Isobaric	Constant pressure	Exchange of gas or liquid from an external reservoir	
Isochoric	Constant volume	Pressure decrease	Intersection point of cooling and heating isochors (nonvisual technique)

In the isothermal and isobaric methods, where the pressure and temperature are held constant respectively, the equilibrium conditions are determined by visual observation of phase change: hydrate crystals disappearance. The most widely used method is the isochoric one.

In a typical isochoric experiment, by decreasing the system´s temperature, hydrates start forming. The differential pressure change (∂P) with respect to differential temperature

change (∂T) is measured in a constant volume cell. At every load of known composition, pressure is monitored as a function of temperature so that PT isochor will be produced[54]. The quantity $(\partial P/\partial T)_V$ indicates the slope of an isochoric line in a PT phase diagram. In the end, hydrates dissociation occurs through stepwise heating. The intersection of cooling and heating curves depicts a phase transition and the hydrate dissociation (*P,T*) point is revealed[55]. For a given load, by plotting several experimental isochors produced at different pressures, the complete hydrate phase boundary of a system is created.

In the isochoric method, the equilibrium condition is recognized through temperature and pressure measurement. This method includes no visual observation or complicated calculations so reliable hydrate equilibrium data are obtained. In addition, the technique covers the entire range of hydrate formation temperatures and pressures and, thus, fewer amounts of fluids are implemented due to the elimination of volume changes. Moreover, the technique is aligned to automated control of experiments[56]. Thus, isochoric method, compared to isobaric and isothermal, is regarded more convenient for investigating phase behavior of multicomponent mixtures. The *P*,*T* path for determination of hydrate equilibrium point is shown in Figure 2.4.

More specifically, researchers[57] used CO_2-H_2 (40:60) mixture gas hydrate systems with TBAB additives to investigate the kinetic characteristics under the same driving force condition. The volume is kept constant and the temperature was changed during the experiment. The procedure is as follows: as the cell temperature was lowered, the pressure decreased linearly without hydrate formation occurring (from point A to B) due to the gas contraction as well as increased gas solubility upon cooling at constant volume. At point B, the hydrates started to form and the pressure dropped rapidly to point C. The catastrophic growth was observed from point B to C. Hydrate dissociation began when the cell was heated from point C but hydrate was remaining until Point D. Between points C and x, the cell temperature was rapidly increased, and waited at least 5 h until reaching equilibrium condition. To avoid obtaining an erroneous dissociation temperature and pressure, the dissociation part of the loop must be performed at a heating rate sufficiently slow to allow the system to reach equilibrium: heating rate of about 0.1 K/h from point x

to D. Finally, the hydrate equilibrium condition (or hydrate dissociation temperature and pressure) is determined at point D[58].

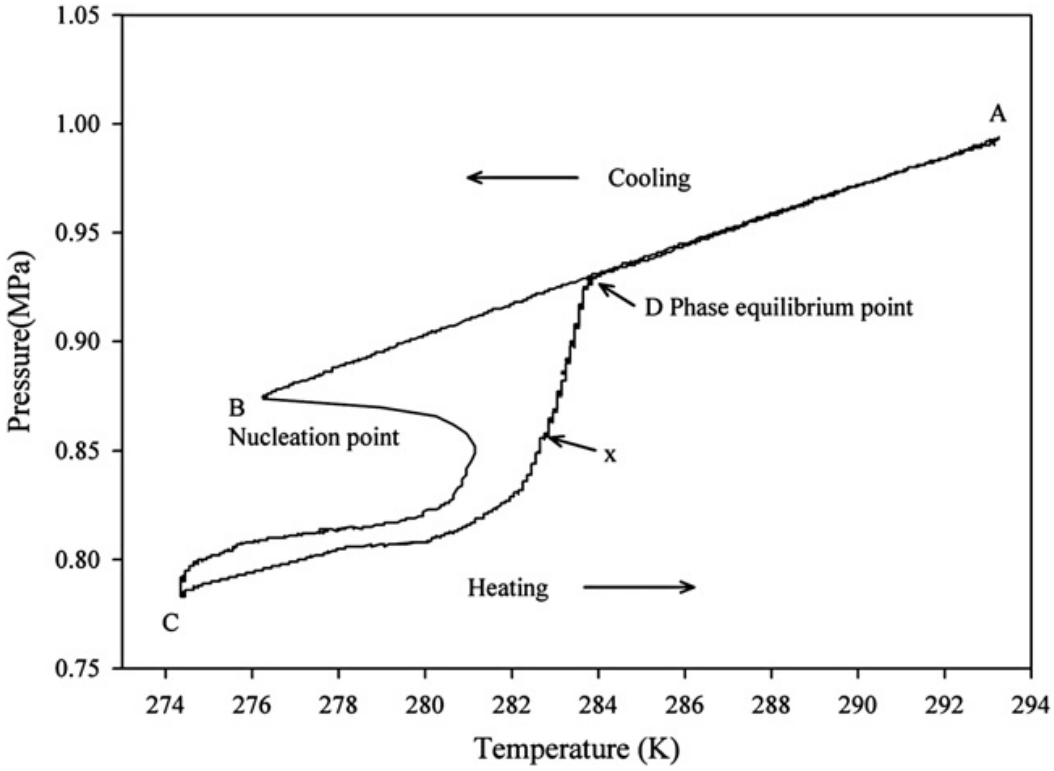

Figure 2.4 Temperature and pressure trace for determination of equilibrium point of CO_2-H_2 (40:60) mixture gas hydrate systems with TBAB additives at initial temperature of 293.15 K and pressure of 0.99 MPa[57].

2.3.2 Macroscopic and microscopic techniques

For macroscopic hydrate experiments, the most common techniques used are[24]: High pressure visual autoclave cell, Figure 2.5, rocking cell, Figure 2.6, Quartz Crystal Microbalance (QCM) in high pressure cell, Figure 2.7, and High-pressure Differential Scanning Calorimetry (HP-DSC), Figure 2.8.

High pressure visual autoclave cell can determine P_{diss},T_{diss}, gas consumption rate during growth/decomposition and visual imaging of growth/decomposition. Quartz Crystal Microbalance (QCM) is also used for P_{diss},T_{diss}. Its major advantage is the small samples (in the order of mg) so equilibration times (hence experimental time) reduced[24]. According to Lee *et al.*[59], the experimental time can be reduced nearly 30 times. Rocking cell is

typically used for Low Dosage Hydrate Inhibitor (LDHI) testing and can specify P_{diss},T_{diss} and gas consumption rate during growth/decomposition.

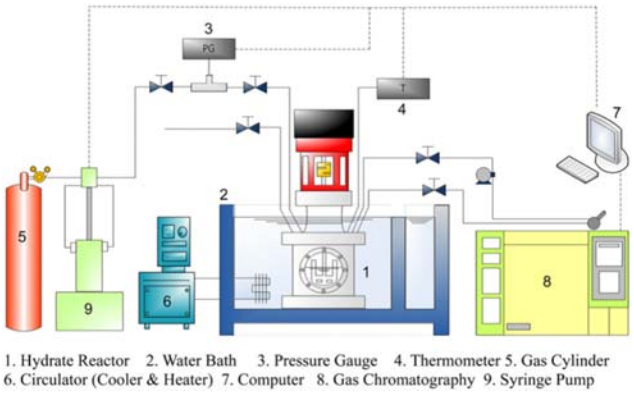

Figure 2.5 Schematic diagram of high pressure visual autoclave cell[60].

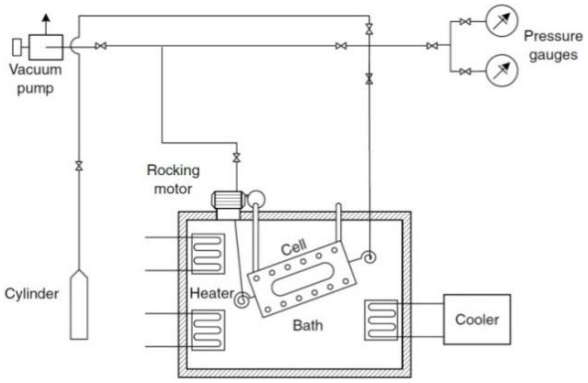

Figure 2.6 Rocking cell apparatus[24].

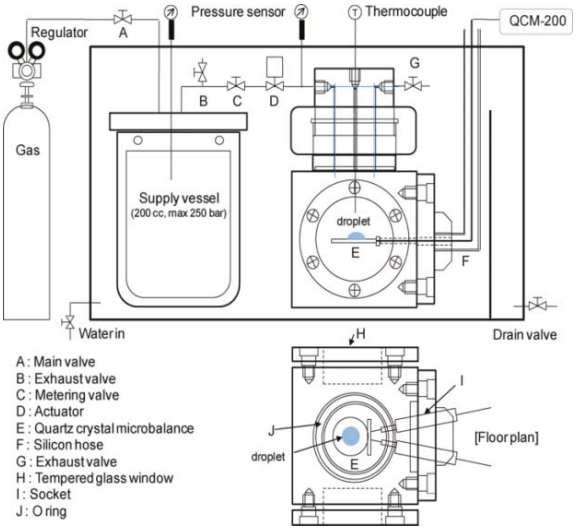

Figure 2.7 Quartz crystal microbalance apparatus[59].

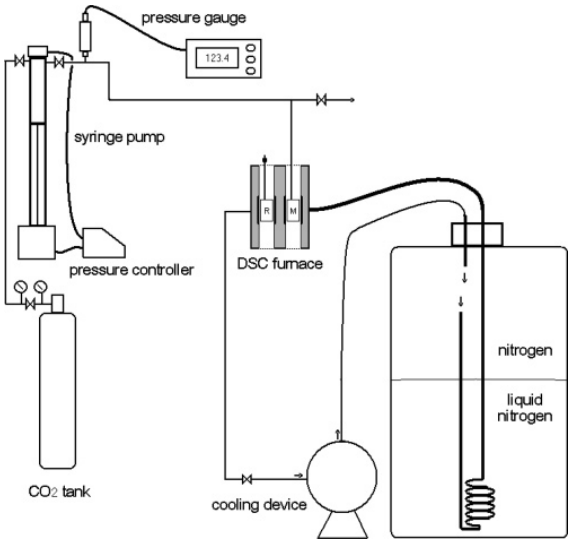

Figure 2.8 DSC device: R, reference vessel; M, sample vessel[61].

Finally, High-pressure Differential Scanning Calorimetry (HP-DSC) can delimitate T_{diss}, heat capacities, heat of dissociation, gas hydrate structure, emulsion stability and hydrate agglomeration. The Table 2.4 summarizes the techniques.

Table 2.4 Most common techniques for macroscopic hydrate measuring[24].

Technique	Phase equilibria data	Kinetic data	Other info
High pressure visual autoclave cell	*P,T*	*P(t), T(t)*, film growth rate vs time	Sapphire/quartz window limits: typically 35 MPa Stirred
Quartz Crystal Microbalance (QCM)	*P,T*	*P(t), T(t)*	Typically 40 MPa
Rocking cell (isochoric technique)	*P,T*	*P(t), T(t)*	Typically 70 MPa (blind cell); 35 MPa (visual cell) Stirred
High-pressure differential scanning calorimetry	*P,T*	Hydrate phase vs. time	<40 MPa, 230 – 400 K

New apparatuses have been also recently proposed[62,63].

Table 2.5 Most common techniques for microscopic hydrate measuring[24].

Technique	Phase equilibria data	Kinetic data	Other info
Solid-state NMR spectroscopy	Hydrate phase and structure	Hydrate phase vs time (min)	typically 0.1 MPa, or use glass bulbs <7 MPa
Raman spectroscopy with high pressure windowed cell	Hydrate phase and structure	*P(t), T(t)*, hydrate phase vs time (min)	typically for sapphire window <70 MPa (for capillary tubes <420 MPa; diamond anvil cell GPa´s)
X-ray diffraction (lab/synchrotron)	Hydrate, water and gas phase distribution and structure	*P(t), T(t)*, hydrate phase vs time (min)	Typically 70 MPa (blind cell); 35 MPa (visual cell) Stirred

For microscopic hydrate experiments techniques, Solid-state NMR spectroscopy, Raman spectroscopy with high pressure windowed cell and X-ray diffraction are widely applied. NMR spectroscopy can delimitate guest occupancy, structure, structural transitions, dynamics, hydration number, hydrate formation and dissociation kinetics. Raman spectroscopy can determine guest occupancy ratios, structure and structural transitions.

X-ray diffraction can specify structure and structure transitions, hydrate crystal growth, decomposition and thermal expansivity[24]. The Table 2.5 summarizes the techniques. The next Table 2.6 summarizes the techniques according to their measuring capabilities.

Table 2.6 Techniques presented according to their measuring capabilities[24].

Capabilities	Technique	Capabilities	Technique
P_{diss}, T_{diss}, *P(t), T(t)*	High pressure visual autoclave cell, Rocking cell, Quartz Crystal Microbalance (QCM)	Hydrate phase development vs time (kinetic data)	Solid-state NMR spectroscopy, Raman spectroscopy with high pressure windowed cell, X-ray diffraction (lab/synchrotron)
Gas consumption rate during growth/ decomposition	High pressure visual autoclave cell, Rocking cell	Guest occupancy, structure, structural transitions	Solid-state NMR spectroscopy, Raman spectroscopy with high pressure windowed cell, X-ray diffraction (lab/synchrotron)
Film growth rate vs time	High pressure visual autoclave cell	Dynamics, hydration number, hydrate formation and dissociation kinetics	Solid-state NMR spectroscopy
		Hydrate crystal growth, decomposition, thermal expansivity	X-ray diffraction (lab/synchrotron)

2.4 Thermodynamic promoters

2.4.1 Hydrate promotion

Hydrate promotion is a new field of study: less than 15 years old. Currently various promoters and mixtures of them are under examination. Promoters (or formers) are classified in two groups: thermodynamic and kinetic. The first ones extend the hydrate formation region in a *P,T* diagram. Thermodynamic promoters are considered as kinds of ionic liquids (ILs). ILs are organic salts that are generally liquid at room temperatures[64]. The disadvantage of using these thermodynamic promoters is that the amount of CO_2 captured in the hydrate form decreases since the thermodynamic promoters occupy some water cavities[65]. The most well experimentally examined example is cyclic aliphatic

ether: tetrahydrofuran (THF). THF in water forms nonideal mixture which shows high immiscibility at low-temperatures and complex liquid-phase behavior at high temperature[66]. THF forms also s(I) structure. Kinetic promoters enhance the hydrate formation rate e.g. sodium dodecyl sulfate (SDS)[67-69], dodecyl trimethyl ammonium chloride (DTAC)[70].

The selection of appropriate thermodynamic additives is subjected to the potential field of application. Various intermediate sized hydrocarbons have been identified as thermodynamic promoters such as cyclopentane[65,71], cyclohexane[72-74], neohexane[75], propane[76] are known as heavy hydrate formers. They exhibit low water solubility which is important for desalination or wastewater treatment[77]. On the other hand, water soluble promoters find attractive application in oil and gas application processes where it is desirable to separate the hydrate promoters from the remaining hydrate formers under atmospheric pressure. Organic substances of that kind are THF[22,78-98,d], acetone[99], 1,4-dioxane[92,99] and also tetra-n-butyl ammonium bromide (TBAB)[100-101], tetra-n-butyl ammonium fluoride (TBAF)[102-103], tetra-n-butyl ammonium chloride (TBAC)[102,104,105], tetra-n-butyl ammonium nitrate ($TBANO_3$)[16,106], tetra-n-butyl phosphonium bromide (TBPB)[107,108], tetra-iso-amyl ammonium bromide (TiAAB)[109] and tri-n-butyl methyl ammonium chloride (TBMAC)[110].

The Figure 2.9 shows THF+H_2O hydrate system at equilibrium. It can be readily come out that the use of THF lessens the formation pressure and increase the formation temperature of a hydrate which results in substantially lower operating cost of a process plant.

Some tetra-alkylammonium halides, which are water-soluble, such TBAB, TBAF, TBAC, and so forth, and some tetra-alkylphosphonium halides like TBPB have already been proposed as promoters of gas hydrates. Especially TBAB is generally considered as promising materials for various innovating processes. Because of its high latent heat and suitable temperature of melting, TBAB semi-clathrate hydrate has been proposed as a phase change material (PCM) for cold transport in a novel refrigeration process[86,110].

[d] The authors presented in two articles part of their hydrate equilibrium results for CO_2+THF+H_2O systems[97, 98].

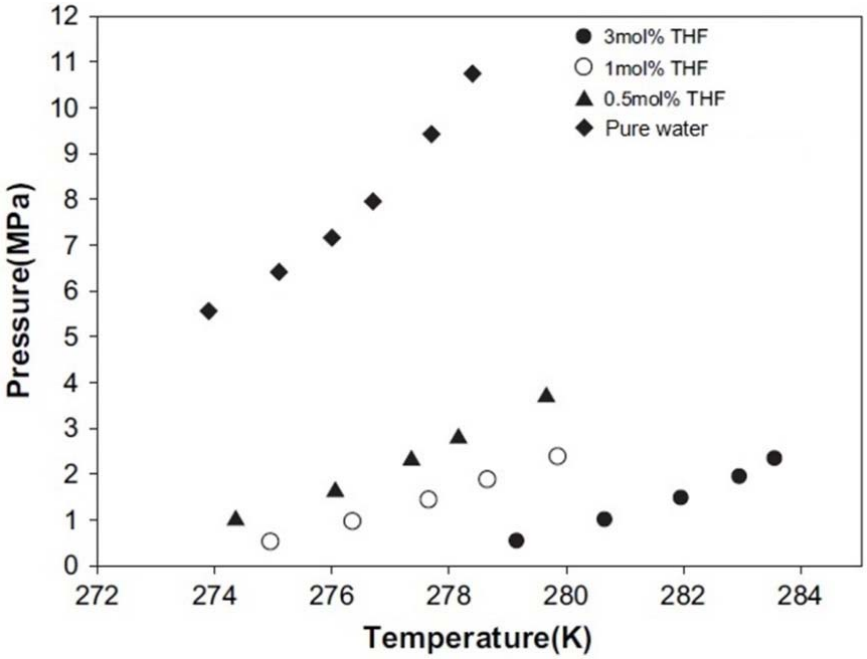

Figure 2.9 Equilibrium hydrate formation conditions for CO_2/H_2 mixture using THF[111].

The phase behavior of tetra-n-butylammonium bromide (TBAB) + water system is rich and complex, as it exhibits vapor-liquid equilibria at low pressures, liquid-liquid equilibria at very high pressures, ion pairing at moderate concentrations, and a complex solid-liquid phase diagram[112]. TBAB forms two types of semi-hydrates: type A ($TBAB{\cdot}26H_2O$) and type B ($TBAB{\cdot}38H_2O$). Type A is formed for concentrations >1.4 mol% and type B exists for lower concentrations[13]. The highest stabilization for type A is achieved on stoichiometric concentration at 3.7 mol% (or 41 wt%)[13]. Higher TBAB concentration will cause inhibition effect.

TBAF forms also two types of semi-hydrates: cubic (Css-I) ($TBAF{\cdot}29.7H_2O$) and tetragonal (Ts-I) ($TBAF{\cdot}32.8H_2O$)[113, 114]. The transition of Css-I to Ts-I may occur at >10 MPa and >1.8 mol%[115]. The stoichiometric concentration of TBAF occurs at higher than 2.3 mol% (or 33 wt%)[113]. Recently it has been shown that TBAF hydrates are formed two times faster than TBAB hydrates and four times than THF hydrates[116].

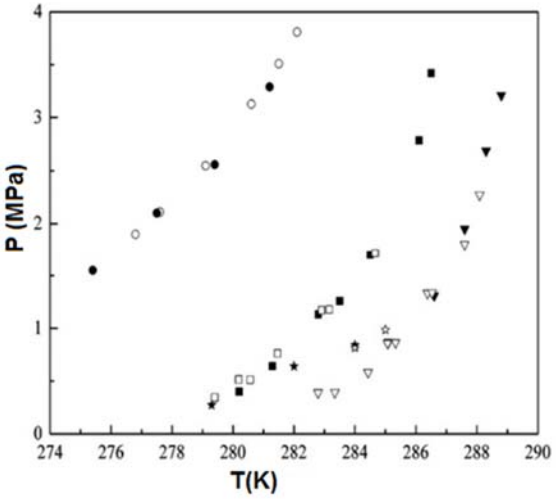

Figure 2.10 Phase equilibrium conditions for CO_2 + H_2O and CO_2 + TBAB + H_2O. CO_2 + H_2O: ●, Li *et al.*[104]; ○, Adisasmito *et al.*[117]. CO_2 + TBAB + H_2O: ■, 2.93 mol%, Li *et al.*[104]; ▼, 6.17 mol%, Li *et al.*[104]; □, 2.58 mol%, Lin *et al.*[118]; ▽, 5.51 mol%, Lin *et al.*[118]; ★, 2.90 mol%, Duc *et al.*[9]; ☆, 6.10 mol%, Duc *et al.*[9].

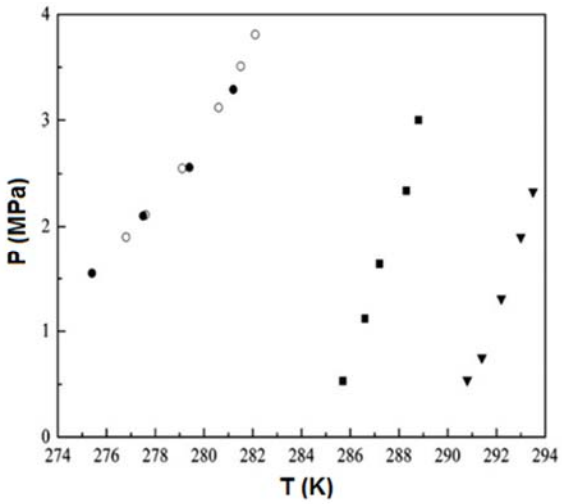

Figure 2.11 Phase equilibrium conditions for the CO_2 + H_2O and CO_2 + TBAF + H_2O. CO_2 + H_2O: ●, Li *et al.*[104]; ○, Adisasmito *et al.*[117]. CO_2 + TBAF + H_2O: ■, 2.93 mol%; ▼, 6.17 mol%, Li *et al.* [104].

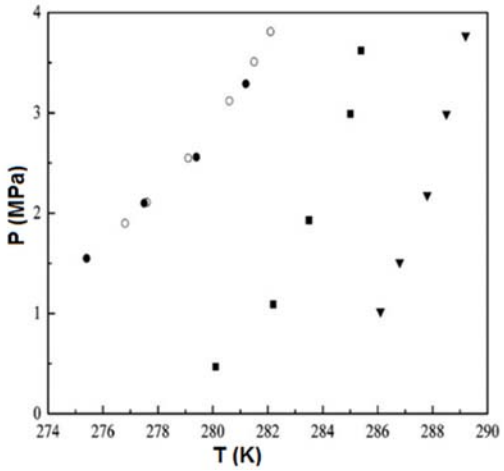

Figure 2.12 Phase equilibrium conditions for the CO_2 + water and CO_2 + TBAC + H_2O. CO_2 + H_2O: ●, Li *et al.*[104]; ○, Adisasmito *et al.*[117]. CO_2 + TBAC + H_2O: ■, 2.93 mol%; ▼, 6.17 mol%, Li *et al.*[104].

Moreover, the space velocity of the hydrate reactor increases with increasing feed pressure and it is almost two times larger for TBAF than TBAB (13.46 h^{-1} for TBAB and 25.96 h^{-1} for TBAF). At higher pressures, for constant temperature, CO_2 concentration in gas phase decreases while in the hydrate phase increases[118,119]. At higher temperatures,

CO_2 concentration in gas phase increases. The CO_2 amount in CO_2+N_2 hydrates increases greatly with a small increase of CO_2 in vapor phase[26]. Li *et al.*[104] have used TBAB, TBAC and TBAF as shown in Figure 2.10, Figure 2.11 and Figure 2.12 respectively.

Another promising promoter seems to be propane (C_3H_8). The system[120] of CO_2/H_2 is presented in Figure 2.13.

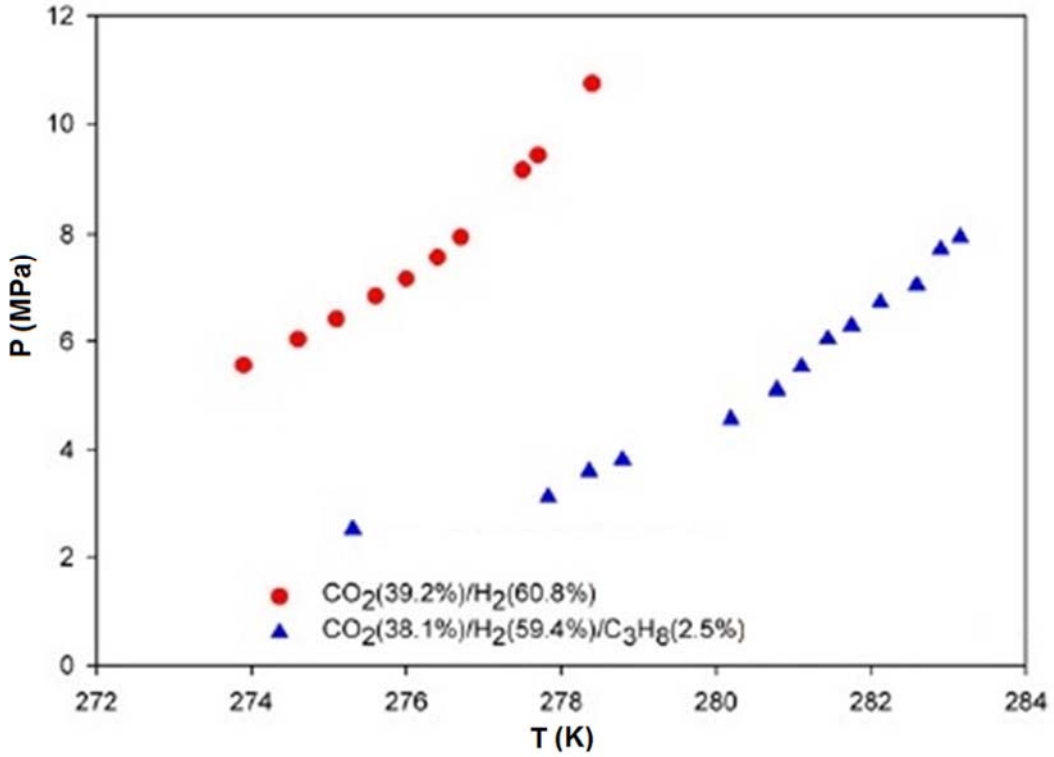

Figure 2.13 Hydrate phase equilibrium[120] for the gas mixture containing mol fraction 0.392 CO_2, 0.608 H_2 and the ternary gas mixture containing mol faction 0.381 CO_2, 0.594 H_2 and 0.025 C_3H_8.

Another promoter, which is also potential phase material for cold storage and transportation in refrigeration and air-conditioning processes, is TBPB. Its capabilities are shown in Figure 2.14. TBPB can store two to four times more CO_2 per H_2O than TBAC and tetra-n-butyl ammonium nitrate ($TBANO_3$)[121].

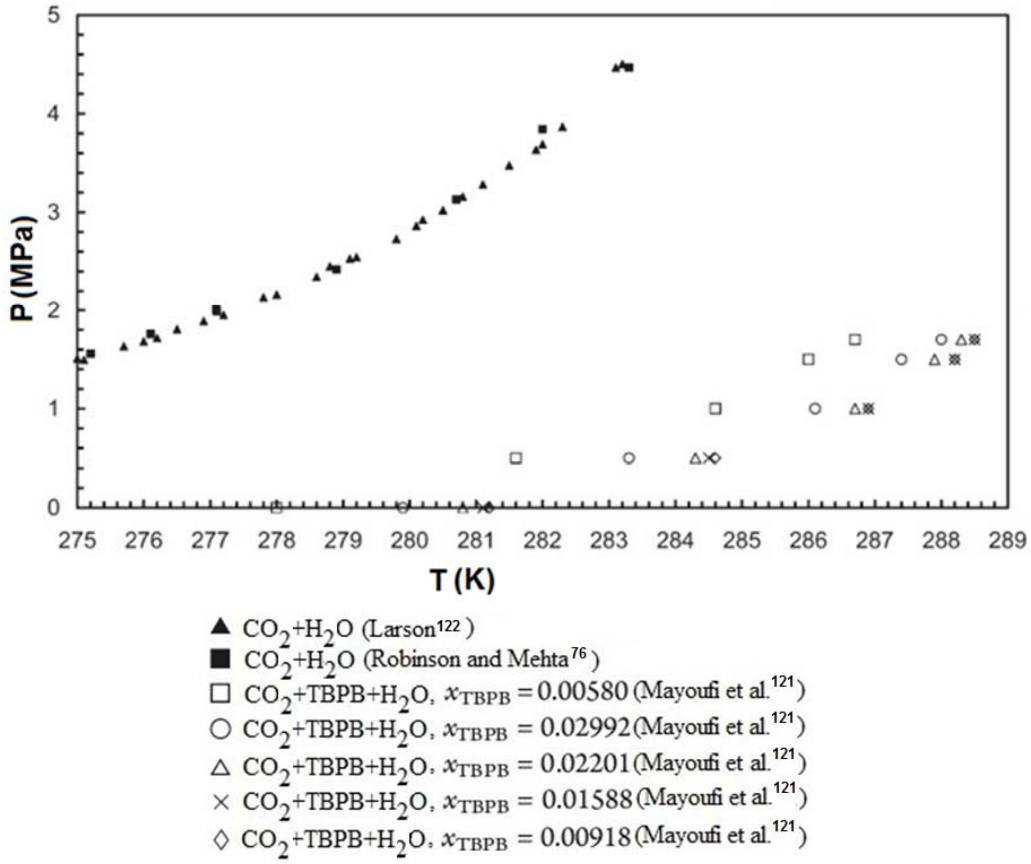

Figure 2.14 CO_2 pressure, P_{CO2}, versus temperature, T, H-L-V equilibrium data for the systems CO_2+H_2O[76,122] and CO_2+TBPB+ H_2O[121].

Cyclopentane (CP) is also a potential promoter. CP is water immiscible cyclic hydrocarbon. The merits of CP over THF and TBAB can be concluded to the following three statements[65]:

a) the melting point of CP hydrates is higher than that of THF hydrates
b) CP is less toxic than THF and
c) the equilibrium pressure of CP+CO_2 binary hydrates is independent of CP concentrations due to immiscibility of CP + water.

In addition, the hydrate formation rate with CP/water emulsion is higher than that of CP aqueous solution due to the larger contact area of gas and liquid which controls hydrate formation rate[71].

Quite recently, mixture of promoters (THF and CP) has been tested[22]. The following Figure 2.15 shows four-phase equilibrium of CP+THF+H_2O and CP+H_2O hydrate

system[22]. It presents the significant reduction in equilibrium pressures caused by the addition of 4 wt% THF to the aqueous phase (CP and water). It can readily come out the synergetic effect of promoters´ mixture, namely THF and CP which lessen the formation pressure and increase the formation temperature of hydrates[111]. CO_2 hydrate formation systems are also presented in Appendix A, Figures A.1 and A.2.

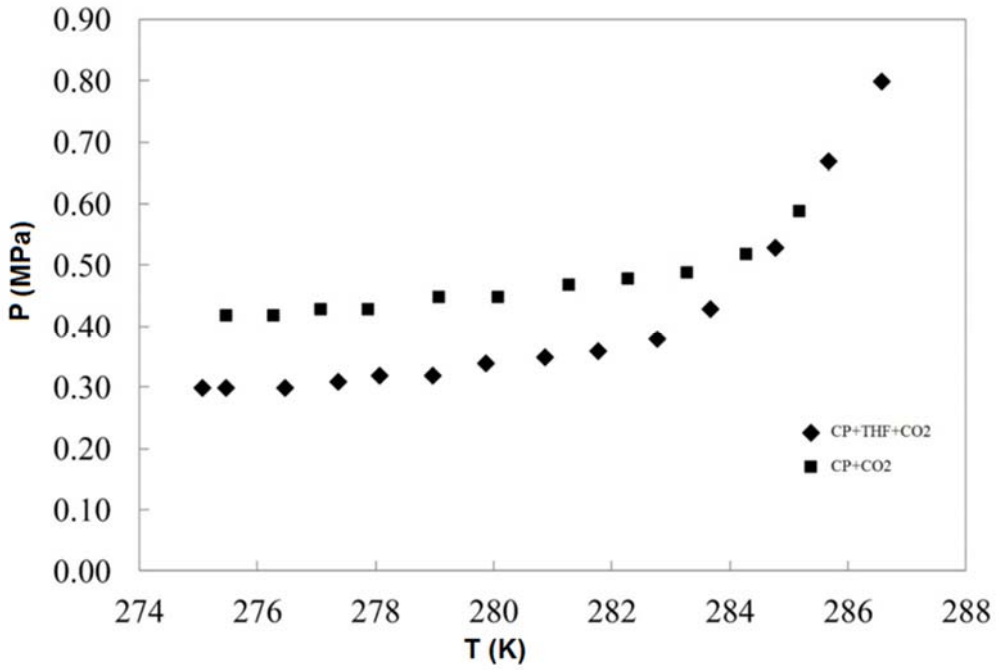

Figure 2.15 Four-phase (H-L_w-L_a-V) equilibrium pressures (absolute) as functions of temperature for mixed hydrates of CP/THF/CO_2. Hydrates formed from a two-liquid phase system prepared from an aqueous solution containing 4 wt% THF and an organic phase containing pure CP. For comparison, (H-L_w-L_a-V) hydrate equilibrium data exhibiting a mixed CP/CO_2 hydrate phase of the ternary system {H_2O + CP + CO_2} are included. The initial vapor phase consists of pure CO_2 in both cases. (◆) CP/THF/CO_2, Herslund *et al.*[22], (■) CP/CO_2, Herslund *et al.*[22].

Finally, there are also kinetic promoters which are only used to accelerate hydrate formation and have no impact on formation thermodynamics. In this work, kinetic promoters have not been used. Most examined examples of this category are sodium dodecyl sulfate (SDS), Figure 2.16, biorfuctants[123] or minerals[11,12]. SDS is a surfactant which can effectively reduce the interfacial tension of gas-liquid contact and accelerate the rate of gas hydrate formation[124,125]. Another kinetic promoter, which is currently under examination, is silica gel[60,126,127]. Silica gels with a nominal diameter of 100.0 nm have

exhibited increased gas consumption during gas hydrate formation, suggesting higher conversion of water into gas hydrate[60].

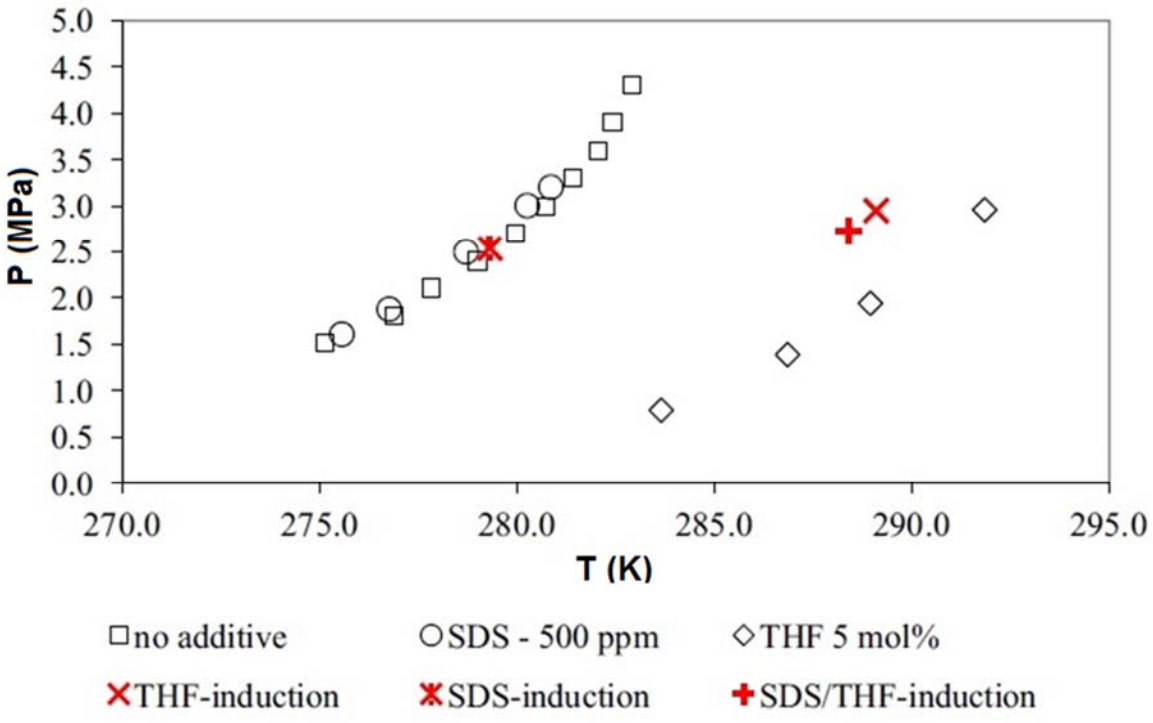

Figure 2.16 CO_2 H-LW-V equilibrium curves for pure water, 500 ppm SDS and 5mol% THF and induction point for THF 5 mol%, SDS- 500ppm and SDS-500ppm/THF-5mol%. Sources: no additive; SDS-500ppm, THF 5 mol%, THF- induction, SDS-induction and SDS/THF induction[124].

2.4.2 Critically Reviewed PT diagrams for CO_2 + promoter systems + H_2O

A sequence of *P,T* Figures of CO_2+THF/TBA Halides +(other gas)+H_2O are presented so that a more in depth view of most of the available literature results in CO_2 hydrate promotion can be acquired. All compositions are given in mol fractions. The first *P,T* Figure 2.17 shows CO_2+THF+H_2O system at various concentrations. An article of CO_2+H_2O equilibrium[128] is added for comparison purposes in order to show the promotion effect of every chemical. Most of the results agree very well with each other, especially at lower pressures, but there are some discrepancies at higher pressures, e.g. above 2 MPa. The red square (■) and blue (⋇) markers that correspond to 1% THF from Shin *et*

al.[92] and Seo *et al.*[79] respectively seem to be slightly inconsistent. In conclusion, the results from different authors are in good agreement with each other.

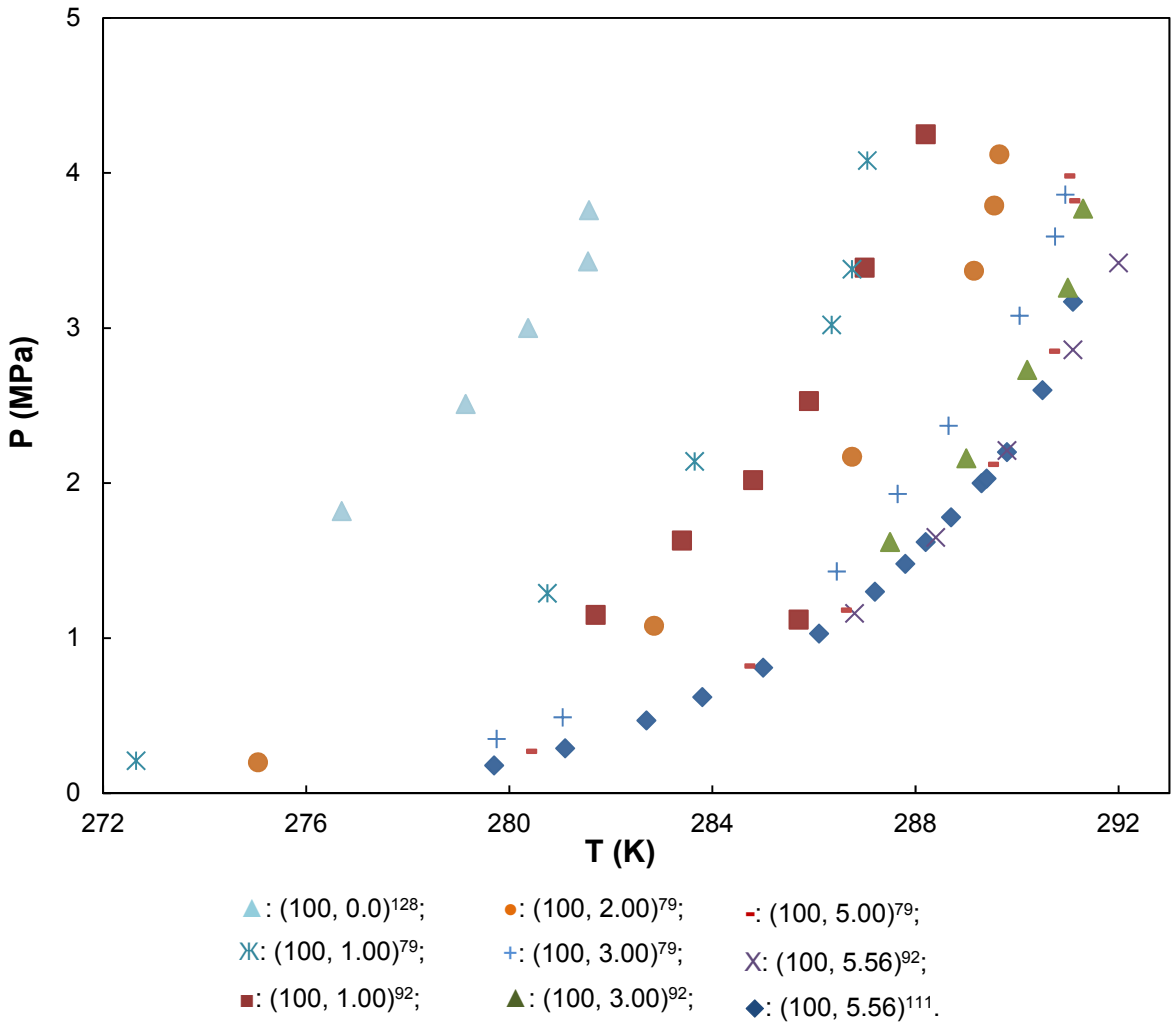

Figure 2.17 CO_2+THF+H_2O system. For clarity reasons, the systems are presented by two numbers in brackets. The first number denotes the mol fraction of CO_2 of a potential binary gas mixture and the second one denotes the promoter concentration. References are presented according to their presence in figure from left to right.

The next Figure 2.18 depicts *P,T* equilibrium points of the system CO_2+CH_4+TBAB+H_2O at various concentrations. As shown previously, an article of CO_2+CH_4 equilibrium with pale blue cross (+) marker is added for comparison purposes. The blue rhombus (◆) and filled orange circle (●) markers of Acosta *et al.*[129] and Mohammadi *et al.*[61] respectively that correspond to 40% CO_2 and 0.29% TBAB mol fractions are in good accordance. The

rest systems have different compositions which prohibits further comparison. Nevertheless, there is consistency in the fact that as TBAB concentration increases, the promotion effect becomes more significant. In conclusion, the results from different authors are in very good agreement with each other.

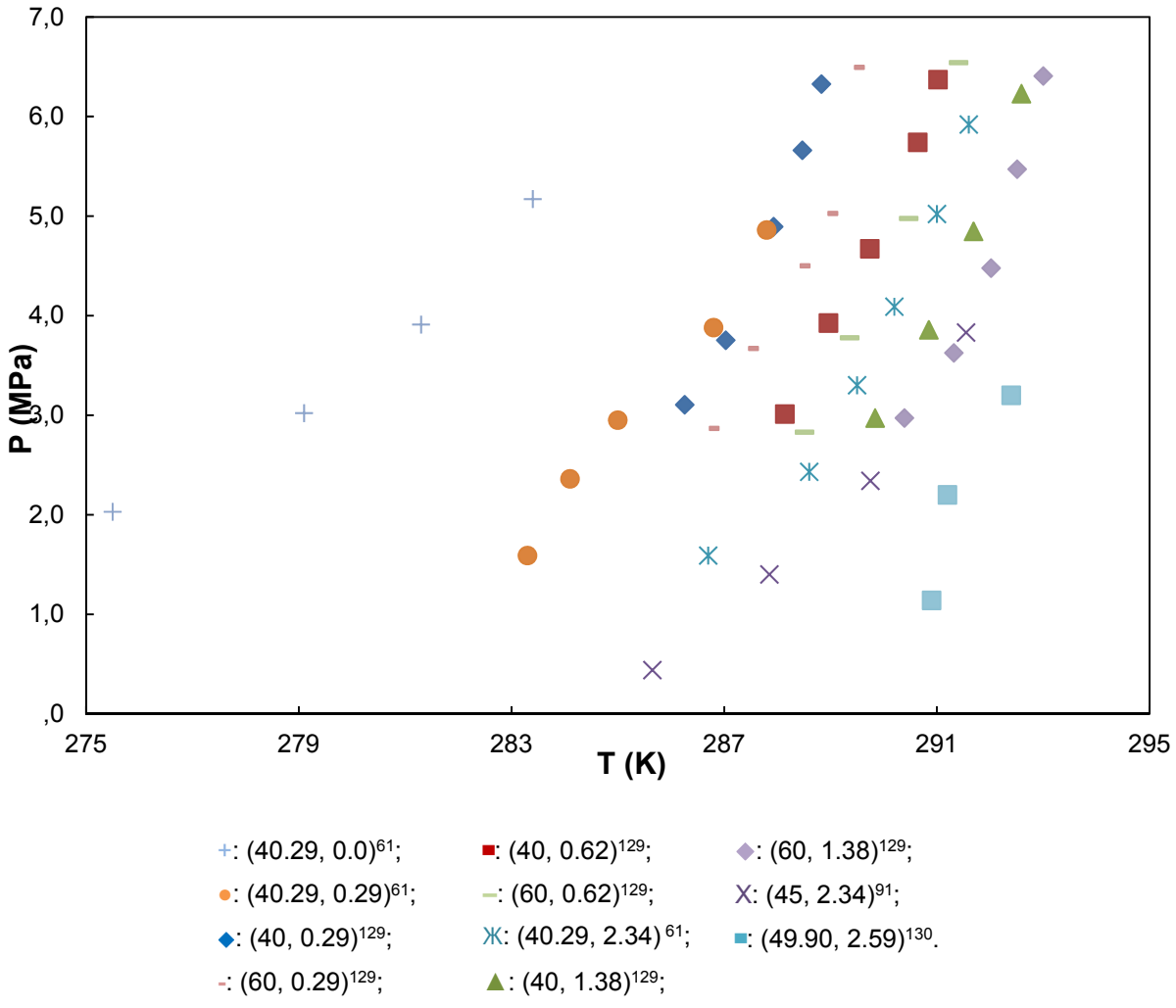

Figure 2.18 CO_2+CH_4+TBAB+H_2O system. For clarity reasons, the systems are presented by two numbers in brackets. The first number denotes the mol fraction of CO_2 in CO_2+CH_4 gas mixture and the second one denotes the promoter concentration. References are presented according to their presence in figure from left to right.

The Figure 2.19 represents the system CO_2+H_2+TBAB+H_2O at various concentrations. The points marked with green triangle (▲), a green dash (–), a filled orange circle (●) and purple cross (+) markers show CO_2+H_2 systems for comparison purposes. The purple

cross (+) markers of Li *et al.*[102] shows CO_2+H_2+H_2O system as well but it does not appear correct because for the low CO_2 concentration being used, the results should have been located at higher pressures. The filled green circle square (●) and (Ж) markers of Li *et al.*[102] and Kim *et al.*[57] respectively, that correspond to app. 40% CO_2 and app. 3% TBAB coincide excellently. Moreover, from the same authors, the blue (X) and the pale green triangle (▲) markers that correspond to app. 40% CO_2 and 0.5% TBAB are in very good agreement. In addition, the red (Ж) and pale purple (X) markers of the same authors that correspond to app. 40% CO_2 and 1% TBAB are in very good agreement. In conclusion, the results from different authors are in good agreement with each other.

In general, the concentrations below 1 mol% TBAB of Li *et al.*[102], the filled orange circle (●) markers of Mohammadi *et al.*[61] for CO_2+H_2+H_2O system and purple cross (+) markers for the same system of Li *et al.*[102] seem to be problematic concerning visual observation.

Figures 2.20, 2.21 and 2.22 show CO_2+TBAR+H_2O systems where R is bromide, chloride or fluoride anion accordingly. In Figures 2.20 for CO_2+TBAB+H_2O systems, the purple (X) and the pale blue (◆) rhombus markers of Lee *et al.*[11] and Li *et al.*[104] respectively that corresponds to app. 0.6% TBAB are in good agreement. In addition, the pale purple (X) and the red dash (-) markers of Lin *et al.*[118] and Mohammadi *et al.*[50] respectively that correspond to app. 0.29% TBAB are in good agreement. In addition, the green dash (–) and triangle (▲) markers of Lin *et al.*[118] and Mohammadi *et al.*[50] respectively that correspond to app. 0.6% coincide excellently. A TBAB concentration of 2.7 mol% (stoichiometric) proves to be the most efficient. Above that concentration inhibition effect is observed as it is shown by the filled orange circle (●) of Lee *et al.*[11], orange dash (–) of Ye and Zhang[131] and pale blue (X) of Mohammadi *et al.*[50].

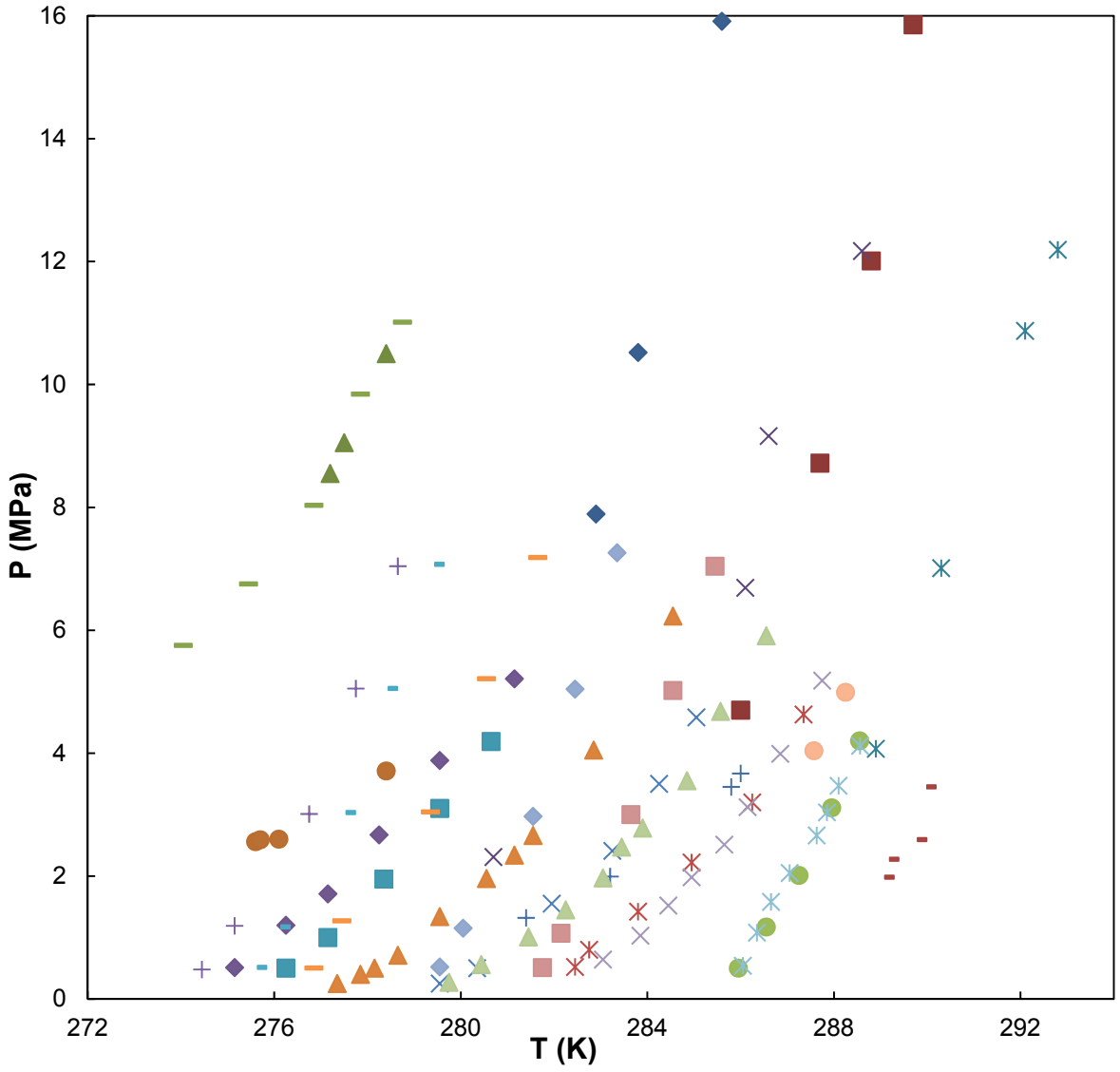

–: (39.20, 0.0)[102]; ■: (39.20, 0.21)[102]; X: (39.52, 0.29)[61]; X: (40.10, 1.00)[57];
▲:(39.52, 0.0)[61]; –: (18.50, 0.21)[102]; X: (39.20, 0.50)[102]; ●: (40.10, 6.00)[57];
+: (18.50, 0.0)[102]; ◆: (14.81, 0.29)[61]; ▲: (40.10, 0.50)[57]; ●: (39.20, 2.67)[102];
●: (75.01, 0.0)[61]; ◆: (18.50, 0.50)[102]; +: (75.01, 0.29)[61]; ✳: (39.52, 2.34)[61];
-: (18.50, 0.14)[102]; ▲: (39.20, 0.29)[102]; ■: (14.81, 2.34)[61]; ✳: (40.10, 2.00)[57];
◆: (39.20, 0.14)[102]; ■: (18.50, 1.00)[102]; ✳: (39.20, 1.00)[102]; -: (75.01, 2.34)[61].

Figure 2.19 CO_2+H_2+TBAB+H_2O system. For clarity reasons, the systems are presented by two numbers in brackets. The first number denotes the mol fraction of CO_2 in CO_2+H_2 gas mixture and the second one denotes the promoter concentration. References are presented according to their presence in figure from left to right.

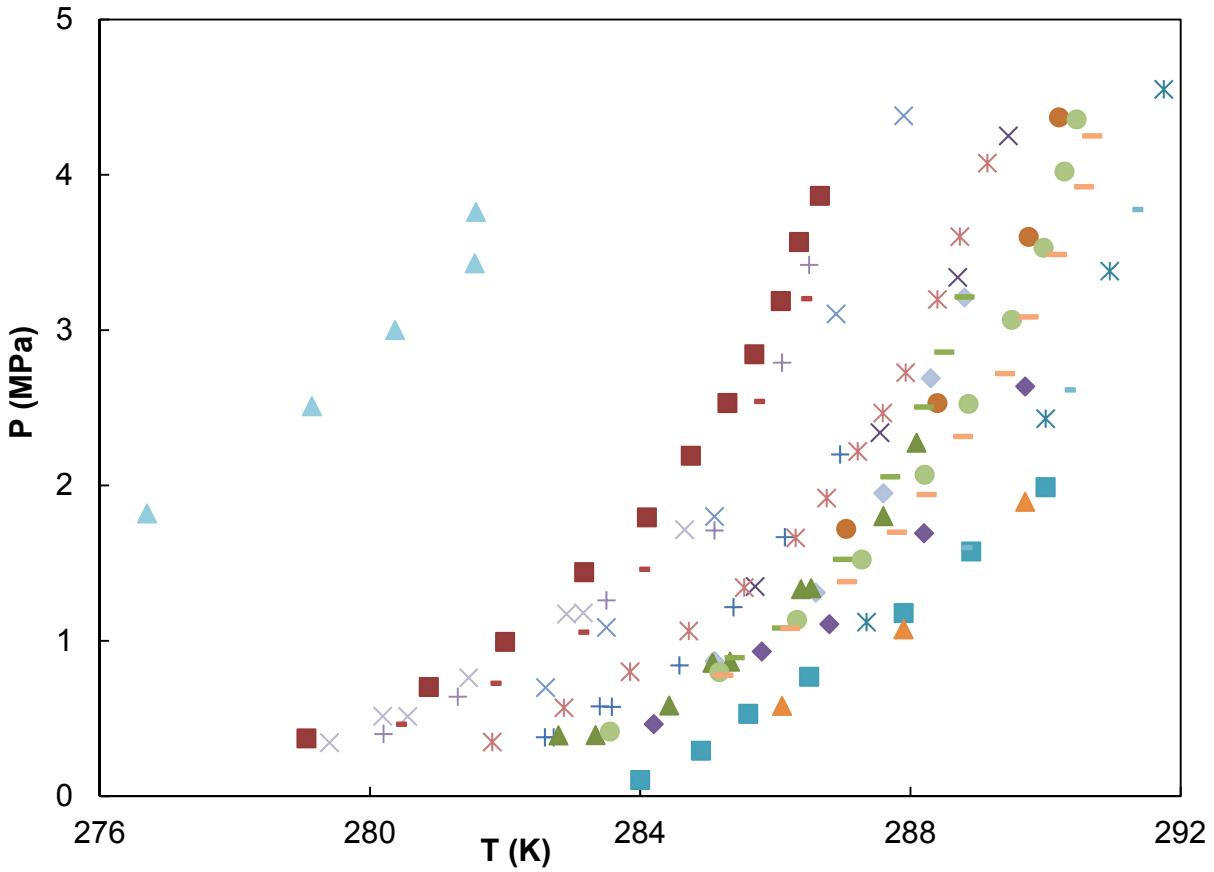

▲: (100, 0.0)[128]; X: (100, 5.29)[50]; ▲: (100, 0.55)[118]; ◆: (100, 1.11)[50];
■: (100, 0.29)[131]; X: (100, 0.60)[11]; ●: (100, 1.29)[131]; Ж: (100, 2.70)[11];
+: (100, 0.29)[102]; Ж: (100, 0.62)[131]; ●: (100, 7.70)[11]; ■: (100, 1.83)[50];
-: (100, 0.29)[50]; +: (100, 0.42)[118]; ◆: (100, 0.62)[104]; ▲: (100, 2.92)[50];
X: (100, 0.26)[118]; –: (100, 0.62)[50]; –: (100, 6.39)[131]; -: (100, 2.56)[131].

Figure 2.20 CO_2+TBAB+H_2O systems. For clarity reasons, the systems are presented by two numbers in brackets. The first number denotes the mol fraction of CO_2 of a potential binary gas mixture and the second one denotes the promoter concentration. References are presented according to their presence in figure from left to right.

The TBAC results are not sufficient for safe conclusions. Nonetheless, the red square (■) markers of Makino *et al.*[105] and the pale red (Ж) markers of Mayoufi *et al.*[14], that correspond to app. 2.3 mol%, are in very good agreement. In addition, the green triangle (▲) markers of Mohammadi *et al.*[13] and the pale blue (-) markers of Li *et al.*[104], that correspond to app. 0.3 mol%, are in very good agreement.

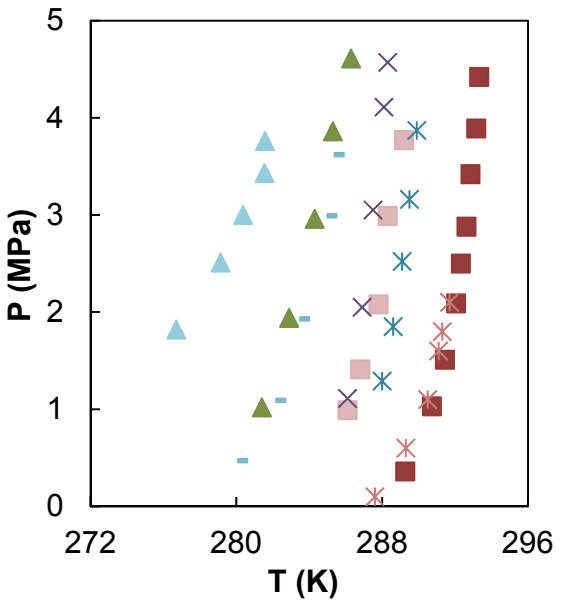

▲: (100, 0.0)[128]; ▪: (100, 0.62)[104];
▲: (100, 0.34)[13]; ✳: (100, 1.79)[13];
-: (100, 0.29)[104]; ■: (100, 2.23)[105];
X: (100, 1.13)[13]; ✳: (100, 2.54)[14].

Figure 2.21 CO_2+TBAC+H_2O systems. For clarity reasons, the systems are presented by two numbers in brackets. The first number denotes the mol fraction of CO_2 of a potential binary gas mixture and the second one denotes the promoter concentration. References are presented according to their presence in figure from left to right.

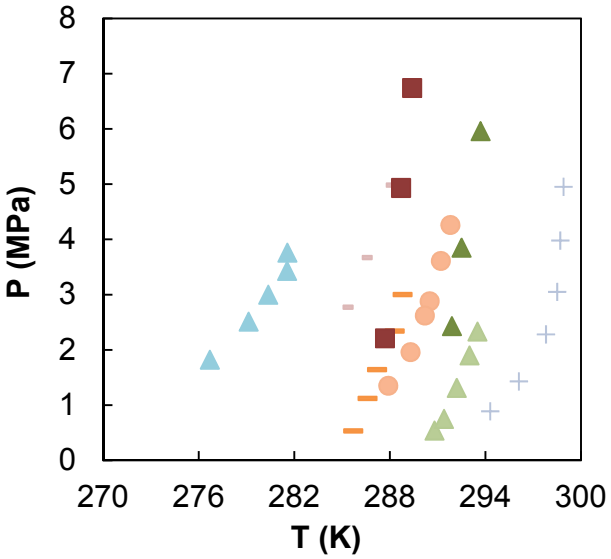

▲: (100, 0.0)[128]; ●: (100, 0.36)[12];
-: (100, 0.14)[12]; ▲: (100, 0.62), [104];
-: (100, 0.29), [104]; ▲: (30, 0.68)[132];
■: (30, 0.36)[132]; +: (100, 1.20)[12].

Figure 2.22 CO_2+TBAF+H_2O systems. For clarity reasons, the systems are presented by two numbers in brackets. The first number denotes the mol fraction of CO_2 in CO_2+N_2 gas mixture and the second one denotes the promoter concentration. References are presented according to their presence in figure from left to right.

The TBAF results are presented in Figure 2.22. The results are not sufficient for safe conclusions but there is consistency in the fact that as TBAF concentration increases, the promotion effect becomes more significant. Moreover, TBAF achieves the maximum promotion effect compared to TBAB and TBAC at similar concentrations according to Li *et al.*[104].

Finally, in Figure 2.23 and 2.24 the systems CO_2+CP+H_2O and CO_2+CH_4+THF+H_2O are investigated by two authors respectively. Their results coincide completely in both cases at same concentrations.

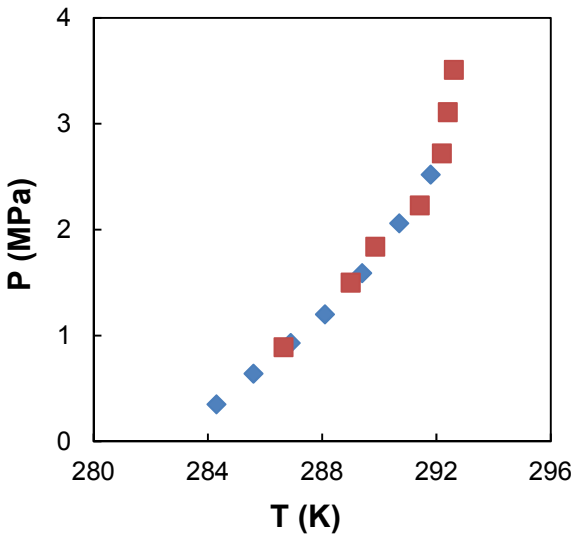

◆: (100, 16.16)[72]; ■: (100, 17.39)[133].

Figure 2.23 CO_2 + CP + H_2O system.

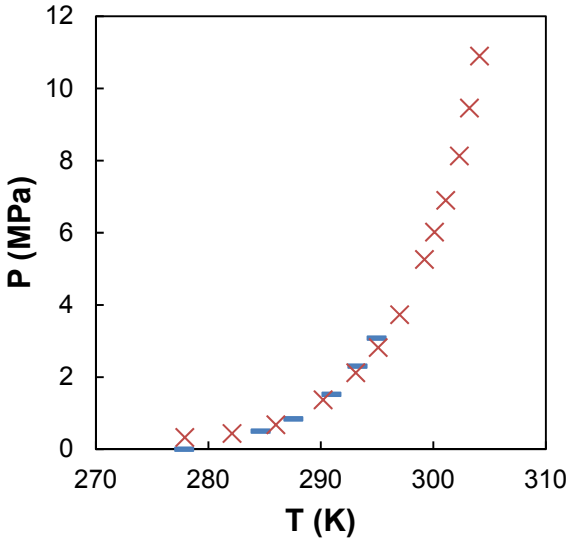

X: (50, 5.56)[90]; –: (45, 5.56)[91].

Figure 2.24 CO_2 + CH_4 + THF + H_2O system.

2.5 Conclusions

In this chapter, an overview of hydrate structures, hydrate measuring techniques together with hydrate promoter systems were reviewed. The chapter presented the theoretical background on hydrate promotion which is necessary for the next chapters. Moreover, the final section presented an overview of the available *P,T* equilibrium data on CO_2 hydrate promotion. The available literature is insufficient on CO_2+N_2 gas mixture which is a common effluent in oil and gas industry[10]. Moreover, TBAC and TBAF promoters are lacking in experimental data. Therefore, the next chapter presents equilibrium data for CO_2+N_2 gas mixture with the use of promoters using gas mixtures of low CO_2 concentration to simulate real systems. The TBAB, TBAF and CP promoters were examined adding new data to the available literature.

3

Experimental methodology

Τοῦτό ἐστι τοῦ Θεοῦ ἐνοίκησις, τὸ διὰ τῆς μνήμης ἐνιδρυμένον ἔχειν ἐν ἑαυτῷ τὸν Θεόν. οὕτω γινόμεθα ναὸς Θεοῦ, ὅταν μὴ φροντίσι γηίναις τὸ συνεχὲς τῆς μνήμης διακόπτηται, ὅταν μὴ τοῖς ἀπροσδοκήτοις πάθεσι ὁ νοῦς ἐκταράσσηται, ἀλλὰ πάντα ἀποφυγὼν ὁ φιλόθεος ἐπὶ Θεὸν ἀναχωρῇ, καὶ ἐξελαύνων τὰ προκαλούμενα ἡμᾶς εἰς κακίαν τοῖς πρὸς ἀρετὴν ἄγουσιν ἐπιτηδεύμασιν ἐνδιατρίβῃ.

Ἁγ. Βασίλειος ὁ Μέγας (329 – 378 μ.Χ.)[e]

[e] *The indwelling of God (in us) is to have foundations of God via memory. In such way we become temple of God when the continuance of memory (of God) is not paused by earthy concerns, when the mind is not disturbed by unexpected passions but (instead when) the pious (mind) avoids everything, he departs to God and he dwells in things that leads to virtue by expelling the provocations towards us for evilness.*

St. Basil the Great (329 – 378 AD)

In this chapter the calibration of transducers, the experimental setup, the measuring procedure and the hydrate equilibrium results are presented and discussed. The results are produced using TBAB, TBAF, CP promoters and mixtures of them. The combination of TBA salts and CP was inspired by Li *et al.*[134] and Herslund[20,22]. The results confirm that synergetic effect between TBA salts and CP indeed occurs which decreases further the hydrate equilibrium pressure at specific *P,T* conditions and aqueous concentrations. This chapter is published in peer-review journals of Fluid Phase Equilibria and Chemical and Engineering Data as shown in Appendix E.

3.1 Equipment used

3.1.1 Calibration of pressure and temperature transducers

The temperature probe was carefully calibrated against a 25-Ω reference platinum resistance thermometer (TINSLEY Precision Instruments). The 25-Ω reference platinum resistance thermometer was calibrated by the Laboratoire National d'Essais (LNE, Paris) based on the 1990 international temperature scale (ITS90). The equilibrium pressure is measured using two calibrated pressure transducers (GE UNIK 5000).

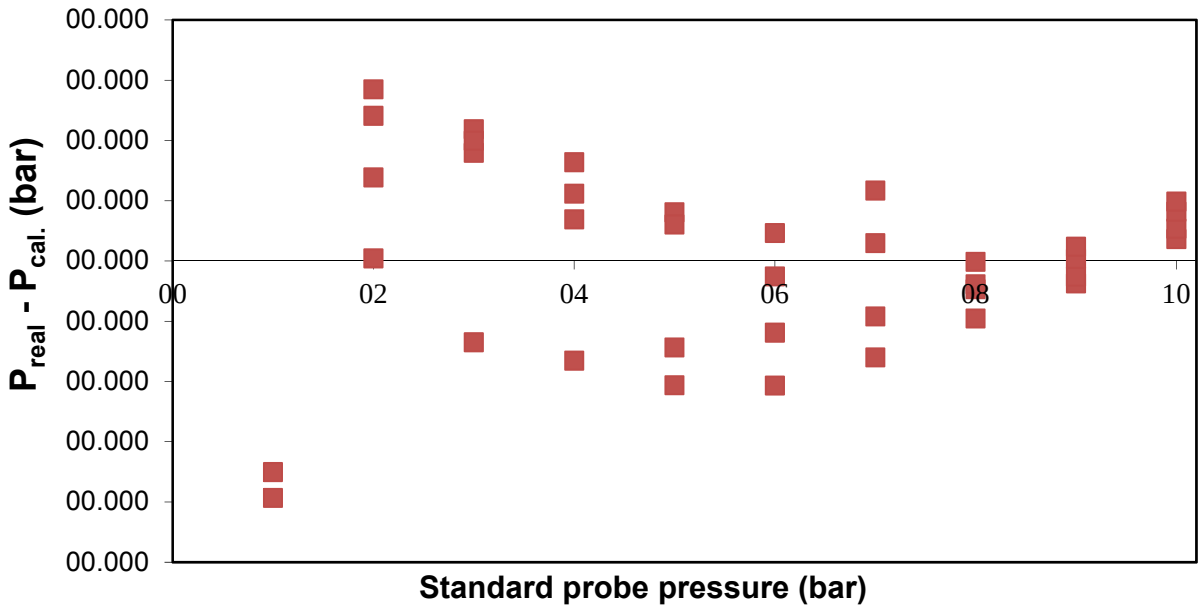

Figure 3.1 Absolute uncertainty of pressure transducer for 0-10 bar.

Two pressure transducers of 10 bar and 100 bar were calibrated. The accuracy was found to be ±0.004 bar and ±0.015 bar for 10 bar and 100 bar accordingly as shown in Figures 3.1 and 3.2. For the temperature transducer, the accuracy was found to be ±0.02 K as presented in Figure 3.3.

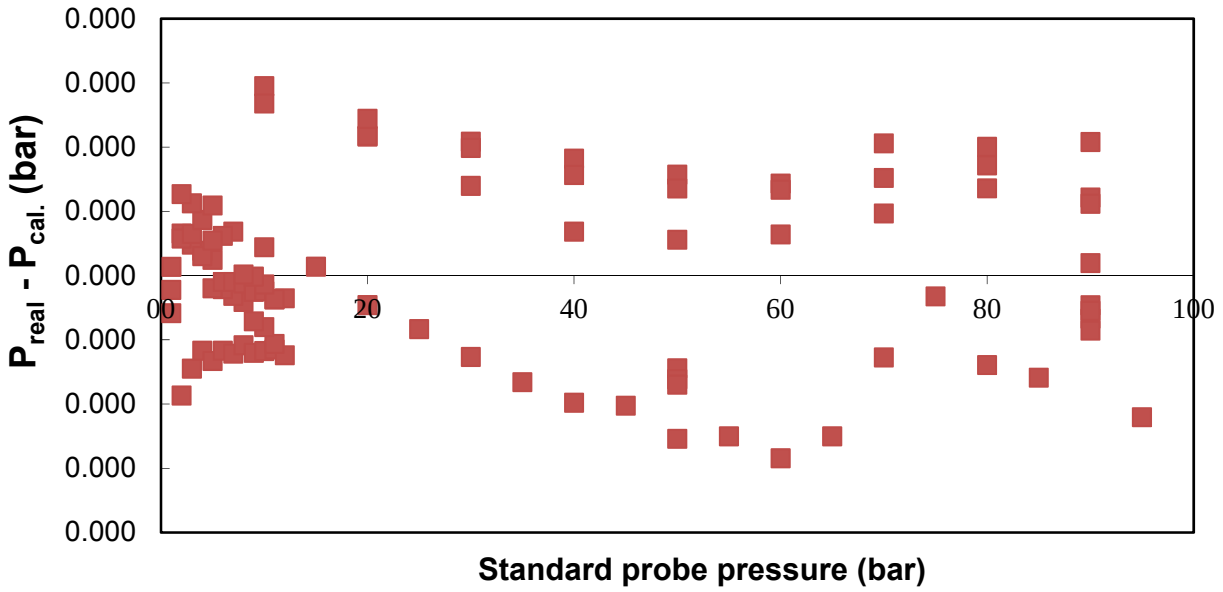

Figure 3.2 Absolute uncertainty of pressure transducer for 0-100 bar.

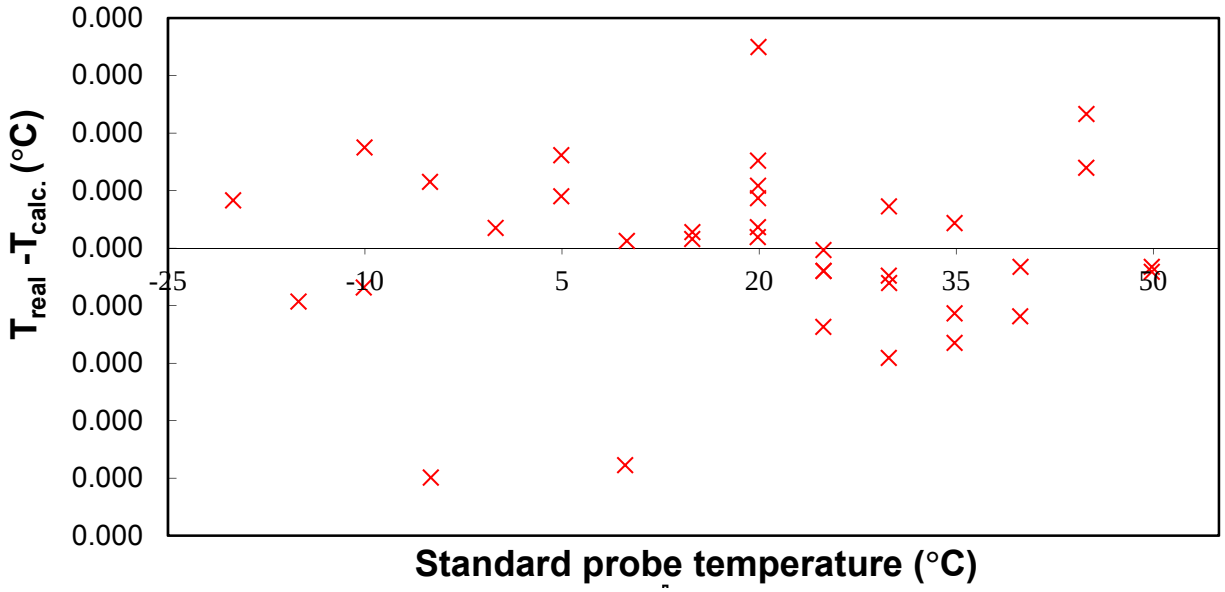

Figure 3.3 Absolute uncertainty of temperature transducer.

The 2nd degree parameters ($X_{cal.}=a \cdot X_{read}^2 + b \cdot X_{read} + c$) used for the temperature and pressure correction are shown in Table 3.1.

Table 3.1 Temperature and pressure parameters as came out from calibration.

Pressure range (bar)	Pressure parameters (2nd degree)			Accuracy
	a	b	c	
0-20	-3.34E-05	1.00075659	-0.00029732	±0.015 bar
20-70	-1.31E-05	1.00248668	-0.05910184	±0.015 bar
0-100	-6.87E-06	1.00051235	0.07324214	±0.015 bar
Temperature parameters (2nd degree)				
	1.19E-05	1.0005044	0.078902	±0.020 K

3.1.2 Calibration of Gas Chromatograph

The first gas mixture (e.g. 6.87/93.13 mol% CO_2/N_2) was produced and then measured with a gas chromatograph (Varian, CP3800). At first, the GC detector (TCD) was calibrated for CO_2 and then for N_2, Figures 3.4 and 3.5 respectively. Similar calibration plots created for the other three gas mixtures.

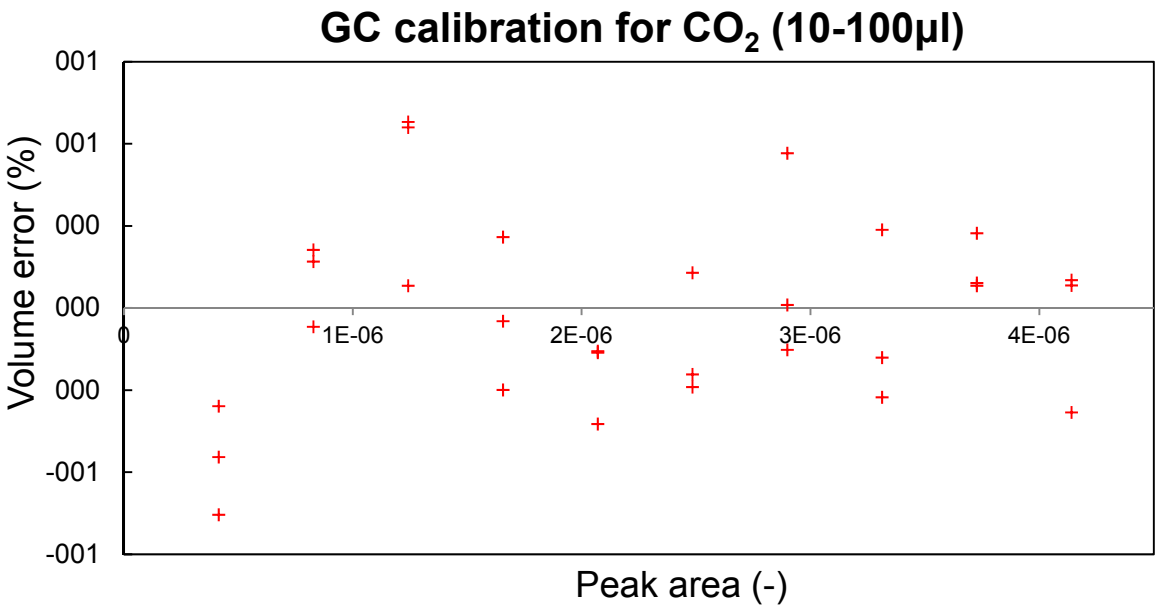

Figure 3.4 CO_2 volume error against peak area as measured with GC.

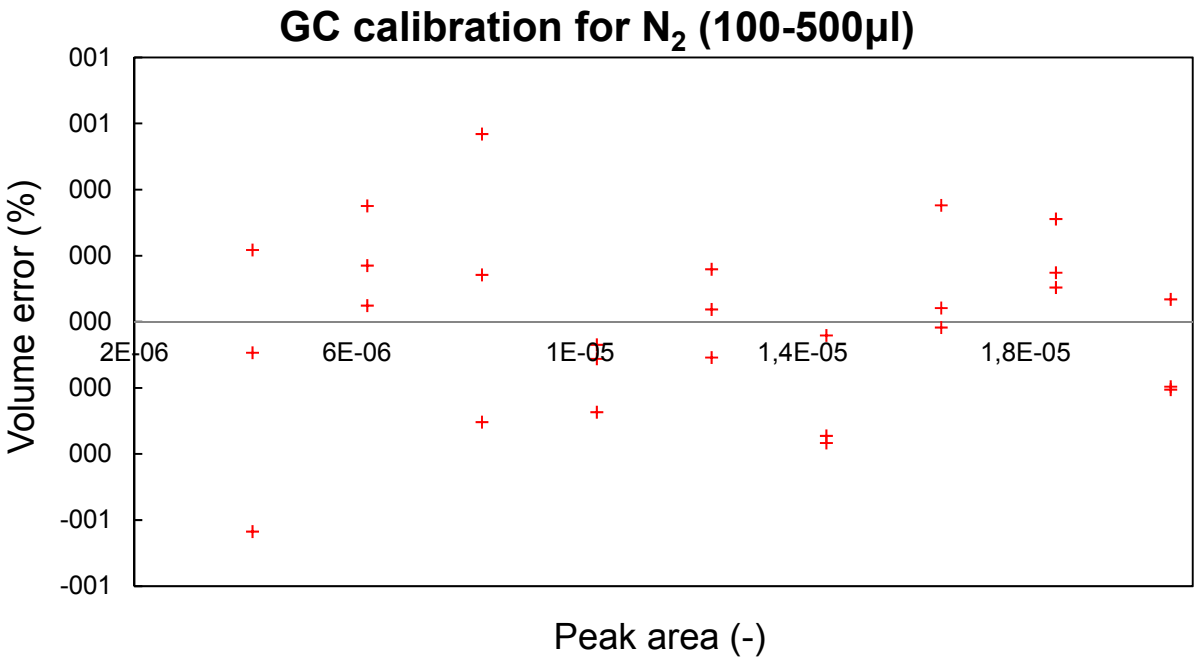

Figure 3.5 N_2 volume error against peak area as measured with GC.

From the area of the peak measured for specific CO_2 or N_2 volumes, which for that case syringes (connected with eVol® Automated Analytical syringe, SGE Analytical Science) of 500μl and 100μl were used, a 2nd order polynomial expression ($n_{cal}=a\cdot S^2+b\cdot S+c$) was derived for each gas at specific range of CO_2 and N_2 concentrations. The polynomial parameters for the first gas mixture are shown in Table 3.2.

Table 3.2 Polynomial expression composition parameters as came out from calibration for CO_2 and N_2.

Gases	Range (μl)	Composition parameters of 2nd degree polynomial			Uncertainty (%)
		a	b	c	
CO_2	0 – 100	1.56E-13	4.64E-09	2.64E-08	±1.0
N_2	100 – 500	-6.18E-14	5.49E-09	2.27E-07	±0.6

3.2 Hydrate equipment description

A brief sketch of the experimental equipment is presented in Figure 3.6. First of all, there are two gas cylinders one of nitrogen and one of mixture of CO_2 and N_2. The first is used for cleaning the cell and the last for providing the gas mixture at desirable pressure. Then there is a vacuum pump to avoid contamination of the tube and to help cleaning the cell.

The cell is immersed in a water bath for controlling the temperature and three sensors are attached to it; two of temperature (on the top and bottom of the cell) and one of pressure on the top. All of them are connected after acquisition units to personal computer. The temperatures are determined by the temperature transducer of the top and pressure transducer of the bottom.

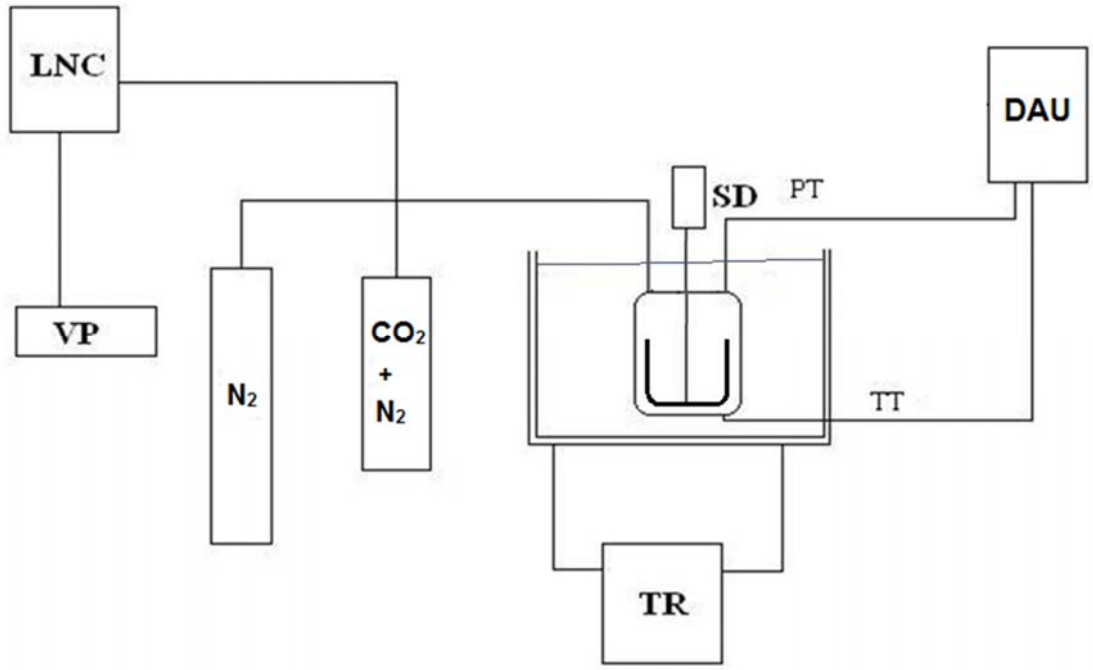

Figure 3.6 Simplified schematic diagram of equilibrium cell equipment. LNP: liquid nitrogen container. VP: vacuum pump. SD: strirring device. TR: temperature regulator. TT: temperature transducer bottom. PT: pressure transducer top. DAU: data acquisition unit.

Figures 3.7, 3.8 and 3.9 show photos of the experimental setup. The cylinder of the CO_2/N_2 mixture is shown in Figure 3.7. Temperature of the cell is controlled using a thermostatic water bath (LAUDA PROLine RP3530). One platinum temperature probe (Pt100) inserted in the cell interior is used to measure the temperature inside the cell within measurement accuracies, which are estimated to be less than 0.02 K with a second order polynomial calibration equation. The data acquisition units (Agilent 34970A, HP 34970A) are coupled with a personal computer to measure and automatically record pressure, temperature and time data. The data acquisition software also allows adjusting the rate of data acquisition, Figure 3.8. Continuous recording of pressures and

temperatures allows detecting any subtle changes in the system and true equilibrium conditions.

Figure 3.7 Cylinder of CO_2 and N_2 gas mixture.

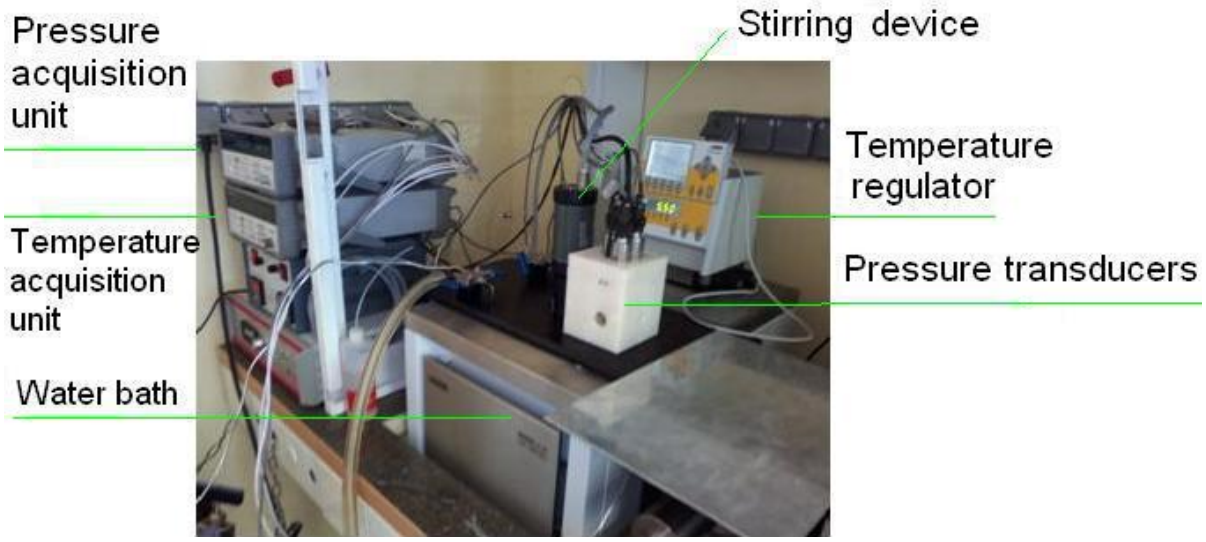

Figure 3.8 The water bath in which the equilibrium cell in immersed with the transducers attached to it.

A motor-driven turbine agitation system (Top Industrie, France) enables to stir the cell contents at a speed up to 2000 rpm to increase the fluids contact and enhance water conversion into hydrate, Figure 3.9.

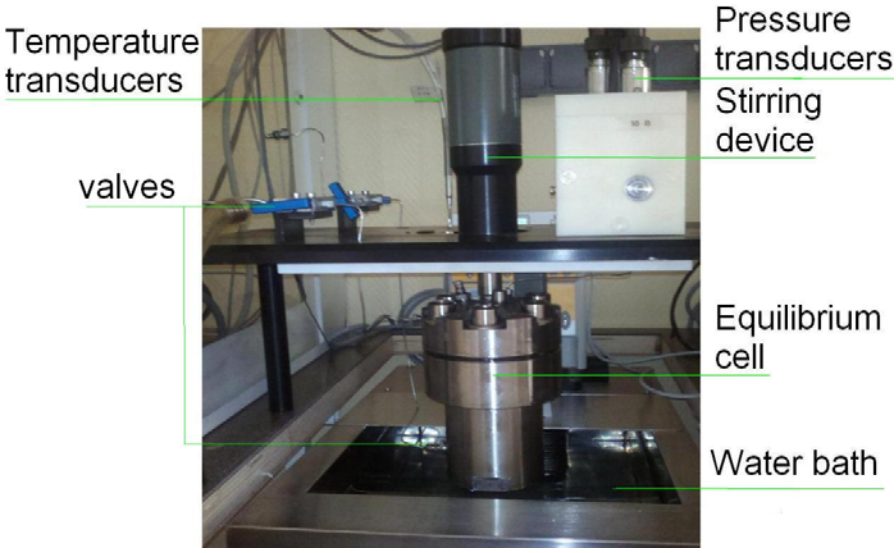

Figure 3.9 The inner volume of the equilibrium cell is approximately 125ml.

3.2.1 Measuring procedure

The four gas mixtures used in this work were prepared thanks to a gas cylinder in which different concentrations of CO_2 and N_2 were utilized. The CO_2 and N_2 gas bottles used in this work were supplied by Air Liquide. The molar fractions of CO_2 were app. 0.15, 0.11, 0.07 and 0.005.

Table 3.3 Chemicals used in this work.

Product Name	Abbreviation	CAS-number	Purity	Supplier	Phase
Carbon dioxide	CO_2	124-38-9	99.998 (vol%)	Air Liquide	gas
Nitrogen	N_2	7727-37-9	99.999 (vol%)	Air Liquide	gas
Tetra-n-butylammonium bromide	TBAB	1643-19-2	≥99+%	Acros Organics	solid
Tetra-n-butylammonium fluoride	TBAF	429-41-4	75 wt% in H_2O	Sigma Aldrich	liquid
Cyclopentane	CP	287-92-3	≥98%	Acros Organics	liquid

The exact concentration was measured by the gas chromatograph (see section 3.1.2). TBAB solutions with mass fractions of (0.05. 0.10 and 0.20) and TBAF solutions with mass fractions of (0.03, 0.05 and 0.10) were prepared by gravimetric method using an accurate analytical balance (Mettler, AT200), with mass accuracy of ±0.0001g. Double-distilled and deionized water from Direct-Q5 Ultrapure Water Systems (MilliporeTM), was used in all experiments. When needed, cyclopentane was added in TBAB and TBAF solutions with use of proper syringes. The chemicals used are presented in Table 3.3.

The schematic diagram of the experimental apparatus employed for measuring hydrate phase equilibrium points in this work is shown in Figure 3.6. Isochoric temperature trace method is applied. There are two cylinders, one of nitrogen gas and one of CO_2 and N_2 gas mixture. The first one is used for cleaning the Equilibrium Cell (EC) and the other one for providing the gas mixture at desirable pressure. The EC is immersed in a water bath for controlling the temperature. The EC temperature is controlled using a thermostatic water bath (LAUDA PROLine RP3530). Two platinum temperature probes (Pt100, JM6081) inserted in the cell interior –at the top (gas phase) and the bottom (liquid phase)– are used to measure the temperature inside the EC within measurement absolute uncertainties, which are estimated to be less than $u(T, k = 2) = 0.02$ K. All of them are connected after acquisition units to personal computer. The results are calculated by the platinum probes of the top and the pressure transducer of the bottom. The pressure in EC is measured using a UNIK 5000 GE absolute pressure transducer with an absolute uncertainty of $u(P, k = 2) = 0.0015$ MPa.

More specifically, the main part of the setup is the EC which is immersed in thermostatic water bath (LAUDA PROLine RP3530) containing double-distilled and deionized water. The EC is made of the 316 stainless steel; its maximum working pressure and its inner volume is 40 MPa and 125 mL respectively. A motor-driven turbine agitation system (Top Industrie, France) enables to stir the cell contents at a speed up to 1200 rpm to increase the fluids contact and enhance water conversion into hydrate. For calibrating temperature and pressure uncertainties second order polynomial calibration equation was used (see section 3.1.1). The data acquisition units (Agilent 34970A, HP 34970A) were coupled with a personal computer to measure and automatically record (every 25s) pressure,

temperature and time data. The data acquisition software also allows adjusting the rate of data acquisition. Continuous recording of pressures and temperatures allows detecting any subtle changes in the system and true equilibrium conditions.

After careful evacuation of the EC using the vacuum pump (Oerlikon leybold vacuum, Trivac D2.5E) for two days, 15-40 ml of promoter solution (TBAB, TBAF, CP,TBAB+CP,TBAF+CP) −that is about 20-30 vol% of EC− was subsequently filled with aqueous solution and then the gas mixture was introduced in the EC from the cylinder. All amounts of substances supplied to the cell were quantified. Pressure and temperature measurements under hydrate stability conditions were carried out as follows: The cell was immersed into the temperature-controlled bath and temperature was decreased to form hydrates, while agitating at a constant speed of about 1070 rpm to increase the fluids contact and enhance water conversion into hydrate.

The temperature of the system was kept constant for at least 7h to overcome the metastable period and to allow complete hydrate formation, which was detected by a noticeable pressure drop. Temperature was then increased step-wisely at rate of about 0.4 °C/h[54,135]. At every temperature step*,* temperature was kept constant until temperature and pressure were established. The stabilization time needed fluctuates from 1h 15 min to 1h 30 min as gas pressure increases from 10 to 80bar. As implemented by Ohmura *et al.*[55], a pressure-temperature diagram was obtained for each experimental run from which the hydrate dissociation condition could also be determined. For measuring an equilibrium condition at a higher pressure, the pressure of the system was increased by successively supplying gas mixture to the equilibrium cell until achieving the desired pressure. In this way, several *P,T* equilibrium data were obtained from each experimental run. Pressure and temperature accuracies for transducers were 15 mbar and 0.02 °C respectively.

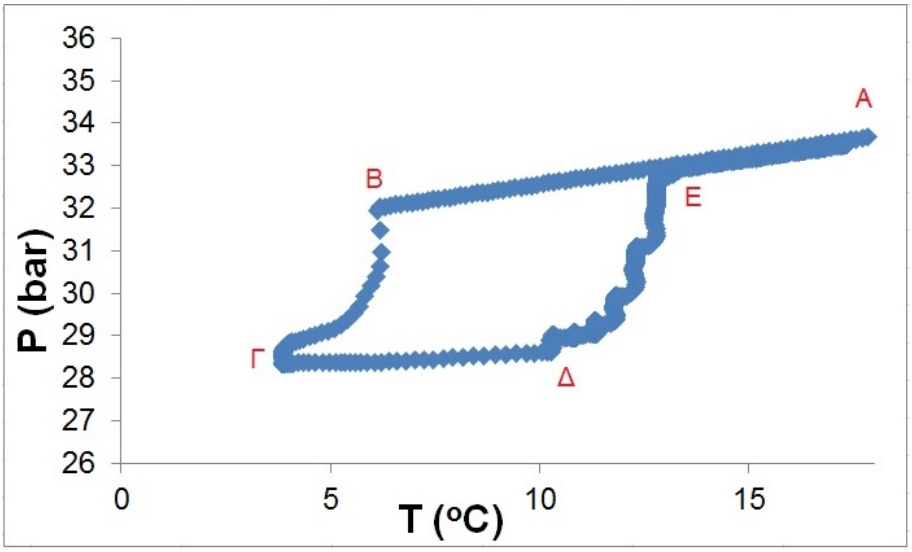

Figure 3.10 Temperature trace method for determination of equilibrium point of CO_2/N_2 (6.87/93.13) gas mixture with 20 wt% TBAB mol fraction.

After two days, a *P,T* diagram was produced, as shown for 20% TBAB and CO_2/N_2 6.87/93.13 in Figure 3.10. The procedure is as follows. At first, the cell was cooled up to 2 °C (from A to Γ). After staying at least 10h at this point equilibrium was achieved which means that hydrates were fully formed. The next day dissociation started. The temperature was increased rapidly (from Γ to Δ) and then step-wisely so that every temperature step corresponded to hydrate equilibrium dissociation points (from Δ to A). Finally, the dissociation point is calculated by the intersection of the HVL polynomial line with the VL equilibrium line (see also chapter 4.1).

3.3 Hydrate equilibrium results

3.3.1 TBAB results

The TBAB results for CO_2+N_2 mixture concentrations are summarized in Figure 3.11. The results are compared with literature data. At first, for comparison purposes, the unpromoted system CO_2+N_2 is reported[136]. In general, it is observed good agreement of results of this work with the literature data for similar systems of 5%, 10% and 20 wt% TBAB solutions which correspond to 0.29%, 0.62% and 1.38 mol% respectively. For clarity reasons, the systems are presented by two numbers in brackets.

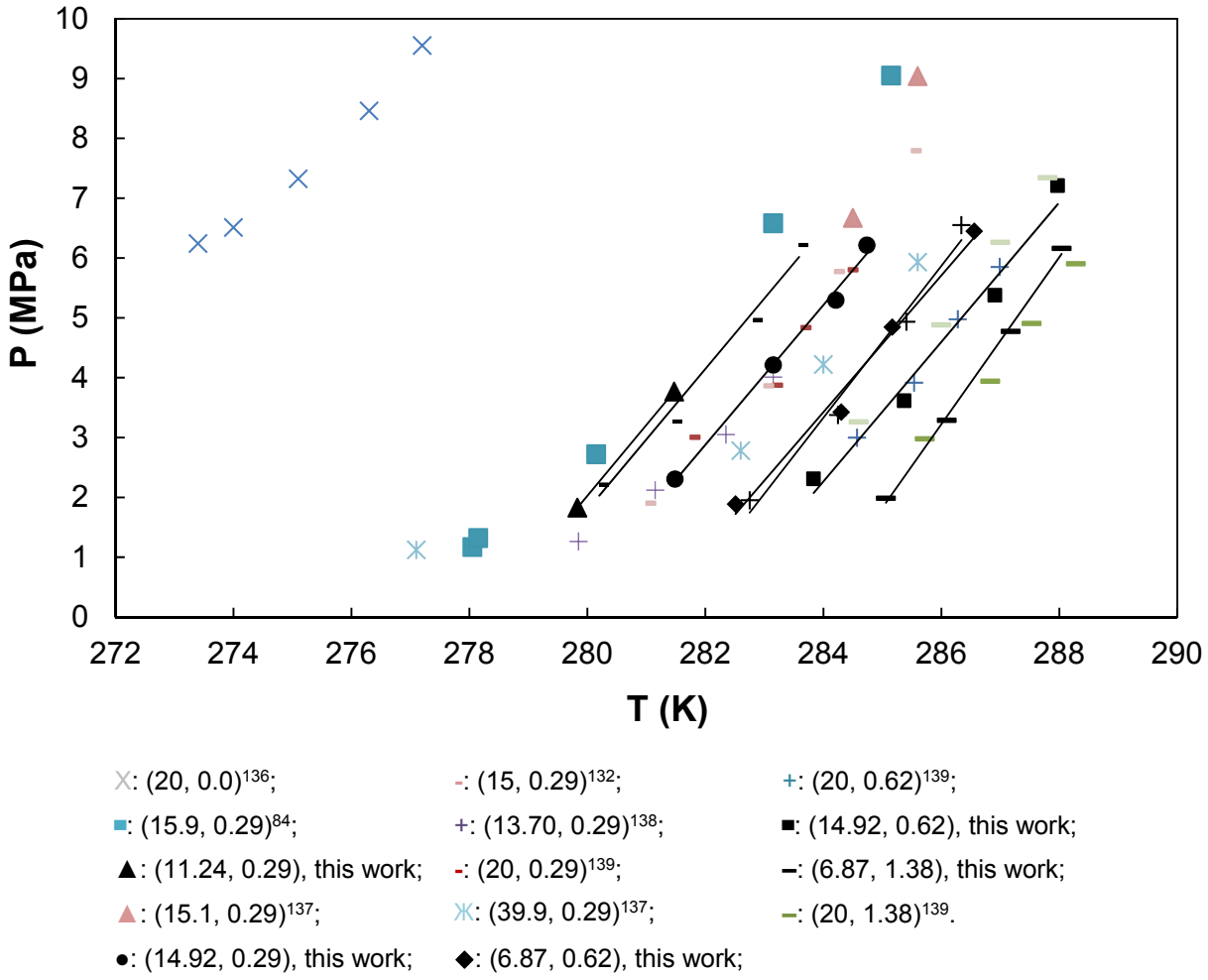

Figure 3.11 Hydrate dissociation points for different systems using TBAB as promoter. The Figure contains systems of this work and systems of CO_2+N_2+TBAB+H_2O from literature. For clarity reasons, the systems are presented by two numbers in brackets. The first number denotes the mol fraction of CO_2 in CO_2+N_2 gas mixture cylinder and the second one denotes the promoter concentration. Black markers connected with trendlines correspond to results of this work. References are presented according to their presence in figure from left to right.

The first number denotes the mol fraction of CO_2 in CO_2+N_2 gas mixture cylinder and the second one denotes the promoter concentration expressed in mol%. Black markers connected with trendlines correspond to results of this work. From Gibbs phase rule, the parameters that suggest where the equilibrium lines should be located are the gas mixture concentration, the promoter concentration in aqueous solution and the gas-to-liquid ratio (mol/mol). For simplicity reasons and owning to the fact that gas-to-liquid ratio is not always mentioned in literature, it was omitted from this study.

In general, the higher the CO_2 in CO_2+N_2 gas mixture concentration, the more on the right of the *P,T* diagram the hydrate dissociation results are located. This results in further decreasing of hydrate formation pressure. At higher temperatures, CO_2 is captured easier than N_2. In modeling, the analogy of Langmuir absorption approximates successfully hydrate crystallization (see chapter 5). So, the size and the kinetic energy of CO_2 at higher temperatures enhance more CO_2 capture than N_2 capture.

The results of similar promoter and gas mixture concentrations are in excellent agreement, e.g. with (14.92, 0.29) from this work, with (13.70, 0.29)[138], with (20, 0.29)[139] and with (15, 0.29)[132]. Another observation is that the system of (6.87, 0.62) of this work is approximately placed on the left of (20, 0.62)[139] which shows that CO_2 hydrates are formed at lower pressures than N_2 hydrates.

Similarly, for higher TBAB concentrations, the results of similar promoter and gas mixture concentrations are in good agreement, e.g. with (6.87, 1.38) from this work, with (20, 1.38)[139]. According to the literature, there is mismatch of (13.70, 0.29)[138] with the system (15.9, 0.29)[84] respectively as shown in Figure 3.10.

For a more detailed comparison of results of this work, Figures 3.12 and 3.13 include systems of this work and for CO_2 or N_2 plus TBAB+H_2O from literature respectively. In Figure 3.12 the results of this work are located between the system of pure CO_2 hydrate and systems of CO_2+TBAB+H_2O from literature. This is expected due to the high content of N_2 that was used in results of this work. The results from literature are smoothly shifted to the right-hand side of the diagram as TBAB concentration increases. In Figure 3.13, results of this work are located between systems of N_2+TBAB+H_2O from literature. This is expected because of the high content of N_2 in the gas mixture used. Specifically, the system of (11.24, 0.29) of this work is located as expected on the right side of the systems of (0.0, 0.29)[11] and (0.0, 0.29)[50].

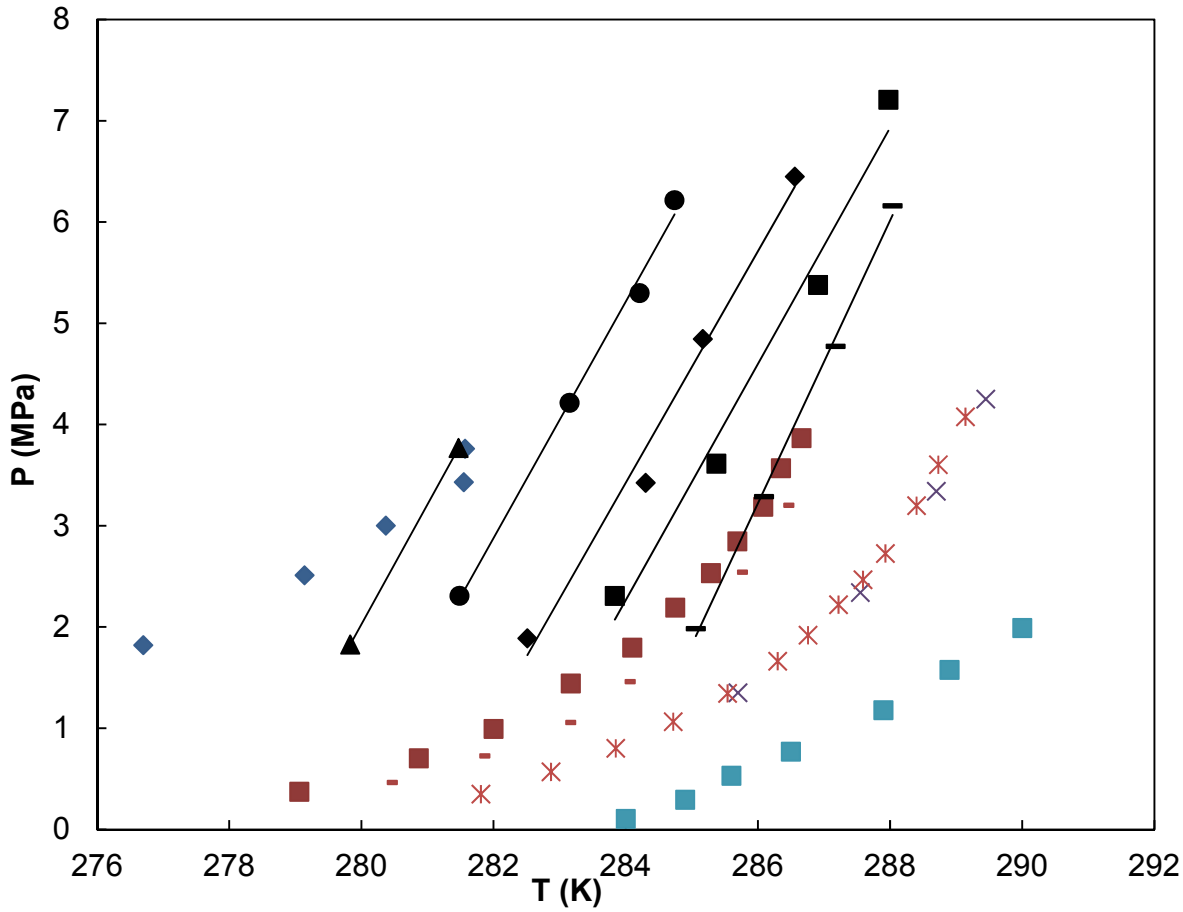

◆: (100, 0.0)[128]; ■: (14.92, 0.62), this work; ✳: (100, 0.62)[131];
▲: (11.24, 0.29), this work; –: (6.87, 1.38), this work; X: (100, 0.60)[11];
●: (14.92, 0.29), this work; ■: (100, 0.29)[131]; ■: (100, 1.83)[50].
◆: (6.87, 0.62), this work; -: (100, 0.29)[50];

Figure 3.12 Hydrate dissociation points for different systems using TBAB as promoter. The Figure contains systems of this work and systems of CO_2+TBAB+H_2O from literature. For clarity reasons, the systems are presented by two numbers in brackets. The first number denotes the mol fraction of CO_2 in CO_2+N_2 gas mixture and the second one denotes the promoter concentration. Black markers connected with trendlines correspond to results of this work. References are presented according to their presence in figure from left to right.

The system of (6.87, 1.38) of this work coincides well with the results of (0.0, 2.59)[11] which reveals that the addition of 6.87% of CO_2 in pure N_2 counteracts the additional use of 2.21 mol% TBAB in aqueous solution, which is the deduction of 2.59 mol% and 1.38 mol% of the two systems.

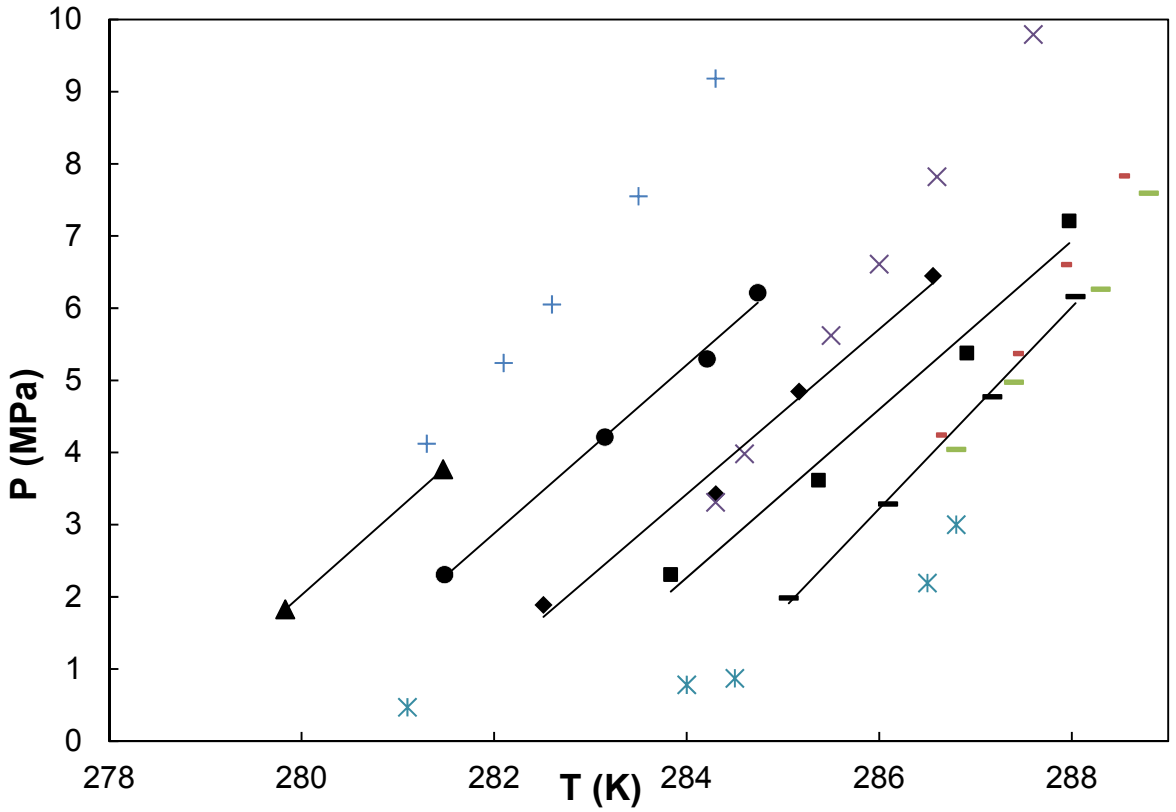

+: (0.0, 0.29)[90]; X: (0.0, 0.62)[50]; –: (0.0, 2.59)[90];
▲: (11.24, 0.29), this work; ■: (14.92, 0.62), this work; –: (6.87, 1.38), this work;
●: (14.92, 0.29), this work; -: (0.0, 1.38)[90]; ✳: (0.0, 1.83)[50].
◆: (6.87, 0.62), this work;

Figure 3.13 Hydrate equilibrium points for different systems using TBAB as promoter. The Figure contains systems of this work and systems of N_2+TBAB+H_2O from literature. For clarity reasons, the systems are presented by two numbers in brackets. The first number denotes the mol fraction of CO_2 in CO_2+N_2 gas mixture cylinder and the second one denotes the promoter concentration. Black markers connected with trendlines correspond to results of this work. References are presented according to their presence in figure from left to right.

3.3.2 Results for CP as promoter

Similar procedure is followed for the system CO_2+N_2+CP+H_2O. For CO_2/N_2 mixture (6.87/93.13), 15 ml and 25 ml of CP aqueous solution of 20 wt% (6.03 mol%) and 52.57 wt% (22.15 mol%) were prepared respectively. The stoichiometric concentration of CP in the solution for s(II) hydrates is 18.65 wt% (5.56 mol%)[140]. For CP concentrations >27.80 wt%, according to Galfré *et al.*[141], emulsion system is produced. For *P,T* measurements,

stirring velocity is not of importance. It was used relatively high stirring velocity (1070 rpm). It came out that results of this work were similar for both CP concentrations used. Figure 3.14 summarizes the results.

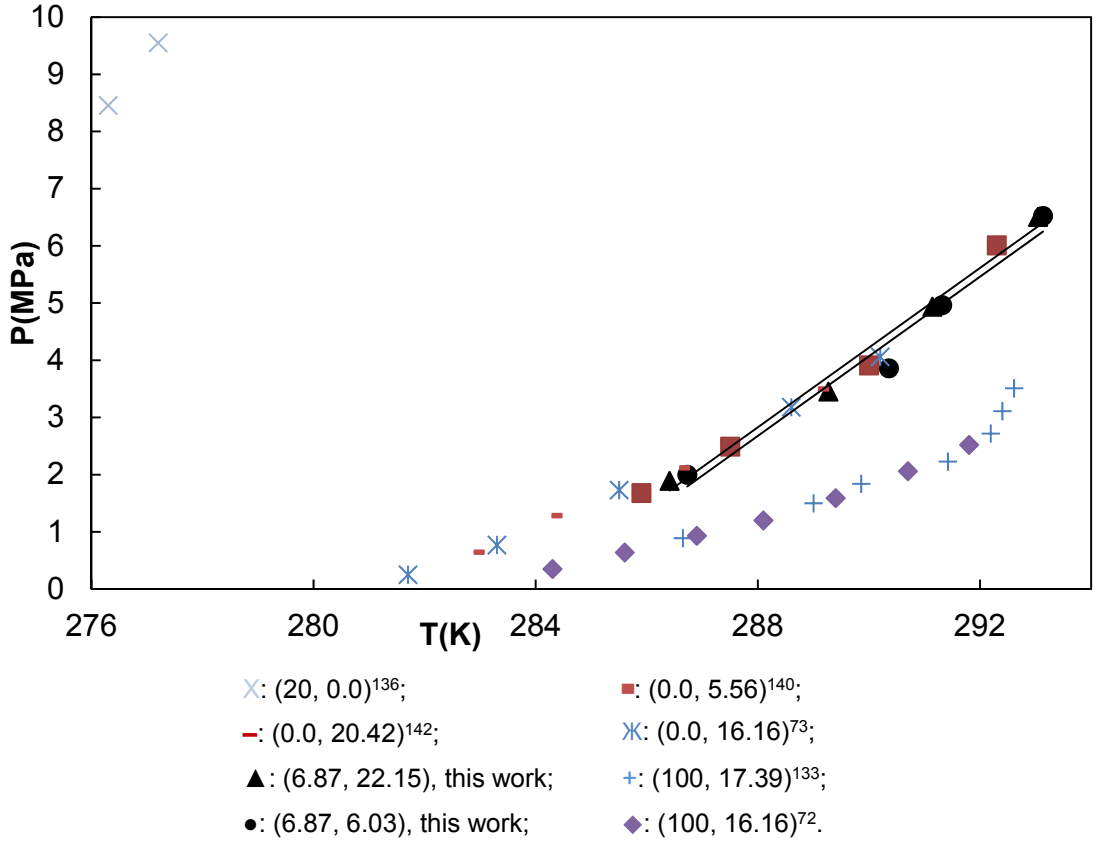

Figure 3.14 Hydrate equilibrium points for different systems using CP promoter. References are presented according to their presence in figure from left to right. For clarity reasons, the systems are presented by two numbers in brackets. The first number denotes the mol fraction of CO_2 in CO_2+N_2 gas mixture cylinder and the second one denotes the promoter concentration. Black markers connected with trendlines correspond to results of this work. References are presented according to their presence in figure from left to right.

In phase equilibrium a mixture may exist between the simple CO_2 hydrate in s(I) and double CO_2-CP hydrates in s(II)[15]. In Figure 3.14, there is a region in which CO_2+N_2 mixture dissociation points should exist based on experimental results[72,73,133]. These are the boundaries of pure CO_2 and pure N_2 plus CP+H_2O systems respectively. The results of this work are included in these boundaries. Another observation is that CP does not ´´sense´´ the small mol fraction of CO_2 (e.g. 6.87 mol%) of CO_2 in CO_2+N_2 gas mixture.

In other words, most probably N_2 is predominantly captured –higher N_2 selectivity– rather than CO_2 since the results between pure N_2 and CO_2+N_2 are identical. According to results of this work and literature[65], the CP concentration does not have any significant impact on the thermodynamic equilibrium in contrast with TBAB due to water immiscibility in cyclopentane. This occurs for both the emulsion and the non-emulsion CP case. In other words, the two systems of different CP concentrations match each other excellently. Very recently it was observed that the decrease in pressure equaled the increase in temperature for the hydrate phase equilibrium[143]. The improvement in the hydrate phase equilibrium temperature produced by CP was limited to ~12 K and the hydrate stability temperature was not increased further when the mol concentration of CP was >1%[143].
The effects of CP on the CO_2 hydrate phase equilibrium conditions can be explained by the theory of hydrate crystalline structure[24]. Typically, CO_2 can easily enter the large cavity ($5^{12}6^2$) of an s(I) hydrate and the small cages of 5^{12} in the presence of other hydrate formers. CP helps to form double s(II) hydrates with CO_2. The large cavity ($5^{12}6^4$) of a s(II) hydrate is occupied by CP and the smaller cavity (5^{12}) is filled with CO_2. The precipitous shift in the CO_2 hydrate phase equilibrium curve is caused by a hydrate crystal change from s(I) (pure CO_2) to s(II) (with the presence of CP)[143]. As the crystal structure changes, a different thermodynamic state (i.e. three-phase temperature and pressure) is required for stability. Small amount of CP encourages the stability of s(II), the occupation of CO_2 in the 5^{12} cavities and provides the large degree of stability to the s(II) large cage. The change in hydrate structure can elucidate in a molecular level the substantial decrease in the hydrate phase equilibrium pressure that is required for a small composition change[143].

3.3.3 TBAF results

The TBAF results for CO_2+N_2 gas mixture global concentrations are summarized in Figure 3.15. The results are compared with literature data. At first, for comparison purposes, the unpromoted system N_2+H_2O is reported[144]. In general, it is observed good agreement of results of this work with the literature data for similar systems of 5% and 10

wt% TBAF solutions which correspond to 0.36% and 0.76 mol% respectively. For 3 wt% TBAF solution no data from literature were found.

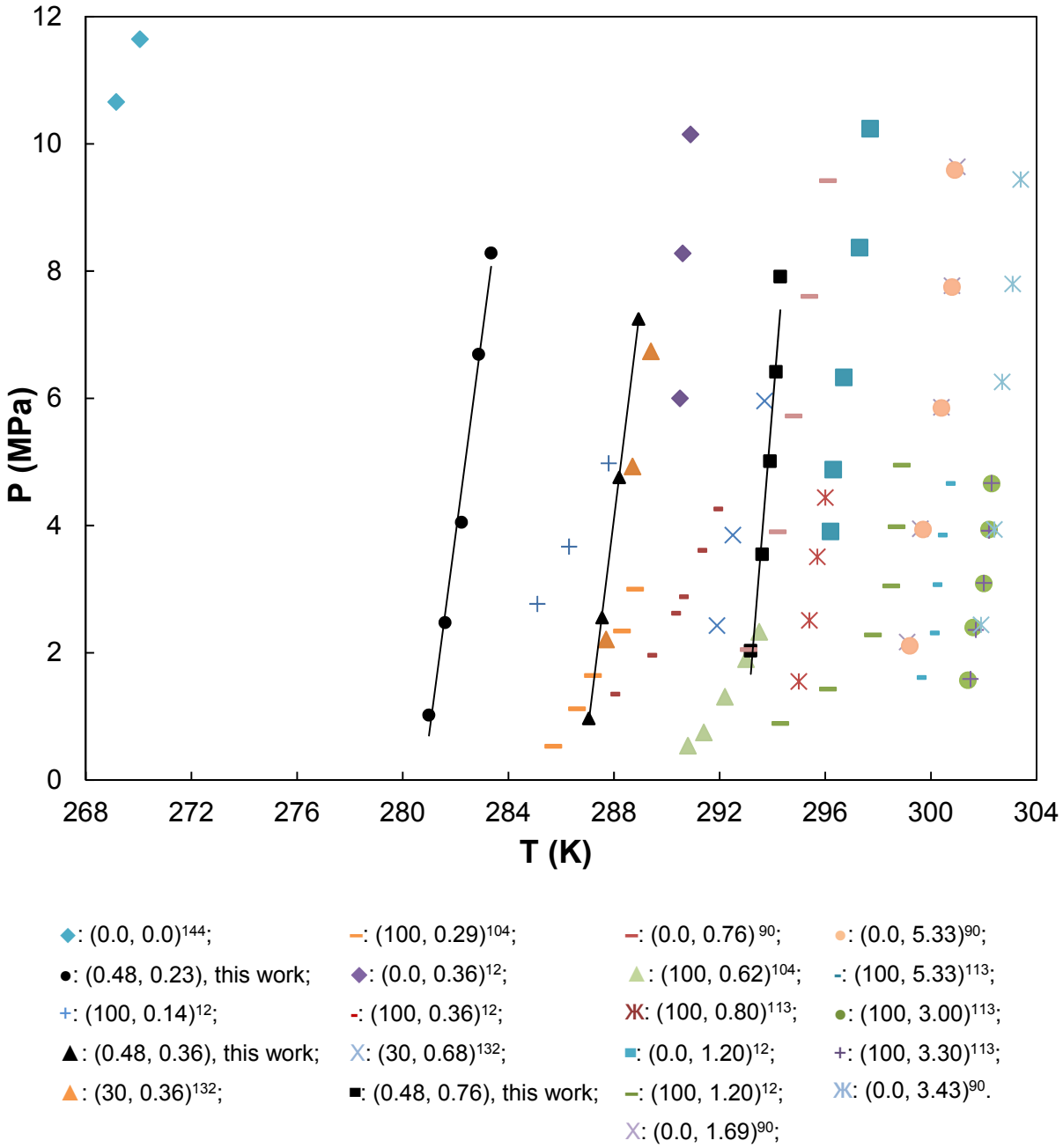

Figure 3.15 Hydrate dissociation points for different systems using TBAF as promoter with CO_2 + N_2 (0.48/99.52) gas mixture. References are presented according to their presence in figure from left to right. The first number denotes the mol fraction of CO_2 in CO_2+N_2 gas mixture cylinder and the second one denotes the promoter concentration used in this work. Black markers connected with trendlines correspond to results of this work. References are presented according to their presence in figure from left to right.

For clarity reasons, the systems are presented by two numbers in brackets. The first number denotes the mol fraction of CO_2 in CO_2+N_2 gas mixture cylinder and the second one denotes the promoter concentration expressed in mol%. Black markers connected with trendlines correspond to results of this work. From Gibbs phase rule, the parameters that suggest where the equilibrium lines should be located are the gas mixture concentration, the promoter concentration in aqueous solution and the water-to-gas ratio (mol/mol). For simplicity reasons and owning to the fact that gas-to-liquid ratio is not always mentioned in literature, it was omitted from this study.

The results for 3.2%, 5% and 10 wt% TBAF, which correspond to 0.23 mol%, 0.36 mol% and 0.76 mol% respectively, seem well placed in the Figure 3.15. The gas mixture, which is 99.52% mol N_2, produced steeper results than with higher CO_2 concentration. In addition, 0.36 mol% TBAF are in good agreement with similar solutions from literature[14,90,132], even though the last correspond to pure N_2 results.

3.3.4 Mixtures of TBAB+CP and TBAF+CP

In Figure 3.16, three systems of this work for mixture of TBAB+CP and systems from literature[132,139] for similar conditions, e.g. CO_2 in CO_2+N_2 and TBAB solution concentrations, are presented. In the caption of Figure 3.17, along with the two numbers in brackets, there is a third number denoting CP addition in TBAB solution in vol%. The addition of 5 vol% CP in TBAB have shown that for TBAB 1.38 mol%, there is synergetic effect between TBAB and CP which means that the results are better when CP is added compared to pure TBAB. The effect is more significant for P > 2.5 MPa as shown in Figure 3.16. When TBAB 0.62 mol% fraction is used, the results of TBAB and CP proved to be identical with those of pure promoter at same concentration.

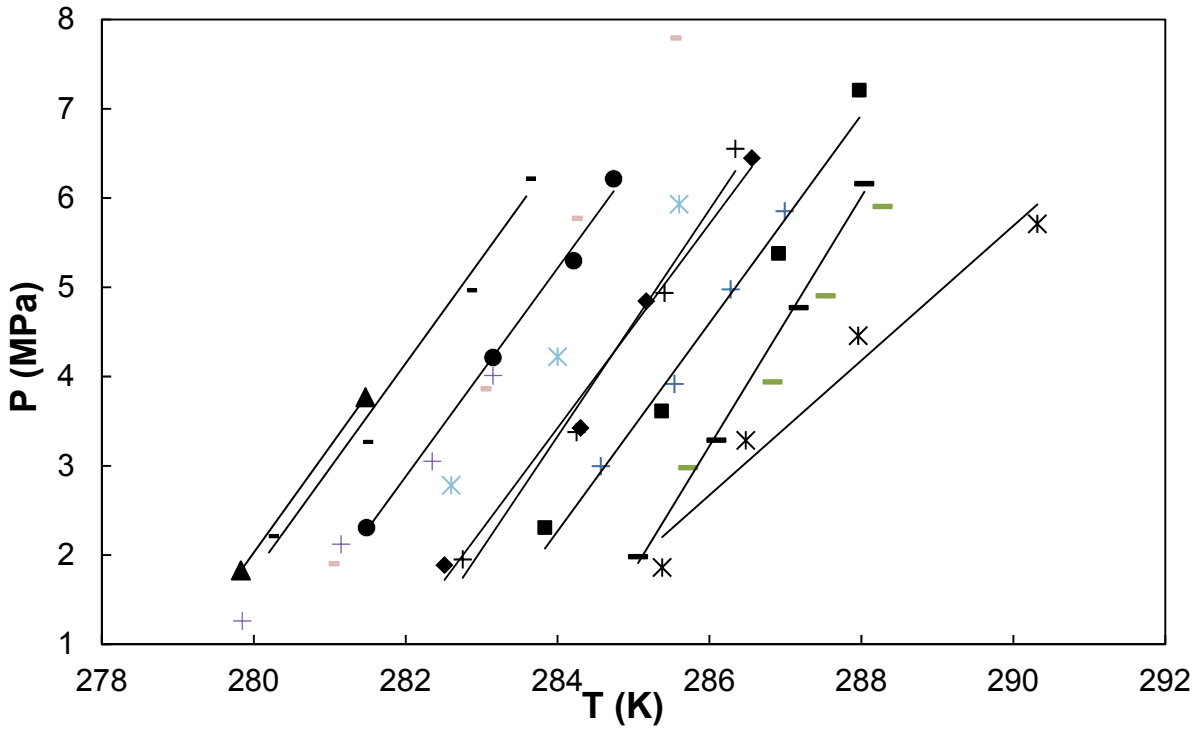

Figure 3.16 Hydrate equilibrium points for different systems using TBAB promoter and mixture of TBAB+CP in this study. References are presented according to their presence in figure from left to right. The first number denotes the mol fraction of CO_2 in CO_2+N_2 gas mixture cylinder, the second one denotes the promoter concentration and the third number is the 5 vol% of CP used in this work. Black markers connected with trendlines correspond to results of this work. References are presented according to their presence in figure from left to right.

For TBAB 0.29 mol% with CP 5 vol%, the gas systems used in this study are different but it is highly improbable that the change in CO_2 concentration would have such a drastical impact on thermodynamic equilibrium that could induce promotion.

Finally, in Figure 3.17 all hydrate dissociation points of this work for TBAF promoter are presented. The use of CP in 0.76 mol% TBAF has no effect in the results compared to pure TBAF results of 0.76 mol% while for 0.36 mol% TBAF the behavior is mixed when CP is present. For low pressures (<30 bar), inhibition effect is observed while for higher pressures (>30 bar) promotion effect appears.

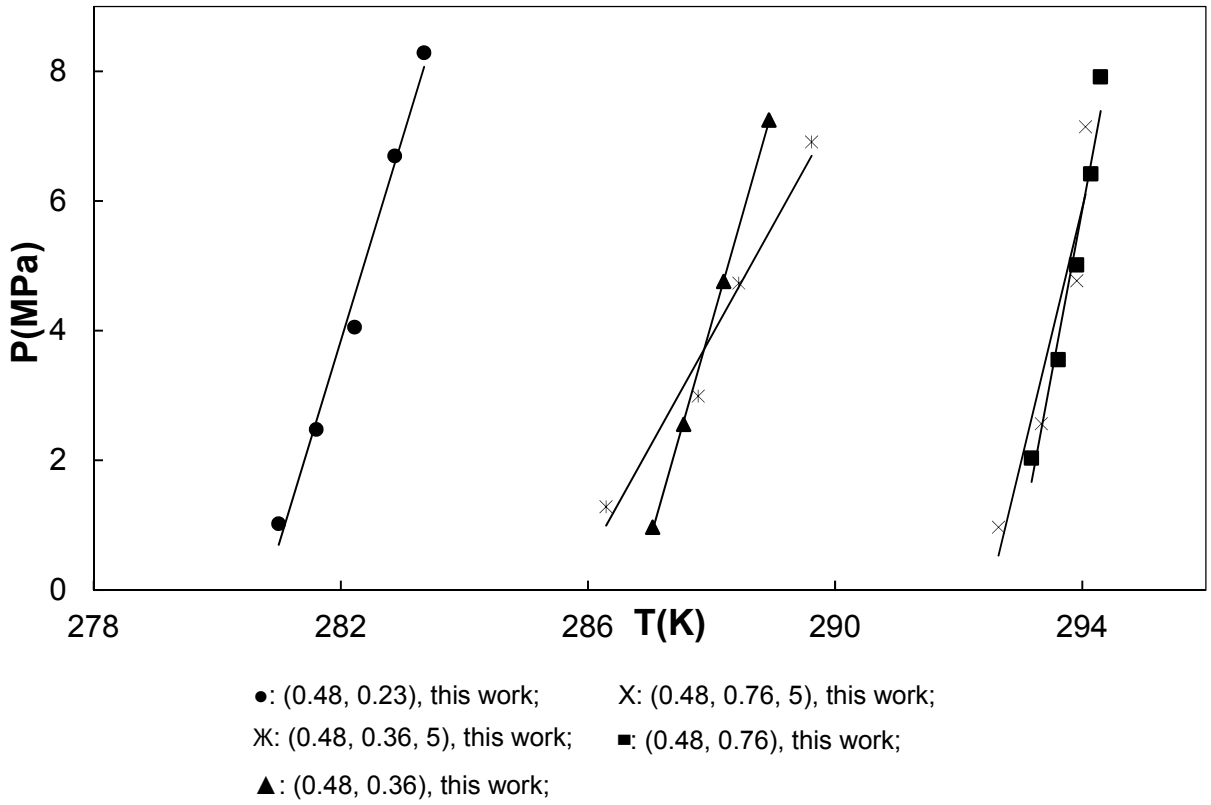

Figure 3.17 Hydrate dissociation points for different systems using TBAF and CP as promoter with CO_2 + N_2 (0.48/99.52) gas mixture. The first number denotes the mol fraction of CO_2 in CO_2+N_2 gas mixture cylinder, the second one denotes the promoter concentration and the third number is the 5 vol% of CP used in this work. Black markers connected with trendlines correspond to results of this work.

Another reason for the promotion enhancement could be attributed to fact that there seems to be some connection between the synergetic effect, the molecular weights and hydrate structures of TBA salts. TBAF is 23% lighter than TBAB and requires 0.26 times (which is the ratio of 0.36/1.38) lower molar concentration so that a synergy between TBAB or TBAF and CP may occur. For the TBAB, it is known that there is phase transition from type B to type A at ~18 wt% (1.21 mol%)[90,94]. TBAF has also two crystal structures: a tetragonal TBAF·32.8H_2O and a cubic TBAF·29.7H_2O at which the phase transition from tetragonal to cubic occurs at ~33 wt% (3.3 mol%)[145]. Moreover, fluoride is more electronegative anion than bromide. These facts might play some role in promotion enhancement.

3.4 Conclusions

Hydrate equilibrium points for CO_2 and N_2 were measured with the use of tetra-n-butylammonium bromide (TBAB), tetra-n-butylammonium fluoride (TBAF), cyclopentane (CP) and mixtures of TBAB and TBAF with CP. The use of higher TBAB concentration (1.38 mol%) and CP (5 vol%) revealed promotion effect and as the pressure rises (>3.5 MPa), the phenomenon becomes more intense as presented in Figure 3.16. In addition, the higher the CO_2 concentration, the stronger the promotion is for every concentration of TBAB aqueous solution. On the contrary, the results have shown that the simultaneous use of TBAB (0.29 mol%) and (0.62 mol%) with CP (5 vol%) did not have any impact on thermodynamic equilibrium. For the system TBAB (0.29 mol%) with CP (5 vol%), even though the gas mixture systems are different, it is rather unlikely that there is positive impact on promotion. However, this fact is not easily observable for low differences of CO_2 concentration in mixtures. Consequently, it came out that the factor of gas mixture concentration has moderate impact for TBAB on hydrate equilibrium points compared to promoter's concentration. All the results of this work are presented in Figure 3.18.

The use of CP solution (even though it is virtually water insoluble) proved to be stronger promoter than TBAB maybe because of the different hydrate structure it induces. According to the hydrate promotion ability of TBAB for 40 wt% (3.60 mol%) TBAB, above of which it acts as inhibitor[146], the promotion results may become similar to CP results. The stoichiometric concentration of CP in the solution for structure II hydrates is 18.65 wt% (5.56 mol%)[140]. When higher CP concentration than was used, e.g. 52 wt% (22.15 mol%), the results showed slight inhibition effect.

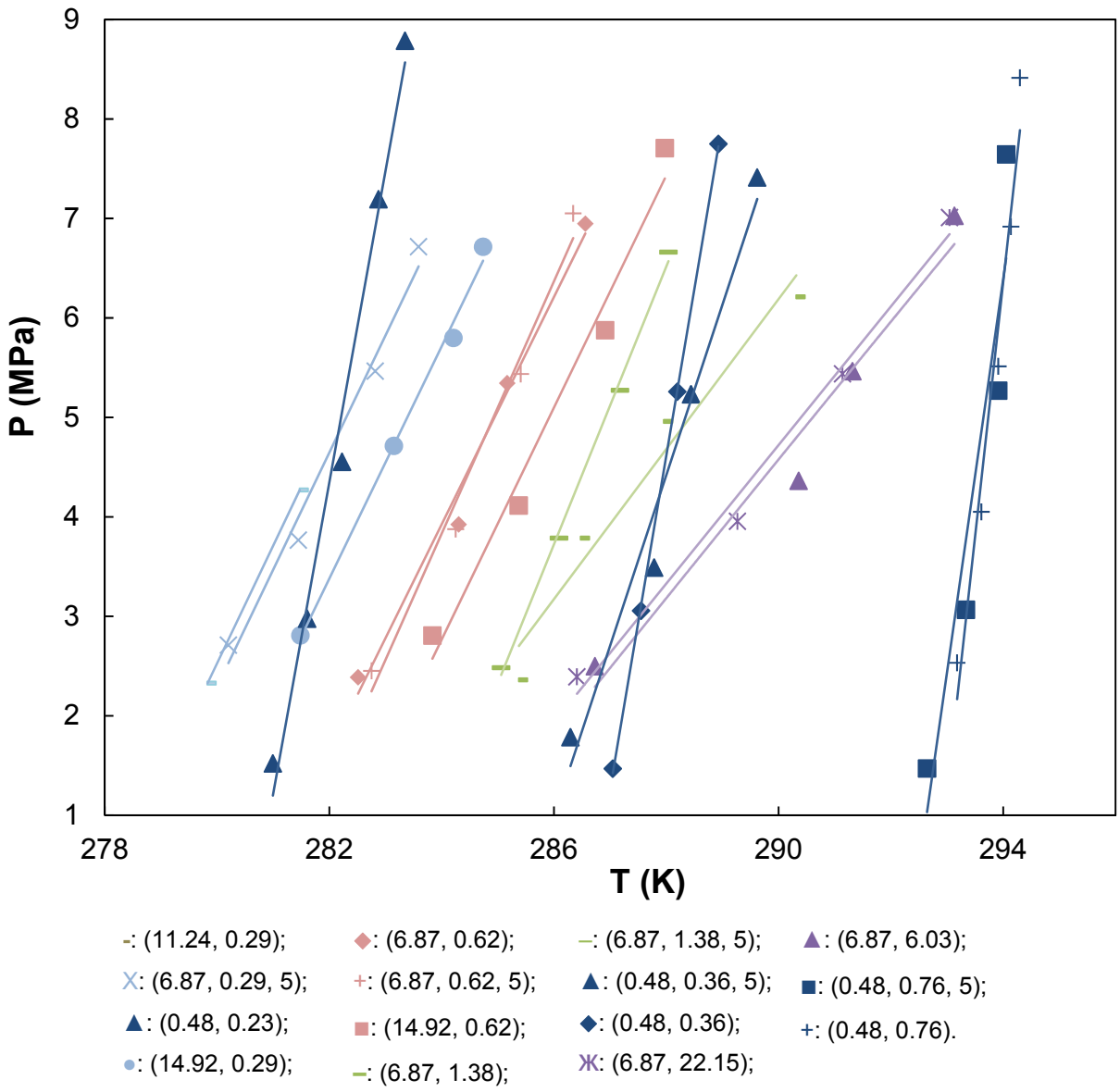

Figure 3.18 Temperature and pressure hydrate equilibrium points for CO_2+N_2+TBAF/TBAB/CP+H_2O systems of this work. Color lines denote same TBAB or CP or TBAF concentration. The open blue colors, red and green are TBAB results. The purple denote CP results and the dark blue stand for TBAF results. The first number denotes the mol fraction of CO_2 in CO_2+N_2 gas mixture cylinder, the second one denotes the promoter concentration and the third number is the 5 vol% of CP used in this work. All results of this work are connected with trendlines.

Finally, TBAF proved to be by far much stronger promoter than TBAB and CP, especially for lower pressures. This is not easily observable because of the almost pure N_2 mixture it was used. The use of TBAF concentration (0.36 mol%) with CP (5 vol%) revealed

promotion effect above 30 bar and as the pressure rises it becomes more intense. Moreover, the gas composition used in TBAF promotion has minor impact on equilibrium results compared to TBAB promotion.

In general, classical gas hydrates generally form at high pressures and/or low temperatures. Flue gas of power stations is emitted in low pressures and high temperatures. The promoters´ examined like TBAB, TBAF, CP can enable hydrate formation at conditions close to ambient pressure and lower temperatures (5 - 10 K) above the normal ice-point of water in constrast to non-promoted systems. The drawbacks of using CP are its high volatility and its hazard towards environment. Furthermore, CP lowers the selectivity towards carbon dioxide in the hydrate phase compared to the unpromoted system as this study has shown. On the other hand, TBA salts are environmental friendly but they exhibit low gas uptake due to their unique semi-clathrate structure. Moreover, their promoting capabilities are lower than CP and as this study has shown their ability depends significantly on the initial CO_2 gas content.

4

Experimental uncertainties and consistency analysis of results

Στερεότητα νοὸς ἐστὶ μετεωροσκοπία τῶν νοητῶν, ἥτις ἁμιλλᾶται τῇ ουρανίῳ χροιᾷ, ἐφ' ᾗ διαυγάζει ἐν τῷ καιρῷ τῆς προσευχῆς τὸ φῶς τῆς ἁγίας Τριάδος.

Ἅγ. Εὐάγριος ὁ Ποντικός (345 – 399 μ.Χ.)[f]

[f] *Firmness of mind is observatory of perceptible, which contend with the heaven skin, upon which illuminates at the time of praying the light of Holy Trinity.*

St. Evagrius of Pontus (345 – 399 AD)

In this chapter the uncertainties of every aspect of the experimental procedure is presented. In addition, the consistency analysis will give an indication of the accurateness of the experimental procedure. This chapter is published in peer-review journals of *Fluid Phase Equilibria* and *Chemical and Engineering Data* as shown in Appendix E.

4.1 Calculation of hydrate equilibrium point

The uncertainties for every hydrate equilibrium point are calculated as the root of the sum of squared uncertainties of transducers and repeatability of the experimental procedure. A *P,T* diagram is produced in order to find dissociation conditions (T_{diss},P_{diss}), as it is shown for 5% TBAB and CO_2/N_2 13.92/83.13 in Figure 4.1. The procedure is as follows. At first, the cell was cooled up to 2°C. After staying at least 10 h at this point, equilibrium is achieved which means that hydrates are fully formed. Then dissociation starts. The temperature is increased rapidly and then step-wisely so that every temperature step corresponds to hydrate equilibrium dissociation point.

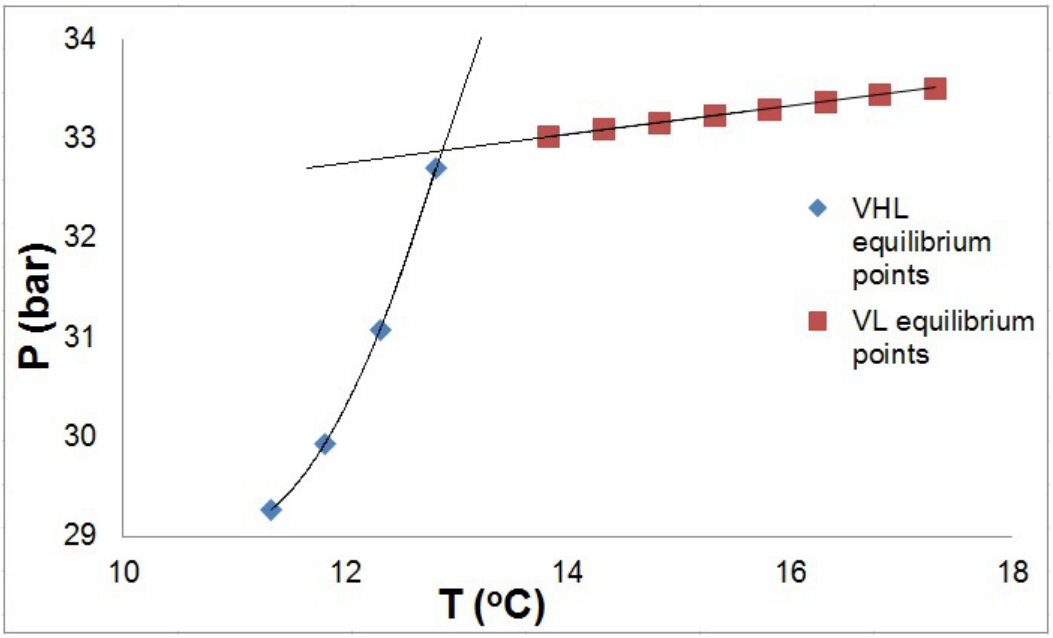

Figure 4.1 Pressure-Temperature trace method diagram for estimating hydrate dissociation point. In this case for 20 wt% TBAB and CO_2/N_2 (6.87/93.13) the dissociation point is found at 32.85 bar and 12.94 °C.

Finally, the dissociation point is calculated by the intersection of the VHL polynomial line with the VL equilibrium line. In this case, the dissociation point was found at 32.85 bar and 12.94 °C, according to eq. 4.1, 4.2, 4.3 and 4.4.

$$P = a'T^2 + b'T + c' \quad \text{for VHL equil.} \tag{4.1}$$

$$P = a\,T + b \quad \text{for VL equil.} \tag{4.2}$$

$$T = \frac{-(b'-a)+\sqrt{\Delta}}{2\,a'} \tag{4.3}$$

$$\Delta = (b'-a)^2 - 4\,a'\,(c'-b) \tag{4.4}$$

where T: equil. dissociation temperature
P: equil. dissociation pressure
Δ: discriminant
a, b: regression coefficients for VHL equil. line
a´,b´,c´: regression coefficients for VL equil. line
u(a), u(b): regression deviations from straight line for VHL equil. line
u(a´), u(b´), u(c´): regression deviations from straight line for VL equil. line

4.2 Hydrate equipment and random uncertainties

At first, the temperature and pressure errors *u(T)* and *u(P)* of the acquisition units were calculated. They consist of the sum of squared roots of calibration (random) and repeatability uncertainties, eq. 4.5 and 4.6. For the calibration (random) uncertainty, it is also assumed maximum error observed from the calibration polynomials, at the limits of rectangular distribution which equals to $(\sqrt{3})^{-1}$. Repeatability uncertainty entails inherently in *P,T* the Gaussian type distribution[147].

$$u(T) = \sqrt{\frac{u_{cal.}^2(T)}{(\sqrt{3})^2} + u_{rep.}^2(T)} \tag{4.5}$$

$$u(P) = \sqrt{\frac{u_{cal.}^2(P)}{(\sqrt{3})^2} + u_{rep.}^2(P)} \quad (4.6)$$

The temperature and pressure calibration error, $u_{cal.}(T)$, $u_{cal.}(P)$, was found by performing temperature and pressure measurements of liquid bath over a range of temperatures (-20 °C to 30 °C) and pressures (10 to 100 bar). The $u_{cal.}(T)$, $u_{cal.}(P)$ are found to be 0.02 K and 0.015 bar, respectively (see 3.1.1 section).

The repeatability temperature and pressure error, $u_{rep.}(T)$, $u_{rep.}(P)$ for every hydrate equilibrium point were calculated by the least square method for VHL and VL hydrate eq. dissociation points, eq. 4.7 and 4.8.

$$u_{rep.}(T) = \sqrt{[\left(\frac{\partial T}{\partial a}\right)u(a)]^2 + [\left(\frac{\partial T}{\partial b}\right)u(b)]^2 + [\left(\frac{\partial T}{\partial a'}\right)u(a')]^2 + [\left(\frac{\partial T}{\partial b'}\right)u(b')]^2 + [\left(\frac{\partial T}{\partial c'}\right)u(c')]^2} \quad (4.7)$$

$$u_{rep.}(P) = \sqrt{[\left(\frac{\partial P}{\partial a}\right)u(a)]^2 + [\left(\frac{\partial P}{\partial b}\right)u(b)]^2 + [\left(\frac{\partial P}{\partial T}\right)u_{rep.}(T)]^2} \quad (4.8)$$

Finally, the relative temperature and pressure uncertainties $U(T)$ and $U(P)$ are calculated using dissociation conditions, T_{diss} and P_{diss}, eq. 4.9 and 4.10. A coverage factor k=2 for 95% confidence level is used assuming Gaussian distribution.

$$U(T) = 2\,u(T) \quad (4.9)$$

$$U(P) = 2\,u(P) \quad (4.10)$$

The results are presented in Tables B.1, B.2 and B.3 in Appendix B. The average standard uncertainty for temperature and pressure is $U(T)$ and U(P) is 0.028 °C and 0.025 bar respectively.

4.3 Gas mixture uncertainties

Then, gas mixture errors were estimated of gas chromatograph (calibration) and repeatability $u_{cal.}(T, P, N_2)$, $u_{cal.}(T, P, CO_2)$ and $u_{rep.}(T, P, N_2)$, $u_{rep.}(T, P, CO_2)$ were calculated for every gas mixture and gas respectively. The calibration error is given by

the ratio of std. deviation of gas concentration for *i* number of measurements divided by the average value of gas concentration for *i* number of measurements. The combined uncertainty for CO_2 and N_2 was calculated by eq. 4.11 and 4.12.

$$U(y_{CO_2}) = 2\sqrt{\frac{u_{cal.}(y_{CO_2})^2}{(\sqrt{3})^2} + \frac{u_{rep.}(y_{CO_2})^2}{(\sqrt{i})^2}} \quad (4.11)$$

$$U(y_{N_2}) = 2\sqrt{\frac{u_{cal.}(y_{N_2})^2}{(\sqrt{3})^2} + \frac{u_{rep.}(y_{N_2})^2}{(\sqrt{i})^2}} \quad (4.12)$$

where *i*: number of gas volume measurements

The $u_{rep.}(T,P)$ represents the ratio of standard deviation deviated by the root of the number for all gas measurement trials of every CO_2 or N_2 molar composition. In this case, denominator,$\sqrt{\mathrm{n}}$, is used due to the assumption of gaussian type distribution. The $u_{cal.}(T,P)$ represents the accuracy of apparatus for gas composition measurement and is shown in Table 4.1. It is also assumed maximum error observed from the calibration polynomials, at the limits of rectangular distribution which equals to $1/\sqrt{3}$.

Table 4.1 Gas mixtures composition uncertainties.

	Gas mixture composition 1 (mol%)		**Gas mixture composition 2 (mol%)**		**Gas mixture composition 3 (mol%)**		**Gas mixture composition 4 (mol%)**	
	CO_2	**N_2**	**CO_2**	**N_2**	**CO_2**	**N_2**	**CO_2**	**N_2**
composition	13.92	85.08	11.24	88.76	6.87	93.13	0.48	99.52
uncertainty ($u_{cal.}$)	1.0%	0.6%	1.0%	0.6%	1.0%	0.6%	0.5%	0.6%
CO and N_2	***U(yCO₂)***	***U(yN₂)***	***U(yCO₂)***	***U(yN₂)***	***U(yCO₂)***	***U(yN₂)***	***U(yCO₂)***	***U(yN₂)***
composition uncertainty	5.9%	1.2%	2.2%	0.7%	2.6%	0.7%	26.8%	0.7%

In the fourth gas mixture, there is high CO_2 uncertainty but the very low CO_2 concentration used contribute to minimization of the absolute uncertainty. In other words, the CO_2 concentration in the fourth gas mixture is 0.48±0.13 mol%.

4.4 Molar composition uncertainties

At first, CO_2, N_2, water and promoter molar masses inserted in equilibrium cell were estimated. The eq. 4.13 was used. The densities ρ_1 and ρ_2 of the inserted gas mixture was found by the pressure and temperature conditions in gas mixture cylinder with help of REFPROP software[148]. The cylinder volume, V_t, is 0.002 m^3 ±0.1%.

$$n_{gas} = V_t\,(\rho_1-\rho_2)\,y_{gas}\frac{1}{MW_{gas}} \tag{4.13}$$

where n_{gas}: mol of gas inserted in equilibrium cell

V_t: total cylinder volume

ρ_1, ρ_2: densities of the inserted gas mixture

y_{gas}: gas molar composition

MW_{gas}: molecular weight of gas

The gas densities ρ_1 and ρ_2 of the inserted gas mixture was found by the pressure and temperature conditions in gas mixture cylinder with help of REFPROP software[148] after each loading. The uncertainty of n_{gas}, $u(n_{gas})$, was estimated by eq. 4.14, 4.15 and 4.16.

$$u(n_{gas}) = \sqrt{\left[\left(\frac{\partial n}{\partial Vt}\right)_{\rho_1,\rho_2} u(V_t)\right]^2 + \left[\left(\frac{\partial n}{\partial \rho 1}\right)_{V_t,\rho_2} u(\rho_1)\right]^2 + \left[\left(\frac{\partial n}{\partial \rho_2}\right)_{V_t,\rho_1} u(\rho_2)\right]^2} \tag{4.14}$$

$$u(\rho_1) = \sqrt{\left[\left(\frac{\partial \rho_1}{\partial T}\right)_{V_t,P} u(T)\right]^2 + \left[\left(\frac{\partial \rho_1}{\partial P}\right)_{V_t,T} u(P)\right]^2} \tag{4.15}$$

$$u(\rho_2) = \sqrt{\left[\left(\frac{\partial \rho_2}{\partial T}\right)_{V_t,P} u(T)\right]^2 + \left[\left(\frac{\partial \rho_2}{\partial P}\right)_{V_t,T} u(P)\right]^2} \tag{4.16}$$

The $\frac{\partial \rho_{1,2}}{\partial T}$ and $\frac{\partial \rho_{1,2}}{\partial P}$ of the 1 and 2 states were estimated numerically. For estimating the gas densities ρ_1 and ρ_2, small changes of T, P (0.01 K and 0.01 MPa respectively) allowed the estimation of gas densities using REFPROP software[148].

Finally, the standard uncertainty $U(n_{gas})$ is estimated by eq. 4.17. The water and promoter inserted quantities were estimated by the known solution volume and promoter

composition. The numerical results are shown in Table B.4 in Appendix B. The average $U(n_{gas})$ is 2.14%.

$$U(n_{gas}) = 2\,\frac{u(n_{gas})}{\sqrt{3}\cdot n_{gas}} \tag{4.17}$$

Other uncertainties are connected to solution and gas mixture preparation. Promoter and water weight are estimated subjectively according to experimental conditions e.g. syringe size and solute weight. The maximum water uncertainties are ±2.0 ml, for TBAF and CP ±0.1 ml respectively and the TBAB weight accuracy is ±0.01 g.

4.5 Consistency analysis of hydrate equilibrium data

For data treatment, Clausius–Clapeyron method is applied, eq. 4.18. Clausius-Clapeyron equation estimates the vapor pressures of liquids or solids. It is used to determine hydrate dissociation pressure as a function of heat of dissociation.

$$\frac{dln(P)}{d(\frac{1}{T})} = \frac{-\Delta H_{dis}}{Z\cdot R} \tag{4.18}$$

where ΔH_{dis} (*kJ/mol*) is the apparent dissociation enthalpy of the hydrate phase, Z is the compressibility factor and R is the gas constant. Lee-Kesler-Plöcker (LKP) Equation of State (EoS)[149] is applied for estimation of Z as a function of T and P using binary interaction parameter κ_{ij}=1.11. It is assumed very low solubility of the gas in the liquid and, thus, no changes in the gas composition.

In this study, the interest lies on the fact that for small changes of dissociation temperature, the Clausius–Clapeyron equation should predict identical (or similar) ΔH_{dis} values. The $\Delta H_{diss.}$ as a function of dissociation temperature shows the goodness of fit (which is shown by the Coefficient of determination (R^2)). Coefficient of determination (R^2) is used to show how well fit the ΔH values (*kJ/mol*) on the straight line of $\Delta H(T)$. Table 4.2 presents the data treatment for TBAF results of this work and from literature. The results of this work are very good (R^2>0.90) except for the systems of 1.38 mol% of TBAB+CP mixture. Most systems from literature are very good.

Table 4.3 presents the data treatment for CP results of this work and from literature. The results of Jianwei *et al.*[140] and Zhang and Lee[133] are not as accurate as the rest. The results from systems of CO_2+TBAB+H_2O and N_2+TBAB+H_2O from literature are presented in Table 4.4.

Table 4.2 Coefficient of determination of $\Delta H_{diss.}$ (*kJ/mol*) in terms of temperature for TBAB and TBAB+CP systems of this work including TBAB literature.

Promoter concentration (mol%)	CO_2 in CO_2+N_2 gas mixture concentration (mol%)	Coefficient of determination (R^2)	Literature
	TBAB+CP		
0.29	6.87	1.000	this work
0.62	6.87	0.999	this work
1.38	6.87	0.822	this work
	TBAB		
0.29	13.92	0.988	this work
0.62	6.87	0.979	this work
0.62	13.92	0.997	this work
1.38	6.87	0.990	this work
0.00	20.0	0.993	Olsen *et al.*[136]
0.29	20.0	0.952	Meysel *et al.*[139]
0.62	20.0	0.996	Meysel *et al.*[139]
1.38	20.0	0.993	Meysel *et al.*[139]
0.29	15.9	0.961	Lu *et al.*[84]
1.00	15.9	0.994	Lu *et al.*[84]
2.90	15.9	0.996	Lu *et al.*[84]
3.70	15.9	0.998	Lu *et al.*[84]
3.50	15.9	1.000	Lu *et al.*[84]
0.29	15.0	0.997	Sfaxi *et al.*[132]
0.55	15.0	0.996	Sfaxi *et al.*[132]
0.55	30.0	0.996	Sfaxi *et al.*[132]
0.29	15.1	0.608	Mohammadi et al.[137]
0.98	15.1	0.707	Mohammadi et al.[137]
2.34	15.1	0.812	Mohammadi et al.[137]
0.29	39.9	0.899	Mohammadi et al.[137]
0.98	39.9	0.972	Mohammadi et al.[137]
2.34	39.9	0.981	Mohammadi et al.[137]

The results for CO_2+TBAB+H_2O systems are very good. Almost all N_2+TBAB+H_2O systems are suspicious (R^2<0.90).

Table 4.3 Coefficient of determination of $\Delta H_{diss.}$ in terms of temperature for systems with CP hydrates.

CP concentration (mol%)	CO_2 in CO_2+N_2 gas mixture concentration (mol%)	Coefficient of determination (R^2)	Literature
6.03	6.87	0.983	this work
22.15	6.87	0.977	this work
16.16	100	0.980	Mohammadi and Richon[72]
17.39	100	0.886	Zhang and Lee[133]
16.16	0.0	0.962	Mohammadi and Richon[73]
20.42	0.0	0.975	Tohidi *et al.*[142]
5.56	0.0	0.703	Jianwei *et al.*[140]

Table 4.4 Coefficient of determination of $\Delta H_{diss.}$ in terms of temperature for CO_2+TBAB+H_2O and N_2+TBAB+H_2O systems.

TBAB concentration (mol%)	CO_2 in CO_2+N_2 gas mixture concentration (mol%)	Coefficient of determination (R^2)	Literature
0.34	100	0.911	Mohammadi *et al.*[50]
0.69	100	0.943	Mohammadi *et al.*[50]
1.29	100	0.941	Mohammadi *et al.*[50]
2.13	100	0.992	Mohammadi *et al.*[50]
6.89	100	0.929	Mohammadi *et al.*[50]
0.29	100	0.917	Ye and Zhang[131]
0.62	100	0.880	Ye and Zhang[131]
1.29	100	0.882	Ye and Zhang[131]
6.39	100	0.929	Ye and Zhang[131]
0.29	0.0	0.759	Mohammadi *et al.*[50]
0.62	0.0	0.558	Mohammadi *et al.*[50]
1.83	0.0	0.809	Mohammadi *et al.*[50]
5.29	0.0	0.662	Mohammadi *et al.*[50]
0.29	0.0	0.624	Lee *et al.*[90]
1.38	0.0	0.773	Lee *et al.*[90]
3.59	0.0	0.725	Lee *et al.*[90]
7.73	0.0	0.893	Lee *et al.*[90]

Finally, the results of this work, from systems of CO_2+TBAF+H_2O and N_2+TBAF+H_2O from literature are presented in Table 4.5. The results of this work are very good (R^2 > 0.90) except for the system of 0.76 mol% of TBAF+CP mixture. The system of 0.29 mol%

in pure CO_2 gas of Li *et al.*[104] and 1.2 mol% in pure CO_2 gas, 0.36 mol% in pure N_2 gas of Mohammadi *et al.*[12] as well as the systems of Lee *at al.*[90] are problematic (R^2 < 0.90). The remaining systems from the literature seem to be very good.

Table 4.5 Coefficient of determination (R^2) of $\Delta H_{diss.}$ *(kJ/mol)* in terms of temperature including TBAF literature.

Promoter concentration (mol%)	CO_2 global concentration of feed in CO_2+N_2 gas mixture (mol%)	Coefficient of determination (R^2)	Literature
	TBAF+CP		
0.36	0.05	0.995	this work
0.76	0.05	0.864	this work
	TBAF		
0.23	0.05	0.997	this work
0.36	0.05	0.991	this work
0.76	0.05	0.993	this work
0.29	100	0.285	Li *et al.*[104]
0.62	100	0.984	Li *et al.*[104]
0.14	100	0.986	Mohammadi *et al.*[12]
0.36	100	0.935	Mohammadi *et al.*[12]
1.20	100	0.734	Mohammadi *et al.*[12]
0.80	100	0.985	Lee *at al.*[113]
3.00	100	0.938	Lee *at al.*[113]
3.30	100	0.958	Lee *at al.*[113]
5.30	100	0.926	Lee *at al.*[113]
0.36	30.0	0.997	Sfaxi *et al.*[132]
0.68	30.0	0.988	Sfaxi *et al.*[132]
0.00	0.0	0.928	Van Cleeff and Diepen[144]
0.36	0.0	0.841	Mohammadi *et al.*[12]
1.20	0.0	0.922	Mohammadi *et al.*[12]
0.76	0.0	0.504	Lee *et al.*[90]
1.69	0.0	0.627	Lee *et al.*[90]
3.43	0.0	0.812	Lee *et al.*[90]
5.33	0.0	0.588	Lee *et al.*[90]

4.6 Conclusions

In this chapter experimental uncertainties and consistency analysis are presented. The temperature and pressure calibration error of transducers $u_{cal.}(T)$ and $u_{cal.}(P)$ are found to be 0.02 K and 0.015 bar, respectively. The average standard uncertainty for temperature and pressure equilibrium points $U(T)$ and U(P) is 0.028 °C and 0.025 bar respectively. In addition, the standard uncertainties of gas in the four different gas mixtures are low in

absolute values. Moreover, the average standard uncertainty of gas molar composition in equilibrium cell $U(n_{gas})$ is 2.14%. Finally, the consistency analysis of every system of this work is shown in Table 4.6. The results are very satisfactory in almost all cases. Some deviations exist for mixtures of promoters but this can be attributed to the high non-ideality of their solutions. The non-ideality of promoter mixtures´ is due to binary gas mixture used and due to ternary aqueous solution.

Table 4.6 Coefficient of determination (R^2) of $\Delta H_{diss.}$ *(kJ/mol)* in terms of temperature for systems of this work.

Promoter concentration (mol%)	CO_2 in CO_2+N_2 gas mixture concentration (mol%)	Coefficient of determination (R^2)
	TBAB	
0.29	13.92	0.988
0.62	6.87	0.979
0.62	13.92	0.997
1.38	6.87	0.990
	TBAB+CP	
0.29	6.87	1.000
0.62	6.87	0.999
1.38	6.87	0.822
	CP	
6.03	6.87	0.983
22.15	6.87	0.977
	TBAF	
0.23	0.05	0.997
0.36	0.05	0.991
0.76	0.05	0.993
	TBAF+CP	
0.36	0.05	0.995
0.76	0.05	0.864

5

Thermodynamic modeling

Καθ' ὅτι ἀν κοινωνήσωμεν ἀληθεύομεν, ὅτι ἀν ἰδιάσωμεν ψευδόμεθα.

Ἡράκλειτος ὁ Ἐφέσιος (544 – 484 π.Χ.)[g]

[g] *Those things we can commune with each other are real, those that we keep in privacy are fake.*

Heraclitus of Ephesus (544 – 484 BC)

5.1 Introduction

In this chapter modeling of CO_2+cycloalkanes (cyclopentane up to cycloctane) using van der Waals-Platteeuw (Vdw-P) hydrate model coupled with CPA EoS are discussed. The CP results of chapter 3 were modeled. This model was previously[20-22] used successfully for fluid phase - hydrate modeling. The model also predicts the hydrate structure (s(I) or s(II)). It is known that cyclopentane and cyclohexane forms s(II) structure[24] which this model predicts. For the rest cycloalkanes examined –e.g. cycloheptane, cyclooctane, methyl-cyclopentane and methyl-cyclohexane– s(H) structure is formed when these chemicals are present. Nonetheless the results are not affected by the misconception of predicting wrong hydrate structure.

5.1.1 Summary of modeling results in literature

The modeling approaches in hydrate phase equilibria modeling can be divided in three groups. The first group includes models which apply Clapeyron eq., Vdw-P model and an EoS for the fluid phases[112,150-157]. The second group contains gas-gravity chart and correlations and in the third group, statistical and neural network approaches are used[150]. A promising hydrate model is developed in ENSTA ParisTech in France. Paricaud[112] used SAFT-VRE model for vapor phases and electrolyte solutions together with Vdw-P model for the hydrate phase. This approach is applied satisfactorily to systems like CO_2+TBAB/TBAC/TBAF/TBPB+H_2O[155], H_2+TBAC+H_2O[156] and CO_2+H_2+TBAB/TBAF/TBPB/$TBNO_3$+H_2O[157].

Moreover, a research group from MINES ParisTech in France has contributed abundantly in hydrate modeling. They have used the vdW–P theory for the hydrate phase and various EoS for the fluid phases like Valderrama–Patel–Teja (VPT)[158], Peng-Robinson[159,160], non random two liquid (NRTL) activity model[151,159], Soave–Redlich–Kwong (SRK)[160], Universal Quasichemical Functional Group Activity Coefficients (UNIFAC)[160] and CPA[161] EoS. Finally, a research group from KAIST in Korea published articles 15 years ago based on SRK[162-165] and UNIFAC[165]. The rest articles in literature are using various EoS. In Table C.1 in Appendix C, literature review on hydrate modeling at the most recent

publications is presented. In Table C.2, average deviations for pressure/temperature are presented for systems from literature.

5.1.2 Paricaud's model

The work of Paricaud[112] aims at proposing a thermodynamic approach to model the SLE involving salt hydrates and gas semiclathrate hydrates. Square-well version of the SAFT-VRE (statistical associating fluid theory with variable range for electrolytes) equation of state is used. The SAFT-VRE is employed satisfactory to compute the properties of electrolyte solutions such as vapor pressures, relative apparent enthalpies, mean activity coefficients and osmotic coefficients. The advantage of electrolyte equations of state in comparison to electrolyte excess Gibbs energy models is the possibility to determine the properties of the liquid and vapor phases at high pressures with the same mathematical expression. Consequently, electrolyte equations of state require usually fewer adjustable parameters.

The SLE equilibrium conditions in electrolyte systems that involve ice and salt hydrates is combined for salt hydrates with the van de Waals-Platteeuw model[19,23] for gas hydrates. Calculations are presented for HI+H_2O, LiBr+H_2O, and TBAB+H_2O binary systems[112]. In next publications the systems of CO_2+TBAB/TBAC/TBAF/TBPB+H_2O[155], H_2+TBAC+H_2O[156] and CO_2+H_2+TBAB/TBAF/TBPB/$TBNO_3$+H_2O[157] are modelled.

The results has shown excellent description of the SLE coexistence curves which can be obtained over a wide composition range by regressing two parameters T_0 and Δh_0 on the *T-x* diagram and dissociation enthalpy data. Moreover, a very good description of the liquid-vapor-semiclathrate hydrate three-phase lines of the TBAB+CO_2+H_2O system is obtained. At high TBAB weight fractions, Paricaud's model predicts a change of hydrate structure from type A to type B as pressure is increased. In addition, for initial TBAB concentrations above the stoichiometric composition, it is predicted that an increase of the initial TBAB weight fraction leads to a destabilization of the semiclathrate hydrate phase, while the opposite behavior is observed at low initial TBAB concentrations[112].

5.2 The van der Waals-Platteeuw Hydrate Model

In this work, an approach which derives from fundamental theory of thermodynamics is applied. J. H. van der Waals and J. C. Platteeuw proposed in 1958 a hydrate model[23]. This model describes only the solid hydrate phase and is typically combined with an equation of state and an activity coefficient model for the description of co-existing fluid phases. The solid phase is treated as a solid solution of hydrate formers in a crystalline host lattice.

The basic assumption in the Van der Waals-Platteeuw model concerns the chemical potential of water which at equilibrium must be equal in all phases, eq. (5.1).

$$\mu_w^{\mathrm{Hydrate}} = \mu_w^{\mathrm{Liquid}} = \mu_w^{\mathrm{Vapor}} \tag{5.1}$$

In van der Waals and Platteeuw model a meta-stable crystalline water phase is defined which preserves the same structure of water as in the actual hydrate phase, instead of evaluating absolute chemical potentials of water in the hydrate phase. This phase is called meta-stable β-phase (empty hydrate lattice).
This meta-stable phase cannot exist without the presence of guest molecules. The stabilization of the actual hydrate structure occurs due to the interaction between the guest molecule and its surrounding water molecules by van der Waals forces.
The difference in chemical potential between the actual hydrate phase and the meta-stable β-phase may be described by eq. (5.2).

$$\mu_w^{\beta} - \mu_w^{\mathrm{Hydrate}} = \Delta\mu_w^{\mathrm{H}} \tag{5.2}$$

The assumptions of the guest molecule in the water cavity for the guest-host interactions were described by an approach similar to the Langmuir adsorption theory[166]. The difference in chemical potential of water between a theoretical empty hydrate water lattice (empty cavities) and the actual hydrate may be described by the presence of guest molecules in the water cavities, according to monolayer Langmuir adsorption theory, eq. (5.3).

$$\Delta\mu(T,P,\theta)_w^{\mathrm{H}} = -R \cdot T \cdot \sum_m \left[\nu_m \cdot \ln(1 - \sum_j \theta(T,P,\tilde{y})_{m,j}\right] \quad (5.3)$$

where ν_m is the number of cavities of type m per water molecule in the hydrate structure, $\theta_{m,j}$ is the fractional occupancy of gas component j in cavity type m. This occupancy is described by eq. (5.4):

$$\theta(T,P,\tilde{y})_{m,j} = \frac{C(T)_{m,j} \cdot f(T,P,\tilde{y})_j}{1+\sum_j \left[C(T)_{m,j} \cdot f(T,P,\tilde{y})_j\right]} \quad (5.4)$$

The fugacity f of the hydrate former is given by eq. (5.5):

$$f(T,P,\tilde{y})_j = \varphi(T,P,\tilde{y})_j \cdot y_j \cdot P \quad (5.5)$$

In eq. (5.4), $C_{m,j}$ is the Langmuir constant for gas component j in cavity type m, φ_j is the fugacity coefficient of component j in the vapor phase, y_j is the mol fraction of component j in the vapor phase. By substitution of eq. (5.4) in eq. (5.3) the following expression, eq. (5.6), for the change in chemical potential of water caused by the presence of the guest molecules is obtained.

$$\Delta\mu(T,P,\theta)_w^{\mathrm{H}} = R \cdot T \cdot \sum_m \left[\nu_m \cdot \ln(1 + \sum_j \left(C(T)_{m,j} \cdot f(T,P,\tilde{y})_j\right))\right] \quad (5.6)$$

Then, it is assumed that hydrate is formed in a co-existing liquid phase. Hence, the combination of eq. (5.1) and eq. (5.2) gives eq. (5.7):

$$\Delta\mu(T,P,\theta)_w^{\mathrm{H}} = \mu(T,P)_w^{\beta} - \mu(T,P,\tilde{x})_w^{\mathrm{liquid}} \quad (5.7)$$

At equilibrium, the chemical potential of water in the liquid phase can be described by eq. (5.8):

$$\mu(T,P,\tilde{x})_w^{\mathrm{liquid}} = \mu(T,P)_w^{*} + R \cdot T \cdot \ln\left[a(T,P,\tilde{x})_w^{\mathrm{liquid}}\right] \quad (5.8)$$

where superscript (*) stands for a pure phase, a is the activity of water in the non-ideal liquid phase including other species. The water activity may be described either in

terms of a symmetric activity coefficient, γ, by an activity coefficient model or in terms of fugacity coefficients, φ, by an equation of state, eq. (5.9).

$$a(T,P,\theta)_w^{\text{liquid}} = \tilde{x}_w^{\text{liquid}} \cdot \gamma(T,P,\tilde{x})_w^{\text{liquid}} = \tilde{x}_w^{\text{liquid}} \cdot \frac{\varphi(T,P,\tilde{x})_w^{\text{liquid}}}{\varphi(T,P)_w^*} \quad (5.9)$$

where $\tilde{x}_w^{\text{liquid}}$ denotes liquid phase composition of water.

Therefore, the difference in chemical potential of water between the meta-stable β-phase and water in the co-existing liquid phase is shown in eq. (5.10):

$$\Delta\mu(T,P)_w^{liquid} = \mu(T,P)_w^{\beta} - \mu(T,P)_w^{liquid} = \Delta\mu(T,P)_w^{hydrate} \quad (5.10)$$

By combining the eqs. (5.6), (5.7), (5.8), (5.9) and (5.10), an explicit expression for the difference of chemical potential between the empty hydrate and the pure liquid phase at specified temperature, *T*, and pressure, *P*, is attained, eq. (5.11):

$$\Delta\mu(T,P)_w^{liquid} = R \cdot T \cdot \left\{ \sum_m \left[\nu_m \cdot \ln\left(1 + \sum_j \left(C(T)_{m,j} \cdot f(T,P,\tilde{y})_j \right)\right)\right] + \ln\left[\tilde{x}_w^{\text{liquid}} \cdot \frac{\varphi(T,P,\tilde{x})_w^{\text{liquid}}}{\varphi(T,P)_w^*} \right] \right\} \quad (5.11)$$

Eq. (5.11) calculates the theoretical chemical potential difference.

In this work, the fugacity and the water activity values were calculated by CPA EoS[167-169]. The last parameter to be specified is the Langmuir adsorption coefficient, *C(T)*. Van der Waals and Platteeuw[23] suggested that the Langmuir adsorption coefficients may be estimated using Lennard-Jones-Devonshire cell theory with a Lennard-Jones 12-6 cell potential. They proposed the following expression, eq. (5.12), for the Langmuir adsorption coefficient:

$$C(T)_{m,j} = \frac{4 \cdot \pi}{k_B \cdot T} \cdot \int_0^{\infty} \exp\left(-\frac{w(r)_{m,j}}{k_B \cdot T}\right) \cdot r^2 \cdot dr \quad (5.12)$$

where k_B is the Boltzmann constant and $w(r)_{m,j}$ is the spherical core cell potential of component *j* in cavity type *m*. *r* is the linear distance from the centre of the cell. McKoy and Sinanoglu[170] evaluated the interactions between the guest molecule and all its

surrounding first layer of water molecules and summed up the contributions in one expression for the spherical core cell potential, eq. (5.13). In 1972, Parrish and Prausnitz[166], presented the final expression for the cell potential of gas constituent *j* in cavity type *m*, in a slightly modified form. In this work, the expression of Parrish and Prausnitz approach is utilized (eq. (5.16)).

$$w(r)_{m,j} = 2 \cdot z_m \cdot \varepsilon_j \cdot \begin{bmatrix} \frac{\sigma_j^{12}}{R_m^{11} \cdot r} \cdot \left(\delta_{m,j}^{10} + \frac{a_j}{R_m} \cdot \delta_{m,j}^{11}\right) \\ -\frac{\sigma_j^{6}}{R_m^{5} \cdot r} \cdot \left(\delta_{m,j}^{4} + \frac{a_j}{R_m} \cdot \delta_{m,j}^{5}\right) \end{bmatrix} \tag{5.13}$$

Where z_m is the coordination number for the guest in cavity type *m*, ε_j is the characteristic energy of guest molecule *j*, a_j is the core radius of molecule *j*, $\sigma_j + 2 \cdot a_j$ is the collision diameter of molecule *j*, R_m is the radius of cavity type *m*. ε_j/k_B, a_j and σ_j are called Kihara parameters. ${\delta^N}_{m,j}$ is defined as shown in eq. (5.14):

$${\delta^N}_{m,j} = \frac{1}{N} \cdot \left[\left(1 - \frac{r}{R_m} - \frac{a_j}{R_m}\right)^{-N} - \left(1 + \frac{r}{R_m} - \frac{a_j}{R_m}\right)^{-N}\right] \tag{5.14}$$

where N is an integer equal to either 4, 5, 10 or 11. Kihara potential is evaluated from the cavity centre to the singularity point at $r = R_m - a_j$, Herslund[20]. Thus eq. (5.12) can be rewritten as shown in eq. (5.15):

$$C(T)_{m,j} = \frac{4 \cdot \pi}{k_B \cdot T} \cdot \int_0^{R_m - a_j} \exp\left[-\frac{w(r)_{m,j}}{k_B \cdot T}\right] \cdot r^2 \cdot dr \tag{5.15}$$

Numerical approximation of the integral in eq. (5.15) was applied by using 20 evaluation points in the Gauss-Legendre method and 200 internal sections in the Composite Simpson 3/8 rule (each with four evaluation points). The two methods produce similar results for $C(T)_{m,j}$. Due to the lower number of evaluation points, Gauss-Legendre method was applied[20]. Parrish and Prausnitz[166] proposed a simpler way of calculating the Langmuir adsorption coefficients[171], which is not used in this work, based on *A(T)*, *B(T)* parameters.

In addition to the theoretical chemical potential difference, an experimental reference hydrate potential was introduced by Parrish and Prausnitz[166]. The difference in chemical potential between meta-stable β-phase and pure water at specified temperature and pressure may be derived thermodynamically in terms of measurable quantities. These quantities could be determined indirectly from existing hydrate equilibrium data.

A calculation of the experimental chemical potential difference determined from a reference hydrate at reference temperature, T_0, and reference pressure, P_0, to the actual hydrate at temperature, T, and pressure, P, was done in two steps, when liquid water coexists with hydrate, according to eq. (5.17):

$$\frac{\Delta\mu(T,P_R)_w^{liq.Water}}{R\cdot T} = \frac{\Delta\mu(T_0,P_0)_w^{liq.Water}}{R\cdot T_0} - \int_{T_0}^{T}\frac{\Delta H(T,P_0)^{Ice} + \Delta H(T)^{liq.Water}}{R\cdot T^2}dT + \int_{T_0}^{T}\frac{\Delta V_w^{Ice} + \Delta V_w^{liq.Water}}{R\cdot T}\cdot\frac{dP_R}{dT}d \qquad (5.17)$$

and eq. (5.18):

$$\Delta\mu(T,P)_w^{liq.Water} = \Delta\mu(T,P_R)_w^{liq.Water} + (\Delta V_w^{Ice} + \Delta V_w^{liq.Water})\cdot(P - P_R) \qquad (5.18)$$

where $\Delta\mu(T,P_R)_w^{liq.Water}$ is the chemical potential difference for water at temperature, T and at the dissociation pressure of the reference hydrate phase, $P_R(T)$. $\Delta\mu(T_0,P_0)_w^{liq.Water}$ is the chemical potential difference measured for the reference hydrate at reference temperature T_0 and reference pressure P_0. $\Delta H(T,P_0)^{Ice}$ and $\Delta H(T)^{liq.Water}$ are the differences in molar enthalpy between ice or liquid water and empty hydrate phase respectively. ΔV_w^{Ice} and $\Delta V_w^{liq.Water}$ are the differences in molar volume of between ice or liquid water and empty hydrate phase respectively. The values of reference state are determined at temperature T_0 and pressure, P_0. P_0 is the vapor pressure of ice at temperature, T_0. Since this pressure is small compared to the hydrate dissociation pressure, it is assumed zero. T_0 is equal to 273.15 K. $\frac{dP_R}{dT}$ is the gradient of the experimentally determined pressure-temperature curve of dissociation for the reference

hydrate phase. A three- parameter expression for the temperature dependence of the reference hydrate dissociation pressure is also presented[166].

According to assumption that the water lattice properties are independent of the guest molecule (for a given hydrate structure), the theoretical chemical potential difference provided in eq. (5.11) must be equal to the reference potential difference given by eq. (5.18) at identical temperature and pressure conditions. Hence, by equating these two expressions, and specifying either temperature or pressure, it is possible to calculate the corresponding equilibrium condition (pressure or temperature respectively).

Holder *et al.*[172] suggested a combined and simplified form of eqs. (5.17) and (5.18). In their expression, the use of a reference pressure, P_R, was removed providing a simpler expression that could be easier evaluated analytically, eq. (5.19):

$$\frac{\Delta\mu(T,P_R)_w^{liq.Water}}{R\cdot T} = \frac{\Delta\mu(T_0,P_0)_w^{liq.Water}}{R\cdot T_0} - \int_{T_0}^{T}\frac{\Delta H(T,P_0)^{liq.Water}}{R\cdot T^2}\cdot dT + \int_0^P \frac{\Delta V_w^{Ice} + \Delta V_w^{liq.Water}}{R\cdot T}\cdot \mathrm{dP} \quad (5.19)$$

Holder *et al.*[172] argued that eq. (5.19) provides similar results compared to the before mentioned expression used by Parrish and Prausnitz[158]. The version of Holder *et al.*[172] has also been applied successfully to more recent uses of the van der Waals-Platteeuw gas clathrate hydrate theory[173,174].

Once equilibrium conditions have been established in the model, the hydrate composition may be calculated from the fractional occupancies of the individual guests in each hydrate cavity. A water-free hydrate composition is defined according to eq. (5.20):

$$Y_j = \sum_m \nu_m \cdot \frac{\theta(T,P,\tilde{y})_{m,j}}{\sum_m \nu_m \sum_l \theta(T,P,\tilde{y})_{m,l}} \quad (5.20)$$

The water-free composition accounts only for the guests present in the hydrate cavities. The water lattice is ignored in the composition calculation.

5.3 Cubic-Plus-Association (CPA)

The *Cubic-Plus-Association*[h] *(CPA) Equation of state (EoS)* is used to estimate the fugacities of all fluid phases. It was shown previously[20-22] that CPA predicts well VLE data of CO_2+CP+H_2O hydrate system. Therefore, CPA was used in this study for higher carbon number cyclo-alkanes. CPA comprises of two contributions: a physical and association term, eq. (5.21).

$$Z = Z^{phys} + Z^{assoc} \tag{5.21}$$

The physical term measures the deviation from ideality due to physical forces[172]. The association term consists of three groups of theories. Firstly, chemical theories are based on formation of new species and the extent of association is determined by the number of oligomers formed, as a function of density, temperature and composition[172]. Secondly, lattice theories account for the number of bonds formed between segments of different molecules that occupy adjacent sites in the lattice. The number of bonds determines the extent of association. Thirdly, in perturbation theories, the total energy of hydrogen bonding is calculated from statistical mechanics and the important parameter for hydrogen bonding is in this case the number of bonding sites per molecule[172].
For mixtures, CPA is derived from the summation of Soave-Redlich-Kwong (SRK) EoS (phys. term) and Statistical Associating Fluid Theory (SAFT) (assoc. term)[167,168], eq. (5.22).

$$P = \frac{R \cdot T}{V_m - b} - \frac{a(T)}{V_m \cdot (V_m + b)} - \frac{1}{2}\frac{R \cdot T}{V_m}\left(1 + \rho \frac{\partial \ln g}{\partial \rho}\right) \sum_i x_i \cdot \sum_{A_i} \cdot \left(1 - X_{A_i}\right) \tag{5.22}$$

The energy parameter $a_i(T)$ of the EoS is given by a Soave – type temperature dependency, while *b* is temperature independent[169], eq. (5.23):

$$a_i(T) = a_{0,i}\left[1 + c_{1,i} \cdot \left(1 - \sqrt{T_r}\right)\right]^2 \tag{5.23}$$

[h]Association describes the effect of hydrogen bonding upon a molecule (self–association) or upon two different molecules (cross–association) in a solution.

where $T_r = \frac{T}{Tc,i}$ is the reduced temperature and $c_{1,i}$ is a SRK parameter.

In the expression for the association strength Δ^{AiBj}, the parameters ε^{AiBj} and β^{AiBj} are called the association energy and the association volume, respectively. The key element of the association term is X_A, which represents the fraction of sites *A* of molecule *i* that are not bonded with other active sites, while x_i is the mole fraction of component *i*. X_{Ai} is related to the association strength between two sites belonging to two different molecules, *e.g.* site *A* on molecule *i* and site *B* on molecule *j*, is determined from Kontogeorgis *et al.*[169], eq. (5.24):

$$X_{A_i} = \frac{1}{1+\rho\cdot\sum_j x_j \sum_{B_j}(X_{B_j}\cdot\Delta^{A_iB_j})} \tag{5.24}$$

where the association strength Δ^{AiBj} in CPA is expressed in eq. (5.25) as[166]:

$$\Delta^{A_iB_j} = g(V_m)\left[exp\left(\frac{\varepsilon^{A_iB_j}}{R\cdot T}\right)-1\right] b_{ij}\cdot\beta^{A_iB_j} \tag{5.25}$$

where $b_{ij} = \frac{b_i+b_j}{2}$ and the radial distribution function, $g(V_m)$ was presented in a simplified form by Kontogeorgis *et al.*[168]. The expression for the simplified hard-sphere radial distribution function is shown in eq. (5.26).

$$g(V_m) = \left[1-\frac{1.9\cdot b}{4\cdot V_m}\right]^{-1} \tag{5.26}$$

These two parameters are only used for associating components, and together with the three additional parameters of the SRK term (a_0, b, c_1), they are the five pure compound parameters of the model[169]. They are obtained by fitting vapor pressure and liquid density data. For inert (not self-associating) components e.g. hydrocarbons, only the three parameters of the SRK term are required, which can be obtained either from vapor pressures and liquid densities or calculated in the conventional manner (critical data, acentric factor e.g. as done for gases like CO_2 and H_2S)[169].

When CPA is used for mixtures, the conventional mixing rules are employed in the physical term (SRK) for the energy and co-volume parameters. The geometric mean rule is used for the energy parameter a_{ij}. The interaction parameter k_{ij} is, in the applications for self-associating mixtures, e.g. alcohol, water, glycol or acid with n-alkanes, the only binary adjustable parameter of CPA[169], eq. (5.27):

$$a(T) = \sum_i \sum_j x_i \cdot x_j \cdot a_{ij}(T) \text{ where } a_{ij}(T) = \sqrt{a_i(T) \cdot a_j(T)} \cdot \left(1 - k_{ij}\right)$$

$$b = \sum_i x_i \cdot b_i \tag{5.27}$$

The interaction parameter k_{ij} may be temperature-dependent, eq. (5.28):

$$k_{ij} = a_{kij} + b_{kij} \cdot T^{-1} \tag{5.28}$$

For mixtures containing two associating compounds, e.g. alcohols or glycols, combining rules for the association energy (ε^{AiBj}) and the association volume (β^{AiBj}) are required. The standard Combining Rule (CR-1) and the Elliott Combining Rule (ECR) have been used more successfully in previous applications[20-22,168,169,175]. The expressions of the cross-association energy and cross – association volume parameters with CR-1 are shown in eq. (5.29)[21]:

$$\varepsilon^{A_iB_j} = \frac{\varepsilon^{A_iB_i} + \varepsilon^{A_jB_j}}{2}, \beta^{A_iB_j} = \sqrt{\beta^{A_iB_i} \cdot \beta^{A_jB_j}} \tag{5.29}$$

In CR1 the β^{AiBj} parameter in cases of cross-association involving one non-self-associating molecule (e.g. CO_2+H_2O) is calculated directly by vapor pressure and liquid density data. For systems containing three or more components CPA becomes predictive, since only binary interactions may be accounted for (directly) in the process of parameter estimation.

The methodology presented here, for handling cross-association between self-associating and non-self-association compounds corresponds to the use of the modification of the CR1 combining rule presented by Folas *et al.*[168].

In this work the notation for association schemes is [{X^+};{Y^-}], where X and Y are number of sites. Superscript (+) and (-) denotes whether the sites are accepting electron (+) or donating electron (-). Water is modeled as a self-associating compound with a total of four associating sites. Two sites are electron donating (two sets of oxygen atom lone pair electrons) and two are electron accepting (two hydrogen atoms). Hence, the association scheme for water in the above defined notation becomes [2^+;2^-], corresponding to the 4C association scheme as defined by Huang and Radosz[176].

Self-association between two water molecules is modeled by allowing electron donating sites on one molecule to interact (hydrogen bond) with electron accepting sites on another molecule of the same type. The self-association strength is defined by the pure component association parameters, ε^{AiBj} and β^{AiBj}.

5.4 Algorithm Applied to this work

The classical van der Waals-Platteeuw hydrate model, as presented in section 5.1, has been used with the use of computational tool of FORTRAN[20]. This section describes the numerical methods and solution procedures utilized in the model set-up as well as an overview of the overall model algorithm. The parameters required for the two models, van der Waals-Platteeuw and CPA, are found in sections 5.5.1 and 5.5.2 respectively.

This work utilizes an algorithm for the hydrate dissociation pressure calculation similar to what is presented by Parrish and Prausnitz[166]. Note that the algorithm and the hydrate model as presented above is valid only for describing equilibrium conditions for hydrate systems above the ice point temperature of water. In order to describe hydrate formation below the ice point temperature of water, the water activity correction term in eq. (5.11) must be omitted. Moreover, new reference parameters are needed for eq. (5.19).

Hydrate formation below the ice point temperature of water has not been considered in this work.

The applied procedure for hydrate dissociation pressure calculations is provided below.

1) Specify molar feeds of all components in the initial system.

2) Specify system temperature.
3) Evaluate Langmuir constants for all hydrate formers at the specified temperature of feed (for all cavities in the s(I) and s(II) hydrates).
4) Set an initial guess for pressure according to the reference pressure expressions provided by Parrish and Prausnitz[166].
5) Perform an isothermal-isobaric multi-phase flash calculation (Gibbs energy minimization) at the specified temperature and pressure, using the feed from 1).
6) Using the results from step 3) - 5), evaluate eq. (5.11)
7) Evaluate eq. (5.19) for the reference hydrate at the specified temperature and pressure.
8) Keeping compositions and fugacity coefficients constant solve eq. (5.11) and eq. (5.19) for pressure.
9) If the new pressure is different from the previously assumed, return to step 5) and repeat calculations until convergence of pressure.

The above calculation procedure is performed for both structure I and structure II hydrates. The program then chooses the most stable structure according to the criteria of lowest equilibrium pressure. Incipient hydrate equilibrium pressure, and phase composition of all phases for the specified feed and temperature is finally returned to the user. Figure 5.1 provides a graphical illustration of the calculation procedure.

The main program in the developed module concerns the van der Waals-Platteeuw hydrate model. The flash routine is used to obtain the inputs required for the hydrate model at the specified temperature and pressure.

The program solves eq. (5.11) and eq. (5.19) for the equilibrium pressure at a specific temperature. The integrals in eq. (5.19) are evaluated analytically (as presented in Herri *et al.* [177]), eq. (5.30):

$$\Delta\mu(T,P_R)_w^{liq.Water} = \frac{T\cdot\Delta\mu(T_0,P_0)_w^{liq.Water}}{T_0} - (\Delta CP_0^{liq.water} - b^{liq.water}\cdot T_0)\cdot T\cdot ln\frac{T}{T_0} - \frac{1}{2}\cdot b^{liq.water}\cdot T\cdot(T-T_0) + \Big[\Delta H(T_0,P_0)^{liq.water} - (\Delta CP_0^{liq.water} -$$

$$b^{liq.water} \cdot T_0) \cdot T_0 - \frac{1}{2} \cdot b^{liq.water} \cdot T_0^2\Big] \cdot (1 - \frac{T}{T_0}) + \Delta V_w \cdot (P - P_0) - R \cdot T \cdot ln\left(x_w^{liquid}\right) \quad (5.30)$$

where $b^{liq.water}$ is temperature dependent coefficient of the heat capacity and $\Delta CP_0^{liq.water}$ is molar heat capacity of reference state.

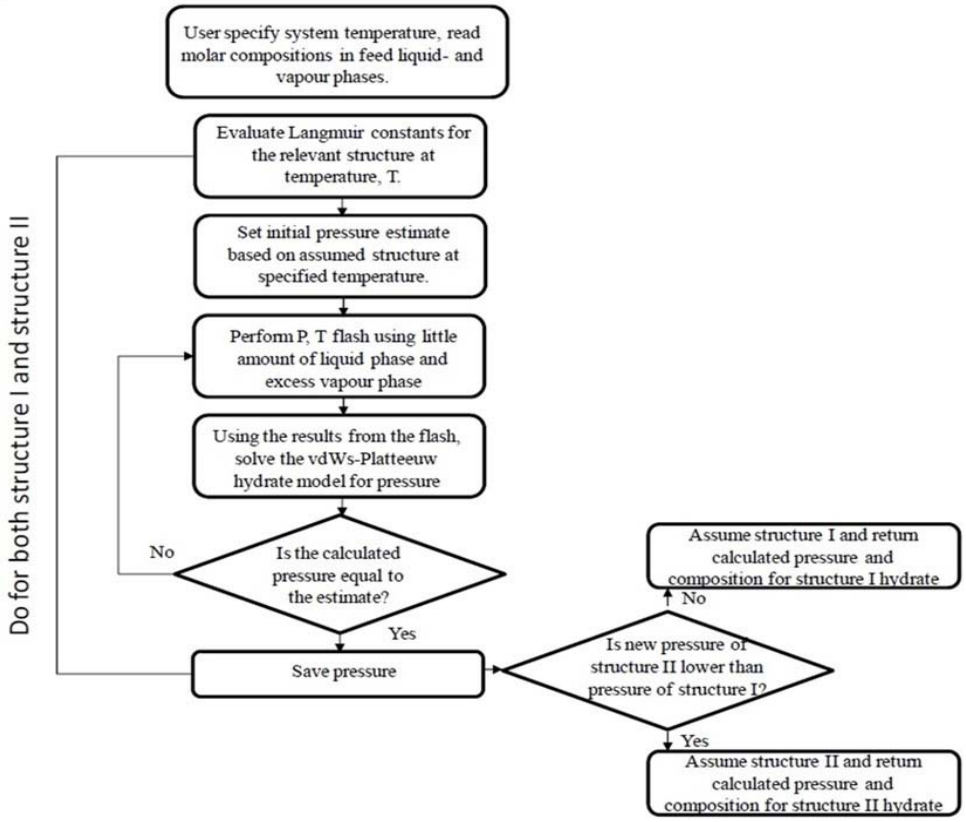

Figure 5.1 Algorithm used for incipient hydrate dissociation pressure calculations for a hydrate forming system of specified composition and temperature[20]. Only for qCPA calculations, the code was developed such that initial pressure estimation is not needed.

The integral of eq. (5.15) is evaluated numerically using a 20-point Gauss-Legendre quadrature method. By subtracting eq. (5.11) from eq. (5.19), the resulting equation may be solved for pressure using the 1st-order Newton-Raphson method. Keeping fugacity coefficients and fluid phase compositions constant (in van der Waals-Platteeuw model) while solving for pressure, the 1st order derivative of the function to be minimized may be approximated by eq. (5.31):

$$\frac{df}{dP} = \Delta V_w^{Ice} + \Delta V_w^{liq.Water} - R \cdot T \cdot \sum_j \left[\nu_m \cdot \frac{\sum_j [C(T)_{m,j} \cdot \varphi(T,\tilde{y})_j]}{1+\sum_l [C(T)_{m,l} \cdot \varphi(T,\tilde{y})_l]} \right] \quad (5.31)$$

where the fugacity coefficients and fluid phase compositions are those obtained in the most recently executed flash calculation. Overall pressure convergence is obtained by successive substitution, where the pressure is substituted back and forth between the flash and the van der Waals-Platteeuw model.

5.5 Model Parameters

5.5.1 Hydrate Model

The van der Waals-Platteeuw hydrate model parameters were found available in the literature[163]. Among these are the structural parameters for the hydrate lattice. These include the average cell radii for each cavity, coordination numbers for specific cavities, number of cavities and water molecules for each hydrate unit cell etc. Such parameters are provided in Table 5.1.

Table 5.1 Water lattice and unit cell parameters for the van der Waals-Platteeuw hydrate model[171].

Structure	**s(I)**		**s(II)**	
Cavity	**5^{12}**	**$5^{12}6^2$**	**5^{12}**	**$5^{12}6^4$**
No. cavities per unit cell	2	6	16	8
Avg. cavity radius·10^{10}/ m	3.95	4.33	3.91	4.73
Coordination number	20	24	20	28
No. water molecules per unit cell	46		136	

Other model specific parameters for the hydrate model are the thermodynamic properties of the reference hydrate. These parameters are given in Table 5.2.

Table 5.2 Thermodynamic properties for the reference hydrate in the van der Waals-Platteeuw hydrate model.

	Units	s(I)	s(II)	Reference
$\Delta\mu(T_0,P_0)_w^{liq.Water}$	J/mol	1297	937	Dharmawardhana *et al.*[178]
ΔH^{Ice}	J/mol	1389	1025	Dharmawardhana *et al.*[178]
$\Delta H(T_0,P_0)^{liq.Water}$	J/mol	-6011	-6011	Herri *et al.* [177]
$\Delta C_p(T)$	J/(mol ·K)	-38.12+0.141·(T-273.1)	-38.12+0.141·(T-273.1)	Sloan[174]
$\Delta V_w^{Ice} + \Delta V_w^{liq.Water}$	m^3/mol	$4.6\cdot10^{-6}$	$4.0\cdot10^{-6}$	Sloan[174]

The thermodynamic properties of the reference hydrates are determined indirectly from experimental investigations of gas hydrate systems. As these thermodynamic properties are not readily measured, the reported values often differ significantly from each other. The difficulty in comparing model results presented in literature by different authors is discussed and emphasised[177]. Often an insufficient amount of information is provided about the parameters used in hydrate models. Moreover, the models are often presented in different forms, making it even more difficult to compare them.

In the present work, the thermodynamic reference properties for the hydrate structures are almost identical to those used by Sloan[174], who (at that time) successfully applied a similar version of the van der Waals-Platteeuw hydrate theory. Sloan[174], however, slightly modified the $\Delta\mu(T_0,P_0)$ for the reference hydrate.

The final parameters needed in the hydrate model are the Kihara cell potential parameters[20,24,174,179,180]. Van der Waals-Platteeuw hydrate model needs *a priori* knowledge of the gas hydrate formers of interest. The Kihara parameters used in this work are presented in Table 5.3 and were obtained from literature. Kihara parameters for cycloalkanes and CO_2, N_2 from literature and the EoS used for their determination are presented in Appendix D, Table D.1.

Table 5.3 Kihara cell potential parameters used in this work.

Component	$a \cdot 10^{10}$ (m)	$\sigma \cdot 10^{10}$ (m)	ε/k_B (K)	Reference
Carbon dioxide	0.6805	2.9643	171.70	Herslund[20]
Nitrogen	0.3526	3.1723	128.07	Strobel *et al.*[181]
Cyclopentane	0.8968	3.1480	250.89	Sloan[174]
Methyl-Cyclopentane (mCP)	1.0054	4.5420	353.66	Mehta and Sloan[179]
Cyclohexane (CC6)	0.9750	4.2675	253.00	Tohidi *et al.*[180]
Methyl-Cyclohexane (mCC6)	1.0693	3.1931	407.29	Mehta and Sloan[179]
Cycloheptane (CC7)	1.0576	3.5902	250.19	Sloan and Koh[24]
Cyclooctane (CC8)	1.1048	3.6550	277.80	Sloan and Koh[24]

5.5.2 Equation of State (CPA)

The cubic-plus-association (CPA) equation of state needs three pure component parameters for non-associating compounds and five pure component parameters for self-associating compounds. Compounds that are non-self-associating, but may cross-associate with other self-associating compounds still have only three pure component parameters. In this work, carbon dioxide is treated in this way.

Pure component parameters for non-self-associating and non-cross-associating compounds are described by their critical properties in a manner identical to the Soave-Redlich-Kwong equation of state (critical temperature, critical pressure and acentric factor). The pure component parameters used in this work are provided in Table 5.4.

Water is the only component treated as self-associating in this work. Carbon dioxide can cross-associate (solvate) with water. CP, CC6, CC7, CC8, mCC6, mCCP and nitrogen are treated as non-self-associating and non-cross-associating. So, their CPA pure component parameters were calculated by their critical properties.

Table 5.4 Cubic-Plus-Association (CPA) equation of state pure component parameters and association schemes.

Compounds	Association scheme	$a_0 \cdot 10^{-5}$ Pa·m^6·mol^{-2}	$b \cdot 10^5$ m^3·mol^{-1}	$c1$	Reference
CO_2	$[0^+;1^-]$	3.5079	2.7200	0.7602	Tsivintzelis *et al.*[182]
N_2	-	1.3820	2.6737	0.5434	Herslund[20]
CP	-	1.7136	0.81727	0.7815	Herslund[20]
mCP	-	2.2158	1.0151	0.8352	This work*
CC6	-	2.2207	0.9790	0.8035	This work*
mCC6	-	2.2158	1.0151	0.8426	This work*
CC7	-	2.8067	1.1335	0.8529	This work*
CC8	-	3.4740	1.3247	0.9225	This work*
H_2O**	$[2^+;2^-]$	1.2277	1.4515	0.6736	Kontogeorgis *et al.*[183]

*calculated by critical properties using a_0 =0.427 · 8.314^2 · T_c^2/P_c, b =0.08664 · 8.314 · T_c/P_c, $c1$ =0.48508 + 1.55171 · ω - 0.15613 · ω^2 (Graboski and Daubert[184]). The critical properties are found in CERE ThermoSystem[185].

**For H_2O the cross association energy and volume used is 0.0692 and 1.6655 Pa·m^3·mol^{-1} respectively[185].

All binary parameters used are presented in Table 5.5. For CO_2–H_2O, cross association volume β_{ij} is found to be 0.1707[20].

Table 5.5 Interaction parameters (k_{ij}) for all binary pairs used in this work.

Binary Pair	k_{ij}	Reference
CO_2 – H_2O	0.4719 - 112.5 ·T^{-1}	Herslund[20]
CO_2 – N_2	-0.0856	Herslund[20]
CO_2 – CP	0.1574	Herslund[20]
CO_2 – CC6/CC7/CC8/mCP/mCC6	0.1	Arya *et al.*[186,*]
N_2 - CP	0.0	Herslund[20]
H_2O – N_2	0.99986 - 368.4·T^{-1}	Herslund[20]
H_2O – CP	0.0211	Herslund[20]

*After personal discussion with Alay Arya, k_{ij} for CO_2 – CC6/CC7/ CC8/mCP/mCC6 was assumed to be 0.1.

It was also used an extension of CPA that accounts for the quadrupole moment of CO_2 which is known as qCPA[187]. The expression for the quadrupolar term is an adaptation of

the 3rd order perturbation theory developed by Stell *et al.*[188-191]. The same base model is used like in Karakatsani *et al.*[192,193] to develop their polar equation of state.

The following Table 5.6 summarizes the parameters used in qCPA. The association scheme in CPA for water is the same used in qCPA. CP parameters were fitted to the saturated properties.

Table 5.6 Adjusted parameters for all binary pairs used in qCPA.

Compounds	$a_0 \cdot 10^{-5}$ Pa·m⁶·mol⁻²	$b \cdot 10^5$ m³·mol⁻¹	$c1$ -	Quad. moment (q) DÅ	Binary Pairs	k_{ij}	References
CO_2	2.9783	2.79	0.68	4.3	CO_2 – CP	0.058	This work
CP	1.6296	7.527	0.7262	-	CO_2 – H_2O	0.41-124 ·T^{-1}	This work
H_2O	1.2277	1.4515	0.6736	-	CP – H_2O	0.0211	Kontogeorgis *et al.*[183]; Herslund[20]

5.6 Modeling Results

The hydrate promotion modeling results for CO_2+cyclo-alkane systems are presented below. The modeling results of this work are presented in Figure 5.2. In this case, feed composition data were used as calculated in this work and presented in Appendix B. The results are satisfactory.

The modeling results for CO_2+CC6/CC7/CC8/mCP/mCC6+H_2O hydrate systems are presented in Figures 5.3, 5.4, 5.5, 5.6, 5.7 and 5.8 respectively.

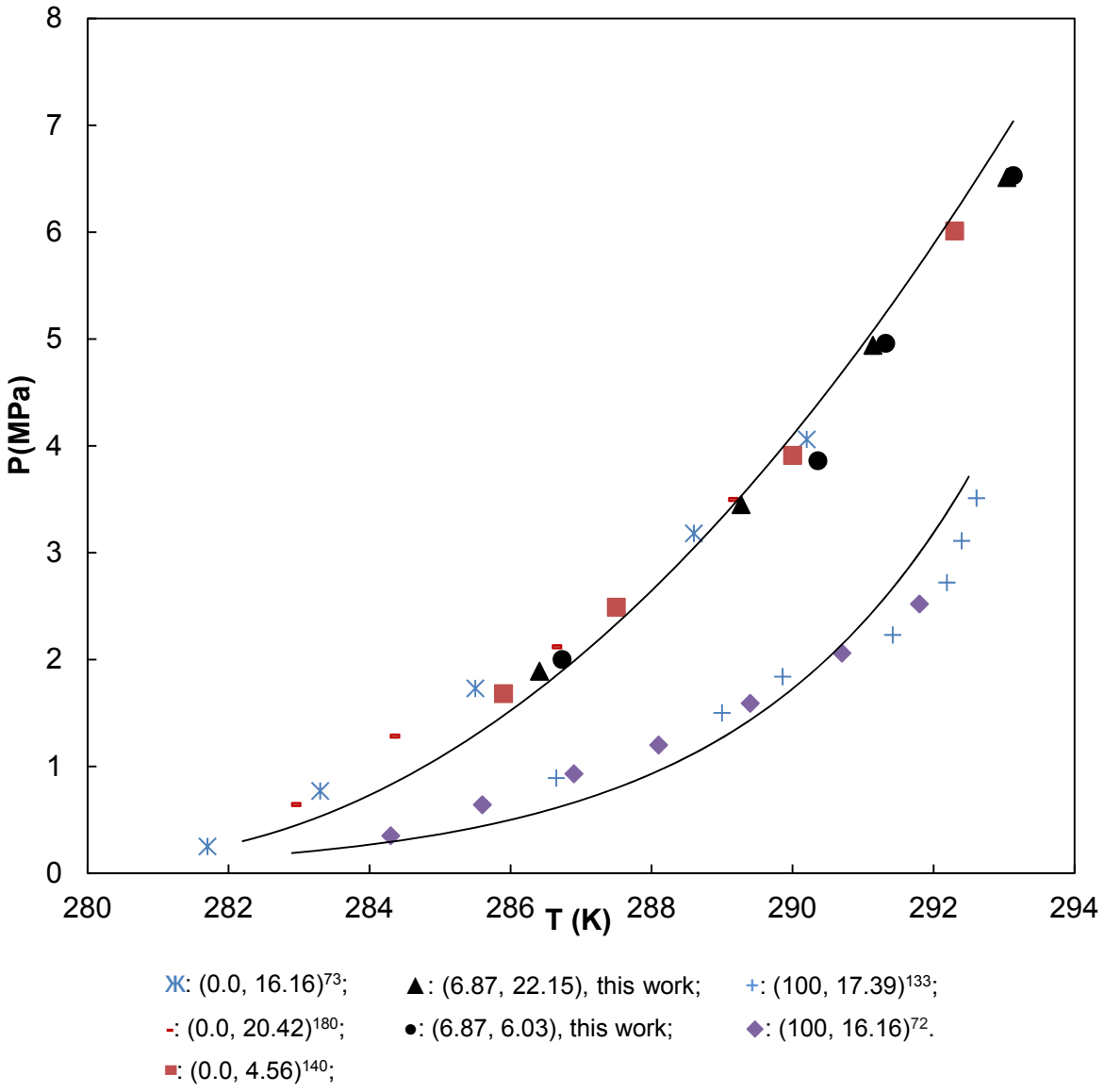

Figure 5.2 Hydrate dissociation points for different systems using CP as promoter and the predictive curves of vdw-P model coupled with CPA EoS for fluid phases. For clarity reasons, the systems are presented by two numbers in brackets. The first number denotes the mol fraction of CO_2 in N_2 gas mixture cylinder and the second one denotes the promoter concentration. Black markers connected with trendlines correspond to results of this work. References are presented according to their presence in figure from left to right. The upper line is produced based on feed composition data from this work. The bottom line is produced based on an assumed feed composition.

Satisfactory results are also obtained for CC7 and CC8 in Figures 5.3 and 5.4 respectively.

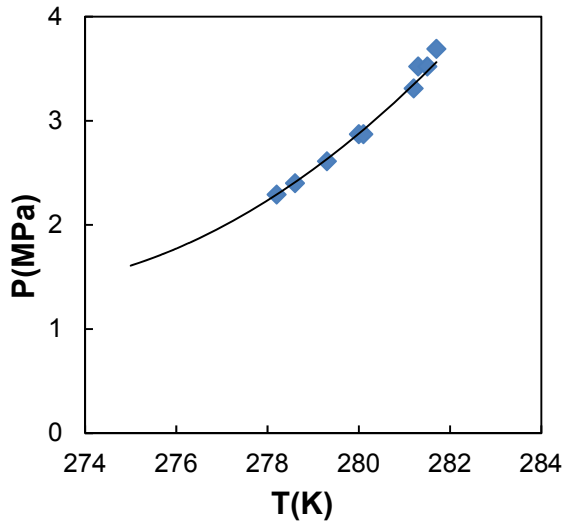

Figure 5.3 Hydrate phase equilibria points and the predictive curve of the system CO_2+CC7+H_2O[194].

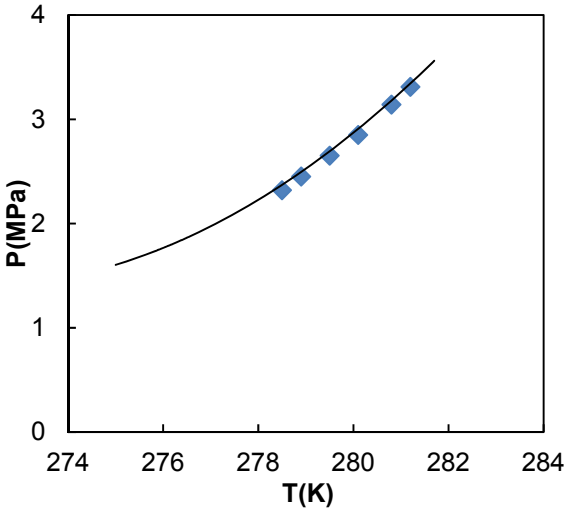

Figure 5.4 Hydrate phase equilibria points and the predictive curve of the system CO_2+CC8+H_2O[194].

For CC6 the results are not so good as presented in Figure 5.5.

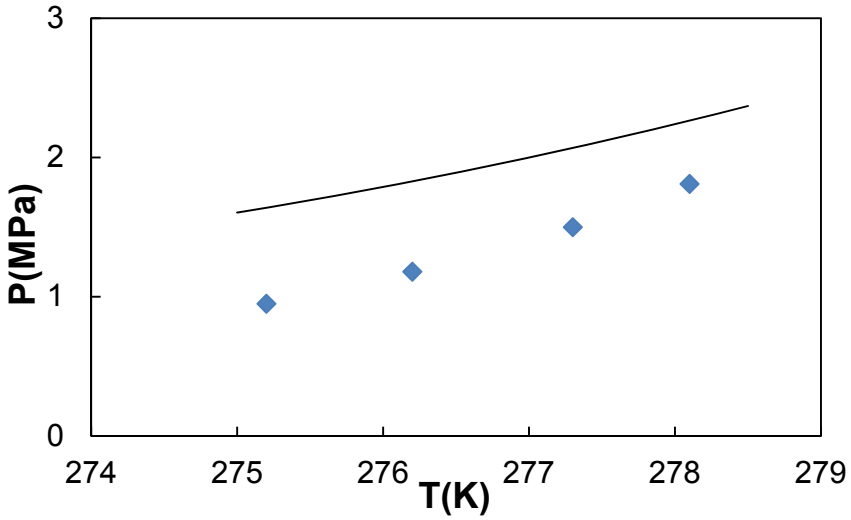

Figure 5.5 Hydrate phase equilibria points and the predictive curve of the system CO_2+CC6+H_2O[72].

In the available literature[180], there was only one set of parameters available for this compound. Every Kihara parameter set in literature for every compound produce (almost) identical results. In general, the results are very much sensitive on Kihara parameters rather than CPA parameters. For mCP and mCC6, the results are not so good as shown

in Figures 5.6 and 5.7. For mCC6, above 280 K, the hydrate formation pressure increases very steeply. Similarly as with CC6, there is difficulty in modeling precisely mCC6. To match the exp. data for higher temperatures, higher k_{ij} values are needed.

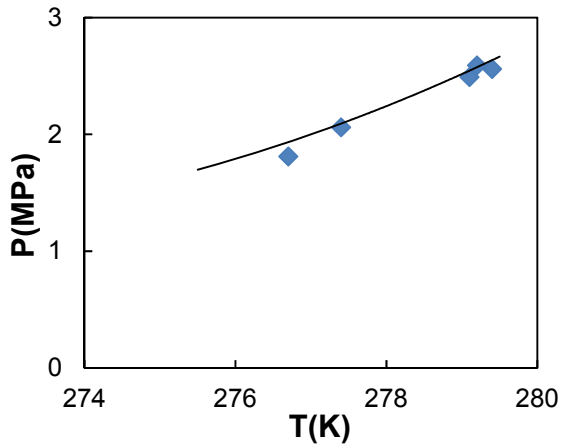

Figure 5.6 Hydrate phase equilibria points and the predictive curve of the system CO_2+mCP+H_2O[72].

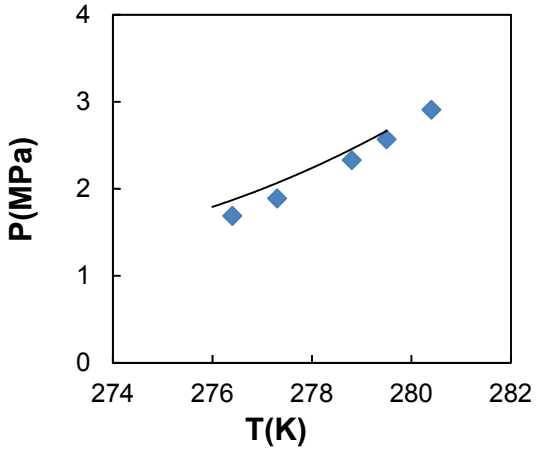

Figure 5.7 Hydrate phase equilibria points and the predictive curve of the system of CO_2+mCC6+H_2O[72].

Finally the results for qCPA compared with CPA are shown in Fig 5.8. The two different versions of CPA are not exhibiting any differences on the results.

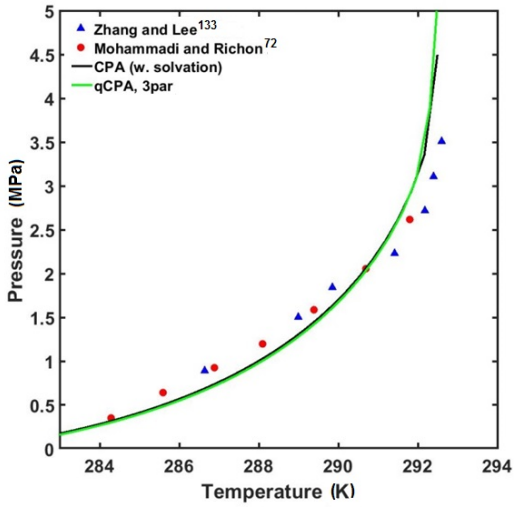

Figure 5.8 Hydrate phase equilibria points and the predictive curves for CPA and qCPA EoS of the ternary system CO_2+CP+H_2O[72,133]. Only for the qCPA case, the model is implemented in MATLAB by Martin Gamel Bjørner.

The average absolute deviation (AAD%) is AAD%= $\frac{1}{NP}\sum_{i=1}^{NP}\left|\frac{x_i^{exp}-x_i^{cal}}{x_i^{exp}}\right| \times 100$ where NP is number of data points. The average absolute error (in MPa) is the difference of predicted hydrate dissociation pressure minus the experimental pressure.

The following Table 5.7 summarises the AAD% for every hydrate system.

Table 5.7 The average absolute deviation for pressure of every system of this work.

System	AAD%	References of experimental data
CO_2+N_2+CP(6.03 mol%)+H_2O	9.1	This work
CO_2+N_2+CP(22.15 mol%)+H_2O	8.2	This work
CO_2+CP+H_2O	8.0	Mohammadi and Richon[72]
CO_2+CC6+H_2O	21.1	Mohammadi and Richon[72]
CO_2+CC7+H_2O	0.0	Mohammadi and Richon[194]
CO_2+CC8+H_2O	2.2	Mohammadi and Richon[194]
CO_2+mCP+H_2O	2.9	Mohammadi and Richon[72]
CO_2+mCC6+H_2O	9.8	Mohammadi and Richon[72]
Average	**8.9**	

5.7 Conclusions - Looking ahead on Modeling of TBA salts

This chapter presented predicitive results of CP systems of this work and for systems of CO_2+cycloalkane+H_2O hydrates. The results are satisfactory in almost all cases even though the Kihara parameters used were excerpted from literature while various EoS were used for their estimation in many of the cases. Only cyclohexane results are not perfectly matching the experimental data and this is caused by the modified VPT with non-density-dependent mixing rules EoS used for the Kihara parameters as shown in Table D.1.

The model used in this work should be extended to deal with TBA salts. This is not straightforward because TBA salts form semi-clathrate hydrates which require, apart from new CPA and Kihara parameters, new thermodynamic parameters (Tables 5.2-5.4). More specifically, there are many structural studies[13,28,112,113,115,118,145,146,152] for water lattice and unit cell parameters for semi-clathrates (as presented in Table 5.1).

Experiments should be carried out in order to find the chemical potential and enthalpies[112] of water lattice and ice for semi-clathrate structures at standard conditions (as presented in Table 5.2). Then, new Kihara parameters (as presented in Table 5.3) could be calculated with this model. CPA could then calculate CO_2 and N_2 solubility in TBAB aqueous solution. Finally, coupled with CPA parameters, this model could then predict TBAB and TBAF results. Fugacities will be more difficult to calculate since TBA salts dissociate in aqueous solution.

6

Conclusions – Future work

Ἐφ᾽ ὅσον χρόνον τίς ἐστιν ἐν τῇ ζωῇ ταύτῃ, κἂν τέλειός ἐστι κατὰ τὴν ἐνθάδε κατάστασιν, καὶ πράξει καὶ θεωρίᾳ, τὴν ἐκ μέρους ἔχει καὶ γνῶσιν καὶ προφητείαν καὶ ἀῤῥαβῶνα Πνεύματος ἁγίου· ἀλλ᾽ οὐκ αὐτὸ τὸ πλήρωμα· ἐλευσόμενὸς ποτε μετὰ τὴν τῶν αἰώνων περαίωσιν εἰς τὴν τελείαν λῆξιν, τὴν πρόσωπον πρὸς πρόσωπον τοῖς ἀξίοις δεικνῦσαν αὐτὴν ἐφ᾽ ἑαυτῆς ἑστῶσαν τὴν ἀλήθειαν· ὡς μηκέτι ἐκ τοῦ πληρώματος μέρος ἔχειν, ἀλλ᾽ αὐτὸ τὸ πλήρωμα τῆς χάριτος κατὰ μέθεξιν ὅλον κομίζεσθαι.

Ἁγ. Μάξιμος ὁ Ὁμολογητής (580 – 662 μ.Χ.)[i]

[i] *As long as somebody exists in this life, even if he is perfect in this (earthy) situation, concerning action and theory, he has partly knowledge and prophesy and engagement of Holy Spirit˙ but this (is) not the fulfillment/all˙ when (he) comes at some point after the ending of centuries in the perfect expiration, face to face to the worthy (people), it will appear the self-sustained Truth˙ so as he may not have any more part of the fulfillment/all, but (he will) acquire all this fulfillment of Grace through communion.*

St. Maximus the Confessor (580 – 662 AD)

6.1 Conclusions

The PhD Thesis dealt with the production of hydrate equilibrium data of TBA salts and cyclopentane and modeling of cycloalkane hydrates. Gas hydrate crystallization can be used as a post-combustion capture process[7]. The scope of this method is to capture CO_2 from flue gas by the mean of hydrates and then its release so that CO_2 is purely concentrated in one stream. This technology is immature, requires high pressure for the hydrates to form and it exhibits large energy penalty[51]. High pressure is linked with high operational costs[9,10] (chapters 1 and 2). Therefore, the use of chemicals (promoters) to produce hydrates at lower pressures is imperative. The available literature review (of chapter 2) showed that there is shortage in data of CO_2+N_2 gas mixture which is a common effluent in oil and gas industry[10]. Moreover, TBAF promoter, which has high capability in reducing hydrate equilibrium pressure, has not been examined as extensively as THF. Hydrate equilibrium points for CO_2 and N_2 were measured with the use of tetra-n-butyl ammonium bromide (TBAB), tetra-n-butylammonium bromide (TBAF), cyclopentane (CP) and mixtures of TBAB and TBAF with CP as promoters (chapter 3). The use of higher TBAB concentration (1.38 mol%) and CP (5 vol%) revealed promotion effect and as the pressure increases (>3.5 MPa), the promotion effect increases. In addition, the higher the CO_2 concentration, the stronger the promotion is for every TBAB solution which is shown by the shift of equilibrium points at higher temperatures. On the contrary, the results have shown that the simultaneous use of TBAB (0.29 mol%) and (0.62 mol%) with CP (5 vol%) did not have any impact on thermodynamic equilibrium. For the system TBAB (0.29 mol%) with CP (5 vol%), even though the gas mixture systems are different, it is rather unlikely that there is positive impact in promotion. However, this fact is not easily observable for low differences of CO_2 concentration in gas mixtures with N_2. Consequently, it came out that the factor of gas mixture concentration has moderate impact on hydrate equilibrium points compared to promoter's concentration. The results of this work are presented in Figure 3.18.

The use of CP solution (even though it is virtually water inmmiscible) proved to be stronger promoter than TBAB maybe because of the different hydrate structure it induces. The CP

drawback, however, is the low CO_2 selectivity in gas hydrate in CO_2 +N_2 gas mixture. The stoichiometric concentration of CP in the solution for structure II hydrates is 18.65 wt% (5.56 mol%). When higher CP concentration than this value was used, e.g. 52 wt% (22.15 mol%), the results showed slight inhibition effect. Finally, the data consistency analysis carried out using Clausius-Clapeyron method revealed that the measurements of this work are satisfactory.

Hydrate equilibrium points for CO_2 and N_2 were measured with the use of tetra-n-butylammonium bromide (TBAF) and mixture of TBAF with CP as promoters. The use of TBAF concentration (0.36 mol%) and CP (5 vol%) revealed a promotion effect at pressures higher than 3.5 MPa. On the contrary, the results have shown that the simultaneous use of TBAF (0.76 mol%) with CP (5 vol%) did not have any impact on thermodynamic equilibrium. The equilibrium results are more dependent on TBAF concentration rather than gas mixture concentration as the comparison with literature data revealed. The consistency analysis has shown that the results of this study are satisfactory.

In addition, experimental uncertainties and consistency analysis are calculated and presented (chapter 3 and 4). The temperature and pressure calibration uncertainties of transducers $u_{cal.}(T)$ and $u_{cal.}(P)$ are found to be 0.02 K and 0.015 bar, respectively. The average standard uncertainty for temperature and pressure equilibrium points are $U(T)$ and U(P) is 0.028 ^{o}C and 0.025 bar respectively. In addition, the standard uncertainties of gas in the four different gas mixtures are low in absolute values. Moreover, the average standard uncertainty of gas molar composition in equilibrium cell $U(n_{gas})$ is 2.14%. The consistency analysis of every system of this work (chapter 4) is shown in Table 4.6. The results are very satisfactory in almost all cases. Some deviations exist for mixtures of promoters. This can be attributed to the high non-ideality of their solutions which Clapeyron equation is not applicable.

Finally, the van der Waals-Platteeuw hydrate model was used for modeling the CP results of this work and for cycloalkanes of higher carbon number (chapter 5). The predictive results of CP systems of this work (Figure 5.2) and for systems of

CO_2+cycloalkane+H_2O hydrates are very satisfactory in almost all cases even though the Kihara parameters used were excerpted from literature while various EoS were used for their estimation in many of the cases. Cyclohexane results are not perfectly matching the experimental data. This is due to the modified PVT with non-density-dependent mixing rules EoS which is used for the estimation of Kihara parameters as shown in Table D.1. Modified PVT is intrinsically different than CPA EoS.

6.2 Future steps to technological scale-up

6.2.1 Process design aspects

The comparison of CO_2 capture technologies against CO_2 hydrate crystallization has shown that hydrate crystallization can be competitive under three conditions:

a) CO_2-rich feed phase[9]

b) High pressure inlet gas such as in oil and gas industry[9,51]

c) Consideration of crystallization as long-term capturing technology[10]

In Figure 6.1, a comparison of different CO_2 capture technologies is presented. It is shown that hydrate technology has comparable cost to other technologies in the iron and steel production where the CO_2 concentration to be treated is typically 30-50 mol%[195].
The process design of a crystallization unit is generally simple. However, the design issues[6-8,196-198] in hydrate crystallization to be considered are:

a) operating temperature
b) minimum pressure
c) rate of hydrate growth
d) gas uptake (separation efficiency).

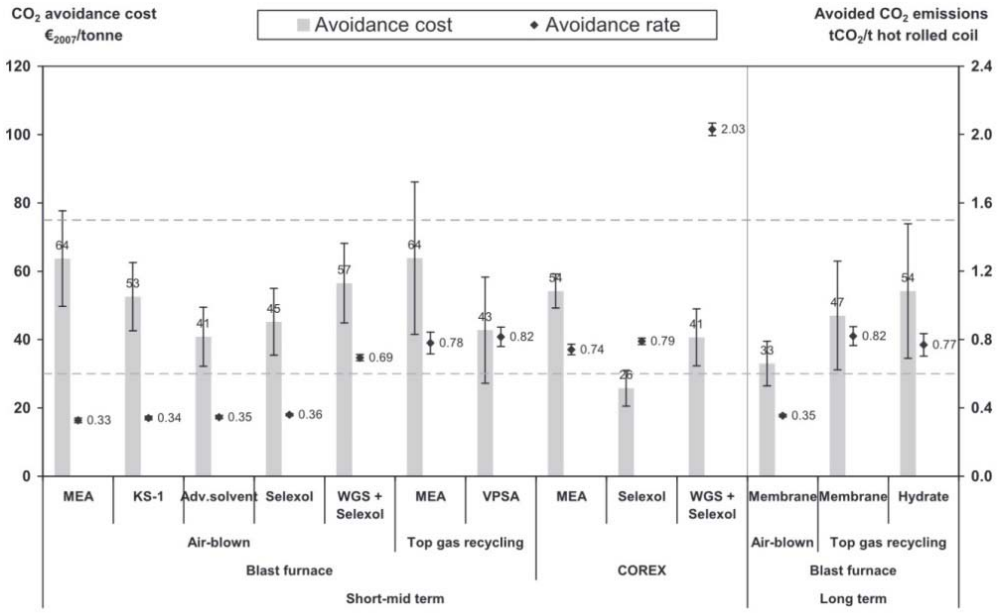

Figure 6.1 CO_2 avoidance costs and avoidance rates for iron and steel production in the short-mid term future (10-15 years) and the long term future (20 years or more). The error bars present uncertainty ranges. The dotted lines indicate the probable future CO_2 price range (30-75 Euro/t)[10].

In this study, the focus was only on pressure reduction. However, the issues (c) and (d) are also crucial. In Figure 6.2, CO_2 uptake is presented for every hydrate structure. The maximum CO_2 uptake can be achieved from s(I) or s(II) hydrate (without promoter). But CO_2 alone cannot stabilize the s(II) hydrates[24]. Promoters like THF, CP or propane occupy some of the large cages of the s(II) hydrate and reduces the CO_2 uptake considerably. Similarly, in case of TBAB semi-clathrate hydrates, only small cages are available for CO_2 and hence a lower CO_2 uptake capacity.

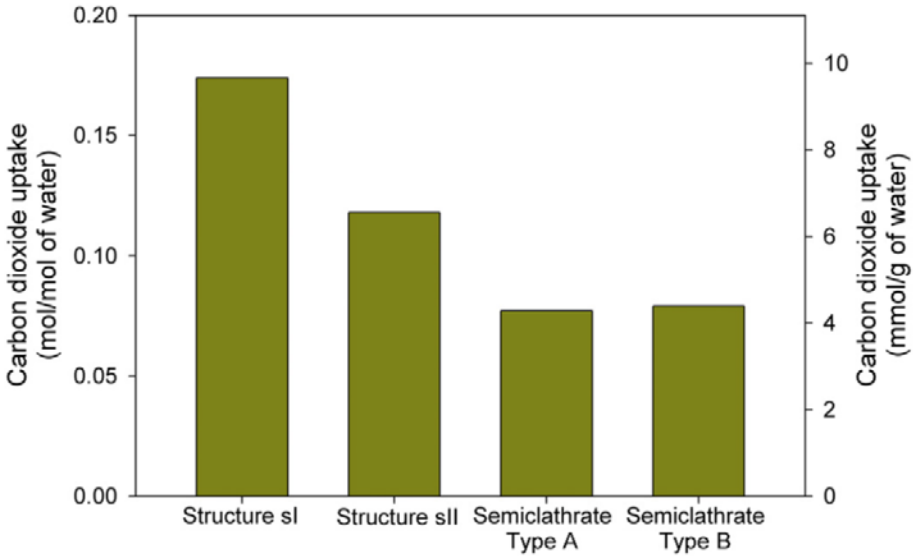

Figure 6.2 CO_2 gas uptake for every gas hydrate structure[196].

Several reactor configurations have been proposed in the literature[78-110]. Most of the studies were carried out in a laboratory scale continuous stirring tank reactor (CSTR). CSTRs are currently used to investigate kinetics of hydrate formation and phase equilibrium measurements. The CSTR has certain disadvantages such as low water conversion to hydrate, gas uptake, slow kinetics and significant energy penalty for stirring. Low water conversion to hydrate is not desirable for scaling up the hydrate crystallisation process for CO_2 capture[196].

Among the various reactor configurations employed so far, fluidized bed reactor (FBR) configuration can be potentially applied at a commercial scale. The drawback of FBR is the requirement of immiscible promoter. The advantages of FBR are the increased gas-liquid contact area; enhanced kinetics and the energy save due to lack of stirring. Moreover, Polyurethane foam or silica sand are cheap and readily available compared to silica gel[60,126,127,199,200] and other porous medium tested until now.

In Figure 6.3, it is to observe the normalised rate of hydrate growth and gas uptake against various promoters for different reactor configurations. The outcome is that propane exhibit the highest CO_2 gas uptake from the until now (2015) available data even though there are relative high fluctuations of the values for same P,T conditions and promoter concentrations.

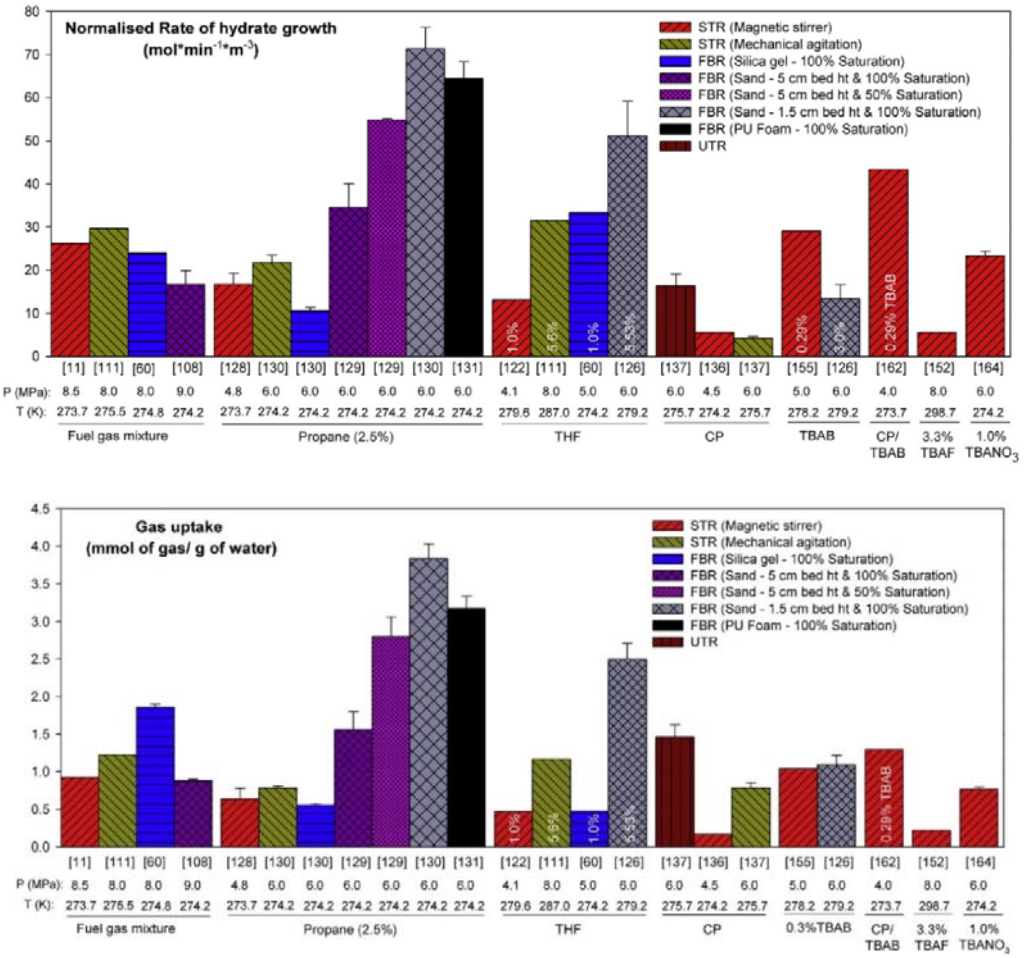

Figure 6.3 Normalised rate of hydrate growth and gas uptake against various promoters for different reactor configurations[196].

There are also other processes proposed in the literature. A continuous reactor was proposed in SMTECHE process[201]. The SIMTECHE process takes advantage of the higher pressure of the pre-combustion streams in an IGCC power plant to remove CO_2 by clathrate hydrate formation. The major limitation of employing continuous mode for the hydrate crystallisation process is the possible plug which is caused by hydrate formation and can block the pipelines e.g. the oil and gas flow lines. The other drawbacks of the continuous operation of the hydrate crystallisation process are insufficient residence time to achieve higher water conversions and higher operating costs involved in gas/liquid agitation for hydrate formation[196].

Moreover, hydrate technology design coupled with membranes for post-combustion capture was presented in 2007 in Figure 6.4. It is the most recent design in literature concerning post-combustion carbon capture. However, there are more recent available designs for pre-combustion carbon capture[190,191].

It is evident from the brief discussion of the hydrate issues of hydrate technology that more work needs to be done both on technological specifications and scale-up.

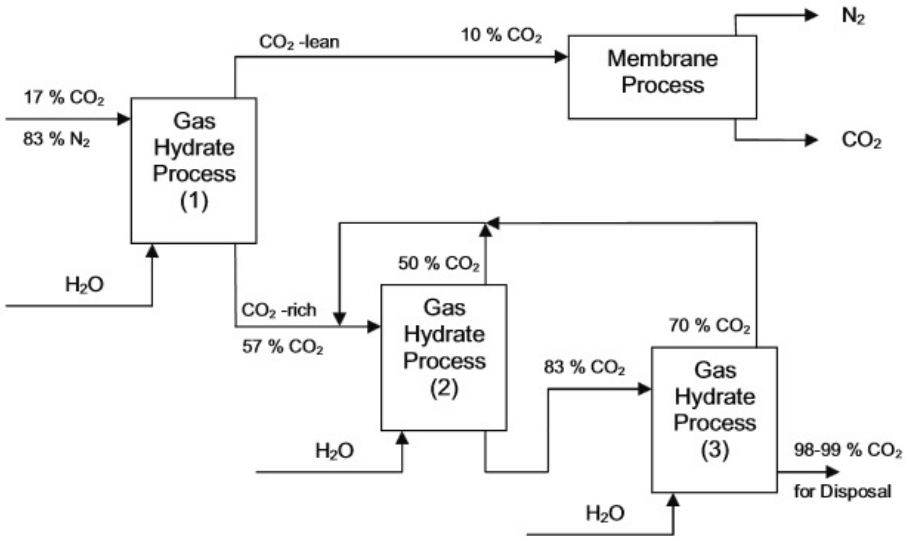

Figure 6.4 A hybrid hydrate-membrane process for CO_2 recovery from flue gas[7].

6.2.2 Future work

It is profound from the existing literature so far that the field of hydrate promotion is lacking in both experimental results and modeling work. The research should focus on examination of new chemicals and combination of them as it was shown in this study as well as to kinetic and structural studies to get a better understanding of their actual capabilities. Techniques with higher efficiency and cost effectiveness are essential but the scale-up challenges of novel technologies from a laboratory to industrial scale has also to be addressed to manage effectively the technical difficulties in CCS.

Apart from testing new components for finding a potential promoter, modeling work should need to provide the necessary aid to this target. The attempts so far are not utterly convincing[198] but, nevertheless, it can be considered as a start: *the beginning is half of*

everything as philosopher Pythagoras stated. In addition, the model used in this work should be extended to deal with TBA salts. This is not straightforward because TBA salts form semi-clathrate hydrates which require, apart from new CPA and Kihara parameters, new thermodynamic parameters (Tables 5.2-5.4). More specifically, there are many structural studies[13,28,112,113,115,118,145,146,150] for water lattice and unit cell parameters for semi-clathrates (as presented in Table 5.1). There should be experiments to find the chemical potential and enthalpies[112] of water lattice and ice for semi-clathrate structures at standard conditions (as presented in Table 5.2). Then, new Kihara parameters (as presented in Table 5.3) could be calculated with this model. CPA could then calculate CO_2 and N_2 solubility in TBAB aqueous solution. Finally, coupled with CPA parameters, this model could then predict TBAB and TBAF results. Fugacities will be more difficult to calculate since TBA salts dissociate in aqueous solution.

In general, pre-combustion (for high pressure, mainly CO_2/H_2 separation), post-combustion (low pressure, mainly CO_2/N_2), and oxy-fuel combustion (predominantly CO_2/H_2O separation) techniques along with new promoters and processes can provide a solution to solve the CO_2 capture and separation (CCS) challenge. To cope with this convoluted issue, multiple technologies would need to be integrated[197].

Bibliography

(1) Todd A.C., 2011, CCS–A multidisciplinary global activity for a global challenge, *Chem. Eng. Res. Des.*, **89**, 1443–1445.

(2) National Research Council, *America's Climate Choices: Limiting the Magnitude of Future Climate Change*, The National Academies Press, Washington, DC, 2010.

(3) Englezos P., 1993, Clathrate hydrates, *Ind. Eng. Chem. Res.*, **32**, 1251–1274.

(4) Collett T.S., 2004, Gas Hydrates as a Future Energy Resource, *Geotimes*, **49**, 24–27.

(5) Osman K., Coquelet C., Ramjugernath D., 2014, Review of carbon dioxide capture and storage with relevance to the South African power sector, *S Afr J Sci.*, **110(5/6)**, Art. #2013-0188.

(6) Kumar R., Englezos P., Moudrakovski I., Ripmeester J.A., 2009, Structure and composition of CO_2/H_2 and $CO_2/H_2/C_3H_8$ hydrate in relation to simultaneous CO_2 capture and H_2 production, *AIChE J.*, **55**, 1584–1594.

(7) Kumar R., Linga P., Englezos P., 2007, The clathrate hydrate process for post and pre-combustion capture of carbon dioxide, *J. Hazard. Mater.*, **149**, 625–629.

(8) Kumar R., Linga P., Ripmeester J. A., Englezos P., 2009, Two-Stage Clathrate Hydrate/Membrane Process for Precombustion Capture of Carbon Dioxide and Hydrogen, *J. Environ. Eng.*, **135**, 411–417.

(9) Duc N.H., Chauvy F., Herri J.M., 2007, CO_2 capture by hydrate crystallization – A potential solution for gas emission of steelmaking industry*, Energy Convers. Manag.*, **48**, 1313–1322.

(10) Kuramochi T., Ramírez A., Turkenburg W., Faaij A., 2012, Comparative assessment of CO_2 capture technologies for carbon-intensive industrial processes, *Prog. Energy Combust. Sci.*, **38**, 87–112.

(11) Lee S., Park S., Lee Y., Lee J., Lee H., Seo Y., 2011, Guest Gas Enclathration in Semiclathrates of Tetra-n-butylammonium Bromide: Stability Condition and Spectroscopic Analysis, *Langmuir*, **27**, 10597–10603.

(12) Mohammadi A., Manteghian M., Mohammadi A.H., 2013, Dissociation Data of Semiclathrate Hydrates for the Systems of Tetra‑n‑butylammonium Fluoride (TBAF) + Methane + Water, TBAF + Carbon Dioxide + Water, and TBAF + Nitrogen + Water, *J. Chem. Eng. Data*, **58**, 3545−3550.

(13) Mohammadi A., Manteghian M., Mohammadi A.H., 2014, Phase equilibria of semiclathrate hydrates for methane + tetran-butylammonium chloride (TBAC), carbon dioxide + TBAC, and nitrogen + TBAC aqueous solution systems, *Fluid Phase Equil.*, **381**, 102–107.

(14) Mayoufi N., Dalmazzone D., Fürst W., Delahaye A., Fournaison L., 2010, CO_2 Enclathration in Hydrates of Peralkyl-(Ammonium/Phosphonium) Salts: Stability Conditions and Dissociation Enthalpies, *J. Chem. Eng. Data*, **55**, 1271–1275.

(15) Cha J.-H., Seol Y., 2013, Increasing Gas Hydrate Formation Temperature for Desalination of High Salinity Produced Water with Secondary Guests, *ACS Sustainable Chem. Eng.*, **1**, 1218−1224.

(16) Jordal K., Anheden M., Yan J., Strømberg L., 2004, *Oxyfuel combustion for coal-fired power generation with CO_2 capture—opportunities and challenges*. In Proceedings of the 7th International Conference on Greenhouse Gas Control Technologies, International Energy Agency Greenhouse Gas Programme.

(17) Jeffrey G.A., 1996, Hydrate inclusion compounds. In: MacNicol, D.D., Toda, F., Bishop, R. (eds.) Comprehensive Supramolecular Chemistry, vol. 6, chap. 23, pp. 757–788. Pergamon, Oxford.

(18) Rodionova T.V., Manakov A.Yu., Stenin Yu.G., Villevald G.V., Karpova T.D., 2008, The heats of fusion of tetrabutylammonium fluoride ionic clathrate hydrates, *J. Incl. Phenom. Macrocycl. Chem.*, **61**, 107–111.

(19) Van der Waals J.H., Platteeuw J.C., 1959, The statistical mechanics of clathrate compounds, *Adv. Chem. Phys.*, **2**, 1–57.

(20) Herslund P. J., 2013, *Thermodynamic and Process Modelling of Gas Hydrate Systems in CO_2 Capture Processes*, Ph.d. Thesis, Technical University of Denmark.

(21) Herslund P.J., Thomsen K., Abildskov J., von Solms N., 2012, Phase equilibrium modeling of gas hydrate systems for CO_2 capture, *J. Chem. Thermodyn.*, **48**, 13–27.

(22) Herslund P.J., Thomsen K., Abildskov J., von Solms N., Galfré A., Brântuas P., Kwatersk M., Herri J.-M., 2013, Thermodynamic Promotion of Carbon Dioxide Clathrate Hydrate Formation by Tetrahydrofuran, Cyclopentane and their Mixtures, *Int. J. Greenh. Gas Control*, **17**, 397–410.

(23) Platteeuw J.C., van der Waals J.H., 1958, Thermodynamic properties of gas hydrates, *Mol. Phys.*, **1**, 91–95.

(24) Sloan E.D., Koh C.A., 2008, *Clathrate Hydrates of Natural Gases*, third ed., CRC Press, Taylor & Francis Group, New York.

(25) Seo Y.T., Lee H., Yoon J.H., 2001, Hydrate phase equilibria and the predictive curve of the Carbon Dioxide, Methane, and Water System, *J. Chem. Eng. Data*, **46***,* 381–384.

(26) Seo Y.T., Lee H., 2004, Structure and Guest Distribution of the Mixed Carbon Dioxide and Nitrogen Hydrates As Revealed by X-ray Diffraction and ^{13}C NMR Spectroscopy, *J. Phys. Chem. B*, **108**, 530–534.

(27) Davidson D.W., 1973, *Water - A Comprehensive Treatise*, Vol. 2, edited by F. Franks, pp. 115–234. New York, London: Plenum Press.

(28) Shimada W., Shiro M., Kondo H., Takeya S., Oyama H., Ebinuma T. and Narita H., 2005, Tetra-n-butylammonium bromide-water (1/38), *Acta Cryst.*, **C61**, o65–o66.

(29) Makogon Y.F., 1974, *Hydrates of Natural Gas, Moscow, Nedra, Izadatelstro,* PennWell Books, Tulsa, Oklahoma, in Russian (1981 in English).

(30) Vysniauskas A., Bishnoi P.R., 1983, A kinetic study of methane hydrate formation, *Chem. Eng. Sci.*, **38**, 1061–1072.

(31) Lederhos J., 1996, *The Transferability of Hydrate Kinetic Inhibitor Results between Bench Scale Apparatuses and a Pilot Scale Flow Loop*, Ph.D. Thesis, Colorado School of Mines, USA.

(32) Parent J.S., Bishnoi P., 1996, Investigations into the nucleation behaviour of methane gas hydrates, *Chem. Eng. Commun.*, **144**, 51–64.

(33) Takeya S., Hori A., Hondoh T., Uchida T., 2000, Freezing-Memory Effect of Water on Nucleation of CO_2 Hydrate Crystals, *J. Phys. Chem. B*, **104**, 4164–4168.

(34) Ohmura R., Ogawa M., Yasuka K., Mori Y.J., 2003, Statistical Study of Clathrate-Hydrate Nucleation in a water/Hydrochlorofluorocarbon System: Search for the Nature of the “Memory Effect”, *J. Phys. Chem. B*, **107**, 5289–5293.

(35) Schroeter J.P., Kobayashi R., Hildebrand M.A., 1983, Hydrate decomposition conditions in the system hydrogen sulfide-methane-propane, *Ind. Eng. Chem. Fundam.*, **22**, 361–364.

(36) Moudrakovski I.L., McLaurin G.E., Ratcliffe C.I., Ripmeester J.A., 2004, Methane and Carbon Dioxide Hydrate Formation in Water Droplets: Spatially Resolved Measurements from Magnetic Resonance Microimaging, *J. Phys. Chem. B*, **108**, 17591–17595.

(37) Lee J.D., Susilo R., Englezos P., 2005, in *Proc. Fifth International Conference on Gas Hydrates*, Trondheim, Norway, June 13–16, Paper 1034.

(38) Servio P., Englezos P., 2003, Morphology of methane and carbon dioxide hydrates formed from water droplets, *AIChE J.*, **49**, 269–276.

(39) Englezos P., Lee J.D., 2005, Gas Hydrates: A Cleaner Source of Energy and Opportunity for Innovative Technologies, *Korean J. Chem. Eng.*, **22**, 671–681.

(40) Booth J.S., Rowe M.M., Fischer K.M., 1996, *Offshore gas hydrate sample database with an overview and preliminary analysis: U.S. Geological Survey Open-File Report 96-272*, 1, 31.

(41) Mahajan D., Taylor C.E., Mansoori G.A., 2007, An introduction to natural gas hydrate /clathrate: The major organic carbon reserve of the Earth, *J. Petrol. Sci. Eng.*, **56**, 1–8.

(42) Ruppel C., *Methane Hydrates and the Future of Natural Gas, Supplementary Paper 4*, MITEI Natural Gas Report, Supplementary Paper on Methane Hydrates, 2011, 1–25.

(43) Uchida T., Ikeda I.Y., Takeya S., Kamata Y., Ohmura R., Nagao J., Zatsepina O.Y., Buffett B.A., 2005, Kinetics and Stability of CH_4-CO_2 Mixed Gas Hydrates during Formation and Long-Term Storage, *Phys. Chem. Chem. Phys.*, **6**, 646–654.

(44) Deschamps J., Dalmazzone D., 2010, Hydrogen Storage in Semiclathrate Hydrates of Tetrabutyl Ammonium Chloride and Tetrabutyl Phosphonium Bromide, *J. Phys. Eng. Data*, **55**, 3395–3399.

(45) Javanmardi J., Nasrifar Kh., Najibi S.H., Moshfeghian M., 2005, Economic evaluation of natural gas hydrate as an alternative for natural gas transportation, *Appl. Therm. Eng.*, **25**, 1708–1723.

(46) Stern L.A., Circone S., Kirby S.H., Durham W.B., 2001, Preservation of Methane Hydrate at 1 Atm, *J. Phys. Chem. B*, **105**, 1756–1762.

(47) Gudmundsson J.S., Andersson V., Levik O., Mork M., 2000, Hydrate Technology for Capturing Stranded Gas, *NY Acad. Sci.*, **912**, 403–410.

(48) Koh C.A., Sloan E.D., Sum A.K., Wu D.T., 2011, Fundamentals and Applications of Gas Hydrates, *Annu. Rev. Chem. Biomol. Eng.*, **2**, 237–257.

(49) Rice W., 2006, Hydrogen production from methane hydrate with sequestering of carbon dioxide, *Int. J. Hydrogen Energy*, **31**, 1955–1963.

(50) Mohammadi A.H., Eslamimanesh A., Belandria V., Richon D., 2011, Phase Equilibria of Semiclathrate Hydrates of CO_2, N_2, CH_4, or H_2 + Tetra-n-butylammonium Bromide Aqueous Solution, *J. Chem. Eng. Data*, **56**, 3855–3865.

(51) Tajima H., Yamasaki A., Kiyono F., 2004, Energy consumption estimation for greenhouse gas separation processes by clathrate hydrate formation, *Energy*, **29**, 1713–1729.

(52) Belandria V., Eslamimanesh A., Mohammadi A.H., Richon D., 2011, Gas Hydrate Formation in Carbon Dioxide+Nitrogen+Water System: Compositional Analysis of Equilibrium Phases, *Ind. Eng. Chem. Res.*, **50**, 4722–4730.

(53) Happel J., Hnatow M.A., Meyer H., 1994, The study of separation of nitrogen from methane by hydrate formation using a novel apparatus, *Ann. NY Acad. Sci.*, **715**, 412–424.

(54) Richon D., de Loos T.W., 2005, *"Vapour-liquid equilibrium at high pressure,"* Measurement of the Thermodynamic Properties of Multiple Phases (Experimental Thermodynamics, Vol VII), R.D. Weir and T.W. de Loos, eds., Elsevier, 90–136.

(55) Ohmura R., Takeya S., Uchida T., Ebinuma T., 2004, Clathrate Hydrate Formed with Methane and 2-Propanol: Confirmation of Structure II Hydrate Formation, *Ind. Eng. Chem. Res.*, **43**, 4964–4966.

(56) Khalil W., 2006, *Développement d'un appareil automatisé de mesure simultanée d'équilibres de phases et de propriétés volumétriques. Exploitation des données volumétriques pour le calcul prédictif de grandeurs thermodynamiques dérivées*, PhD Dissertation, Ecole Nationale Supérieure des Mines de Paris, France.

(57) Kim S.M., Lee J.D., Lee H.J., Lee E.K., Kim Y., 2011, Gas hydrate formation method to capture the carbon dioxide for pre-combustion process in IGCC plant, *Int. J. Hydrogen Energy*, **36**, 1115–1121.

(58) Tohidi B., Burgass R.W., Danesh A., Ostergaard K.K., Todd A.C., 2000, *Improving the accuracy of gas hydrate dissociation point measurements.* In: Holder GD, Bishnoi PR, editors. Gas hydrates: Challenges for the Future, vol. 912. New York: New York Acad Sciences;. p. 924.

(59) Lee B.R., Sa J.-H., Park D.-H., Cho S., Lee J., Kim H.-J., Oh E., Jeon S., Lee J. D., Lee K.-H., 2011, "Continuous" Method for the Fast Screening of Thermodynamic Promoters of Gas Hydrates Using a Quartz Crystal Microbalance, *Energy Fuels*, **26**, 767–772.

(60) Park S., Lee S., Lee Y., Lee Y., Seo Y., 2013, Hydrate-based pre-combustion capture of carbon dioxide in the presence of a thermodynamic promoter and porous silica gels, *Int. J. Greenh. Gas Control*, **14**, 193–199.

(61) Mohammadi A.H., Eslamimanesh A., Richon D., 2013, Semi-clathrate hydrate phase equilibrium measurements for the CO_2+H_2/CH_4+tetra-n-butylammoniumbromide aqueous solution system, *Chem. Eng. Sci.*, **94**, 284–290.

(62) Fonseca J.M.S. and von Solms N., 2012, Development and testing of a new apparatus for the measurement of high-pressure low-temperature phase equilibria, *Fluid Phase Equilibria*, **329**, 55–62.

(63) Belandria V., Eslamimanesh A., Mohammadi A.H., Theveneau P., Legendre H., Richon D., 2011, Compositional analysis and hydrate dissociation conditions measurements for carbon dioxide + methane + water system, *Ind. Eng. Chem. Res.* **50**, 5783–5794.

(64) Tumba K., Reddy P., Naidoo P., Ramjugernath D., Eslamimanesh A., Mohammadi A. H., D. Richon, 2011, Phase Equilibria of Methane and Carbon Dioxide Clathrate Hydrates in the Presence of Aqueous Solutions of Tributylmethylphosphonium Methylsulfate Ionic Liquid, *J. Chem. Eng. Data*, **56**, 3620–3629.

(65) Zhang J., Lee J.W., 2009, Enhanced kinetics of CO_2 hydrate formation under static conditions, *Ind. Eng. Chem. Res.,* **48**, 5934–5942.

(66) Ricaurte M., Torré J.-P., Asbai A., Broseta D., Dicharry C., 2012, Experimental data, modeling, and correlation of carbon dioxide solubility in aqueous solutions containing low concentrations of clathrate hydrate promoters: application to CO_2–CH_4 gas mixtures, *Ind. Eng. Chem. Res.*, **51**, 3157–3169.

(67) Liu N., Gong G., Liu D., Xie Y., 2008, *Effects of additives on carbon dioxide hydrate formation*, Proceedings of the 6th International Conference on Gas Hydrates (ICGH 2008), Vancouver, Canada.

(68) Lim Y.-A., Babu P., Kumar R., Linga P., 2013, Morphology of Carbon Dioxide−Hydrogen−Cyclopentane Hydrates with or without Sodium Dodecyl Sulfate, *Cryst. Growth Des.*, **13**, 2047−2059.

(69) Kang S.-P., Lee J.-W., 2010, Kinetic behaviors of CO_2 hydrates in porous media and effect of kinetic promoter on the formation kinetics, *Chem. Eng. Sci.*, **65**, 1840–1845.

(70) Li X.-S., Xu C.-G., Chen Z.-Y., Wu H.-J., 2010, Tetra-n-butyl ammonium bromide semi-clathrate hydrate process for post-combustion capture of carbon dioxide in the presence of dodecyl trimethyl ammonium chloride, *Energy*, **35**, 3902–3908.

(71) Li S., Fan S., Wang J., Lang X., Wang Y., 2010, Clathrate Hydrate Capture of CO_2 from Simulated Flue Gas with Cyclopentane/Water Emulsion, *Chinese J. Chem. Eng.*, **18**, 202–206.

(72) Mohammadi A.H., Richon D., 2009, Phase equilibria of clathrate hydrates of methyl cyclopentane, methyl cyclohexane, cyclopentane or cyclohexane+carbon dioxide, *Chem. Eng. Sci.*, **64**, 5319–5322.

(73) Mohammadi A.H., Richon D., 2011, Phase equilibria of binary clathrate hydrates of nitrogen + cyclopentane/ cyclohexane/methyl cyclohexane and ethane + cyclopentane/cyclohexane/ methyl cyclohexane, *Chem. Eng. Sci.*, **66**, 4936–4940.

(74) Mooijer-van den Heuvel M.M., Witteman R., Peters C.J., 2001, Phase behaviour of gas hydrates of carbon dioxide in the presence of tetrahydropyran, cyclobutanone, cyclohexane and methylcyclohexane, *Fluid Phase Equil.*, **182**, 97–110.

(75) Uchida T., Ohmura R., Ikeda I.Y., Nagao J., Takeya S., Hori A., 2006, Phase Equilibrium Measurements and Crystallographic Analyses on Structure-H Type Gas Hydrate Formed from the CH_4-CO_2-Neohexane-Water System, *J. Phys. Chem. B*, **110**, 4583–4588.

(76) Robinson D.B., Mehta B. R., 1971, Hydrates in the propane-carbon dioxide-water system, *J. Can. Pet. Technol.*, **10**, 33–36.

(77) Eslamimanesh A., Mohammadi A. H., Richon D., Naidoo P., Ramjugernath, D., 2012, Application of gas hydrate formation in separation processes: A review of experimental studies, *J. Chem. Thermodyn.*, **46**, 62−71.

(78) Ricaurte M., Dicharry C., Broseta D., Renaud X., Torré J.-P., 2013, CO_2 Removal from a CO_2–CH_4 Gas Mixture by Clathrate Hydrate Formation Using THF and SDS as Water-Soluble Hydrate Promoters, *Ind. Eng. Chem. Res.*, **52**, 899−910.

(79) Seo Y., Kang S.-P., Lee S., Lee H., 2008, Experimental Measurements of Hydrate phase equilibria and the predictive curve for Carbon Dioxide in the Presence of THF, Propylene Oxide, and 1,4-Dioxane, *J. Chem. Eng. Data*, **53**, 2833–2837.

(80) Kang S.-P., Lee H., Lee C.S., Sung W.M., 2001, Hydrate phase equilibria and the predictive curve of the guest mixtures containing CO_2, N_2 and tetrahydrofuran, *Fluid Phase Equilib.*, **185**, 101–109.

(81) Kang S.-P., Lee H., Ryu B.-J., 2001, Enthalpies of dissociation of clathrate hydrates of carbon dioxide, nitrogen, (carbon dioxide+nitrogen), and (carbon dioxide + nitrogen + tetrahydrofuran), *J. Chem. Thermod.*, **33**, 513–521.

(82) Linga P., Adeyemo A., Englezos P., 2007, Medium-Pressure Clathrate Hydrate/Membrane Hybrid Process for Post combustion Capture of Carbon Dioxide, *Environ. Sci. Technol.*, **42**, 315–320.

(83) Linga P., Kumar R., Englezos P., 2007, Gas hydrate formation from hydrogen/carbon dioxide and nitrogen/ carbon dioxide gas mixtures, *Chem. Eng. Sci.*, **62**, 4268 – 4276.

(84) Lu T., Zhang Y., Li X.S., Chen Z.Y., Yan K.F., 2009, Equilibrium Conditions of Hydrate Formation in the Systems of CO_2-N_2-TBAB and CO_2-N_2-THF, *Guocheng Gongcheng Xuebao/Chinese J. Proc. Eng.*, **9**, 541–544 (in Chinese).

(85) Lee H.J., Lee J.D., Linga P., Englezos P., Kim Y.S., Lee M.S., Kim Y.D., 2010, Gas hydrate formation process for pre-combustion capture of carbon dioxide, *Energy*, **35**, 2729–2733.

(86) Martinez M.C., Dalmazzone D., Fürst W., Delahaye A., Fournaison L., 2008, Thermodynamic Properties of THF + CO_2 Hydrates in Relation with Refrigeration Applications, *AIChE J.*, **54**, 1088–1095.

(87) Delahaye A., Fournaison L., Marinhas S., Chatti I., Petitet J.-P., Dalmazzone D., Fürst W., 2006, Effect of THF on Equilibrium Pressure and Dissociation Enthalpy of CO_2 Hydrates Applied to Secondary Refrigeration, *Ind. Eng. Chem. Res.*, **45**, 391–397.

(88) Zhang J., Yedlapalli P., Lee J.W., 2009, Thermodynamic analysis of hydrate-based pre-combustion capture of CO_2, *Chem. Eng. Sci.*, **64**, 4732–4736.

(89) Yang M., Song Y., Liu W., Zhao J., Ruan X., Jiang L., Li Q., 2013, Effects of additive mixtures (THF/SDS) on carbon dioxide hydrate formation and dissociation in porous media, *Chem. Eng. Sci.*, **90**, 69–76.

(90) Lee S., Lee Y., Park S., Seo Y., 2010, Phase Equilibria of Semiclathrate Hydrate for Nitrogen in the Presence of Tetra-*n*-butylammonium Bromide and Fluoride, *J. Chem. Eng. Data*, ***55,*** 5883–5886.

(91) Xia Z.-M., Chen Z.-Y., Li X.-S., Zhang Y., Yan K.-F., Lv Q.-N., Xu C.-G., Cai J., 2012, Thermodynamic Equilibrium Conditions for Simulated Landfill Gas Hydrate Formation in Aqueous Solutions of Additives, *J. Chem. Eng. Data*, **57**, 3290−3295.

(92) Shin H.J., Lee Y.-J., Im J.-H., Han K.W., Lee J.-W., Lee Y., Lee J.D., Jang W.-Y., Yoon J.-H., 2009, Thermodynamic stability, spectroscopic identification and cage occupation of binary CO_2 clathrate hydrates, *Chem. Eng. Sci*, **64**, 5125–5130.

(93) Van Denderen M., Ineke E., Golombok M., 2009, CO_2 Removal from Contaminated Natural Gas Mixtures by Hydrate Formation, *Ind. Eng. Chem. Res.*, **48**, 5802–5807.

(94) Hashimoto S., Murayama S., Sugahara T., Ohgaki K., 2006, Phase Equilibria for H_2 + CO_2 + Tetrahydrofuran + Water Mixtures Containing Gas Hydrates, *J. Chem. Eng. Data*, **51**, 1884–1886.

(95) Kang S.-P., Lee H., 2000, Recovery of CO_2 from Flue Gas Using Gas Hydrate: Thermodynamic Verification through Phase Equilibrium Measurements, *Environ. Sci. Technol.*, **34**, 4397–4400.

(96) Sabil K.M., Duartea A.R., Zevenbergen J., Ahmad M.M., Yusup S., Omar A., Peters C. J., 2010, Kinetic of formation for single carbon dioxide and mixed carbon dioxide and tetrahydrofuran hydrates in water and sodium chloride aqueous solution, *Int. J. Greenh. Gas Control*, **4**, 798–805.

(97) Sabil K.M., Witkamp G.-J., Peters C.J., 2010, Estimations of enthalpies of dissociation of simple and mixed carbon dioxide hydrates from phase equilibrium data, *Fluid Phase Equil.*, **290**, 109–114.

(98) Sabil K.M., Witkamp G.-J., Peters C.J., 2010, Phase equilibria in ternary (carbon dioxide + tetrahydrofuran + water) system in hydrate-forming region: Effects of carbon dioxide concentration and the occurrence of pseudo-retrograde hydrate phenomenon, *J. Chem. Thermodyn.*, **42**, 8–16.

(99) Pahlavanzadeha H., Kamran-Pirzamana A., Mohammadi A. H., 2012, Thermodynamic modeling of pressure–temperature phase diagrams of binary clathrate hydrates of methane, carbon dioxide or nitrogen + tetrahydrofuran, 1,4-dioxane or acetone, *Fluid Phase Equil.*, **320**, 32–37.

(100) Kamata Y., Oyama H., Shimada W., Ebinuma T., Takeya S., Uchida T., Nagao J., Narita H., 2004, Gas Separation Method Using Tetra-*n*-butyl Ammonium Bromide Semi-Clathrate Hydrate, *Jpn. J. Appl. Phys.*, **43**, 362–365.

(101) Wang S., Danner M., Kuchling T., Clarke M.A., 2013, Measurement of the three-phase (vapor + liquid + solid) equilibrium conditions of semi-clathrates formed from mixtures of CO_2, CO and H_2, *J. Chem. Thermod.*, **56**, 149–152.

(102) Li X.-S., Xia Z.-M., Chen Z.-Y., Yan K.-F., Li G., Wu H.-J., 2010, Equilibrium Hydrate Formation Conditions for the Mixtures of CO_2 + H_2 + Tetrabutyl Ammonium Bromide, *J. Chem. Eng.*, Data, **55**, 2180–2184.

(103) Park S., Lee S., Lee Y., Seo Y., 2013, CO_2 Capture from Simulated Fuel Gas Mixtures Using Semiclathrate Hydrates Formed by Quaternary Ammonium Salts, *Environ. Sci. Technol.*, **47**, 7571−7577.

(104) Li S., Fan S., Wang J., Lang X., Wang Y., 2010, Semiclathrate Hydrate phase equilibria and the predictive curve for CO_2 in the Presence of Tetra-*n*-butyl Ammonium Halide (Bromide, Chloride, or Fluoride), *J. Chem. Eng. Dat*a, **55***,* 3212–3215.

(105) Makino T., Yamamoto T., Nagata K., Sakamoto H., Hashimoto S., Sugahara T., Ohgaki K., 2010, Thermodynamic Stabilities of Tetra-n-butyl Ammonium Chloride + H_2, N_2, CH_4, CO_2, or C_2H_6 Semiclathrate Hydrate Systems, *J. Chem. Eng. Data*, **55***,* 839–841.

(106) Du J.-W., Liang D.-Q., Li D.-L., Chen Y.-F., Li X.-J., 2011, Phase Equilibrium Conditions of Tetrabutyl Ammonium Nitrate + CO_2, N_2 or CH_4 Semiclathrate Hydrate Systems, *Ind. Eng. Chem. Res.*, **50**, 11720–11723.

(107) Suginaka T., Sakamoto H., Iino K., Sakakibara Y., Ohmura R., 2013, Phase equilibrium for ionic semiclathrate hydrate formed with CO_2, CH_4, or N_2 plus tetra butyl phosphonium bromide, *Fluid Phase Equil.*, **344**, 108–111.

(108) Li X.-S., Zhan H., Xu C.-G., Zeng Z.-Y., Lv Q.-N., Yan K.-F., 2012, Effects of Tetrabutyl-(ammonium/phosphonium) Salts on Clathrate Hydrate Capture of CO_2 from Simulated Flue Gas, *Energy Fuels*, **26**, 2518−2527.

(109) Majumdar A., Maini B., Bishnoi P. R., Clarke M. A., 2012, Three-Phase Equilibrium Conditions of TiAAB Semiclathrates Formed from N_2, CO_2, and Their Mixtures, *J. Chem. Eng. Data*, **57**, 2322−2327.

(110) Mayoufi N., Dalmazzone D., Fürst W., Elghoul L., Seguatni A., Delahaye A., Fournaison L., 2012, Phase behaviour of tri-n-butylmethylammonium chloride hydrates in the presence of carbon dioxide, *J. Therm. Anal. Calorim.*, **109**, 481–486

(111) Lee Y.J., Kawamura T., Yamamoto Y., Yoon J.-H., 2012, Phase Equilibrium Studies of Tetrahydrofuran (THF) + CH_4, THF + CO_2, CH_4 + CO_2, and THF + CO_2 + CH_4 Hydrates, *J. Chem. Eng. Data*, **57**, 3543−3548.

(112) Paricaud P., 2011, Modeling the Dissociation Conditions of Salt Hydrates and Gas Semiclathrate Hydrates: Application to Lithium Bromide, Hydrogen Iodide, and Tetra-*n*-butylammonium Bromide + Carbon Dioxide Systems, *J. Phys. Chem. B*, **115**, 288–299.

(113) Lee S., Lee Y., Park S., Kim Y., Lee J.-D., Seo Y., 2012, Thermodynamic and Spectroscopic Identification of Guest Gas Enclathration in the Double Tetra-n-butylammonium Fluoride Semiclathrates, *J. Phys. Chem. B*, **116**, 9075−9081.

(114) Trueba A.T., Radovi I.R., Zevenbergen J.F., Peters C.J., Kroon M.C., 2013, Kinetic measurements and in situ Raman spectroscopy study of the formation of TBAF semi-hydrates with hydrogen and carbon dioxide, *Int. J. Hydrogen Energy*, **38**, 7326–7334.

(115) Sakamoto J., Hashimoto S., Tsuda T., Sugahara T., Inoue Y., Ohgaki K., 2008, Thermodynamic and Raman spectroscopic studies on hydrogen plus tetra-n-butyl ammonium fluoride semiclathrate hydrates, *Chem. Eng. Sci*, **63**, 5789–5794.

(116) Fan S., Li S., Wang J., Lang X., Wang Y., 2009, Efficient Capture of CO_2 from Simulated Flue Gas by Formation of TBAB or TBAF Semiclathrate Hydrates, *Energy Fuels*, **23**, 4202–4208.

(117) Adisasmito S., Frank R., Sloan E.D., 1991, Hydrates of carbon-dioxide and methane mixtures, *J. Chem. Eng. Data*, **36**, 68–71.

(118) Lin W., Delahaye A., Fournaison L., 2008, Phase equilibrium and dissociation enthalpy semi-clathrate hydrate of CO_2 + TBAB, *Fluid Phase Equilib.*, **264**, 220–227.

(119) Belandria V., Mohammadi A.H., Richon D., 2012, Compositional analysis of the gas phase for the CO_2+N_2+tetra-n-butylammoniumbromide aqueous solution systems under hydrate stability conditions, *Chem. Eng. Sci.*, **84**, 40–47.

(120) Babu P., Yang T., Veluswamy H.P., Kumar R., Linga P., 2013, Hydrate phase equilibrium of ternary gas mixtures containing carbon dioxide, hydrogen and propane, *J. Chem. Thermodyn.*, **61**, 58–63.

(121) Mayoufi N., Dalmazzone D., Delahaye A., Clain P., Fournaison L., Fürst W., 2011, Experimental Data on Phase Behavior of Simple Tetrabutylphosphonium Bromide (TBPB) and Mixed CO_2+TBPB Semiclathrate Hydrates, *J. Chem. Eng. Data*, **56**, 2987–2993.

(122) Larson S.D., 1955, *Phase studies of the two-components carbon dioxide-water system, involving the carbon dioxide hydrate*, Ph.D. Thesis, University of Illinois, Urbana, IL.

(123) Wang W., Huang Z., Chen H., Tan Z., Chen C., Sun L., 2012, Methane hydrates with a high capacity and a high formation rate promoted by biosurfactants, *Chem. Commun.*, **48**, 11638–11640.

(124) Lirio C.F., Pessoa F.L., Uller A.M., 2013, Storage capacity of carbon dioxide hydrates in the presence of sodium dodecyl sulfate (SDS) and tetrahydrofuran (THF), *Chem. Eng. Sci.*, **96**, 118–123.

(125) Torré J.P., Ricaurte M., Dicharry C., Broseta D., 2012, CO_2 enclathration in the presence of water-soluble hydrate promoters: Hydrate phase equilibria and the predictive curve and kinetic studies in quiescent conditions, *Chem. Eng. Sci.*, **82**, 1–13.

(126) Park J., Seo Y.T., Lee J.W., Lee H., 2006, Spectroscopic analysis of carbon dioxide and nitrogen mixed gas hydrates in silica gel for CO_2 separation, *Catal. Today*, **115**, 279–282.

(127) Adeyemo A., Kumar R., Linga P., Ripmeester J., Englezos P., 2010, Capture of carbon dioxide from flue or fuel gas mixtures by clathrate crystallization in a silica gel column, *Int. J. Greenh. Gas Control*, **4**, 478–485.

(128) Sami N.A., Das K., Sangwai J.S., Balasubramanian N., 2013, Phase equilibria of methane and carbon dioxide clathrate hydrates in the presence of (methanol + $MgCl_2$) and (ethylene glycol + $MgCl_2$) aqueous solutions, *J. Chem. Thermodyn.*, **65**, 198–203.

(129) Acosta H.Y., Bishnoi P.R., Clarke M.A., 2011, Experimental Measurements of the Thermodynamic Equilibrium Conditions of Tetra-*n*-butylammonium Bromide Semiclathrates Formed from Synthetic Landfill Gases, *J. Chem. Eng. Data*, **56**, 69–73.

(130) Deschamps J., Dalmazzone D., 2009, Dissociation enthalpies and phase equilibrium for TBAB semi-clathrate hydrates of N_2, CO_2, N_2+CO_2 and CH_4+CO_2, *J. Therm. Anal. Calorim.*, **98**, 113–118.

(131) Ye N., Zhang P., 2012, Equilibrium data and morphology of tetra-n-butyl ammonium bromide semiclathrate hydrate with carbon dioxide, *J. Chem. Eng. Data*, **57**, 1557–1562.

(132) Sfaxi I., Durand I., Lugo R., Mohammadi A., Richon D., 2014, Hydrate phase equilibria and the predictive curve of CO_2+N_2+aqueous solution of THF, TBAB or TBAF system, *Int. J. Greenh. Gas Control*, **26**, 185–192.

(133) Zhang J., Lee J.W., 2009, Equilibrium of Hydrogen + Cyclopentane and Carbon Dioxide + Cyclopentane Binary Hydrates, *J. Chem. Eng. Data*, **54**, 659–661.

(134) Li X.-S., Xu C.-G., Chen Z.-Y., Wu H.-J., 2011, Hydrate-based pre-combustion carbon dioxide capture process in the system with tetra-n-butyl ammonium bromide solution in the presence of cyclopentane, *Energy*, **36**, 1394–1403.

(135) Rovetto L.R., Strobel T.A., Koh C.A., Sloan E.D., 2006, Is gas hydrate formation thermodynamically promoted by hydrotrope molecules?, *Fluid Phase Equilib.*, **247**, 84–89.

(136) Olsen M.B., Majumdair A., Bishnoi P.R., 1999, Experimental Studies on Hydrate Equilibrium-Carbon Dioxide and Its Systems, *Int. J. of The Soc. of Mat. Eng. For Resources*, **7**, 17–23.

(137) Mohammadi A.H., Eslamimanesh A., Belandria V., Richon D., Naidoo P., Ramjugernath D., 2012, Phase equilibrium measurements for semi-clathrate hydrates of the (CO_2 + N_2 + tetra-n-butylammonium bromide) aqueous solution system, *J. Chem. Thermodyn.*, **46**, 57–61.

(138) Chen C., Li X.-S., Chen Z.-Y., Xia Z.-M., Yan K.-F., Cai J., 2014, Equilibrium Hydrate Formation Conditions of CO_2+N_2+SO_2 Ternary Simulated Flue Gas in SO_2 and Tetra-n-butylammonium Bromide Containing Aqueous Solutions, *J. Chem. Eng. Data*, **59**, 103−109.

(139) Meysel P., Oellrich L., Bishnoi P.R., Clarke M.A., 2011, Experimental investigation of incipient equilibrium conditions for the formation of semi-clathrate hydrates from quaternary mixtures of (CO_2+N_2+TBAB+H_2O), *J. Chem. Thermodyn.*, **43**, 1475–1479.

(140) Jianwei D., Deqing L., Dongliang L. and Xinjun L., 2010, Experimental Determination of the Equilibrium Conditions of Binary Gas Hydrates of Cyclopentane + Oxygen, Cyclopentane + Nitrogen, and Cyclopentane + Hydrogen, *Ind. Eng. Chem. Res.*, **49**, 11797–11800.

(141) Galfré A., Kwaterski M., Brântuas P., Cameirao A., Herri J.-M., 2014, Clathrate Hydrate Equilibrium Data for the Gas Mixture of Carbon Dioxide and Nitrogen in the Presence of an Emulsion of Cyclopentane in Water, *J. Chem. Eng. Data*, **59**, 592−602.

(142) Tohidi B., Danesh A., Todd A.C., Burgass R.W., Ostergaard K.K., 1997, Equilibrium data and thermodynamic modelling of cyclopentane and neopentane hydrates, *Fluid Phase Equil.*, **138**, 241–250.

(143) Zheng J., Yang M., Liu Y., Wang D., Song Y., 2017, Effects of cyclopentane on CO_2 hydrate formation and dissociation as a co-guest molecule for desalination, *J. Chem. Thermodynamics* , **104**, 9–15.

(144) Van Cleeff A., Diepen G.A.M, 1960, Gas Hydrates of Nitrogen and Oxygen, *Recl. TraV. Chim. Pays-Bas.*, **79**, 582–586.

(145) Dyadin Y.A., Udachin K.A., 1987, Clathrate polyhydrates of peralkylonium salts and their analogs, *J. Struc. Chem.*, **28**, 394–432.

(146) Lin W., Dalmazzone D., Furst W., Delahaye A., Fournaison L., Clain P., 2013, Thermodynamic Studies of CO_2 + TBAB + Water System: Experimental Measurements and Correlations, *J. Chem. Eng. Data*, **58**, 2233−2239.

(147) Dietrich C.F., *Uncertainty, Calibration and Probability*, 2nd edition (Adam Hilger, Bristol, U.K., 1991)

(148) Lemmon E., Huber M., McLinden M., 2010, *NIST Standard Reference Database 23: Reference Fluid Thermodynamic and Transport Properties-REFPROP*, Version 9.0, Thermophysical Properties Division, National Institute of Standards and Technology.

(149) Plöcker U., Knapp H., Prausnitz J.M., 1978, Calculation of High-Pressure Vapor-Liquid Equilibria from a Corresponding-States Correlation with Emphasis on Asymmetric Mixtures, *Int. Chem. Proc.*, **17**, 324–334.

(150) Shahnazar S., Hasan N., 2014, Gas hydrate formation condition: Review on experimental and modeling approaches, *Fluid Phase Equilib.*, **379**, 72–85.

(151) Eslamimanesh A., Mohammadi A.H., Richon D., 2012, Thermodynamic modeling of phase equilibria of semiclathrate hydrates of CO_2, CH_4, or N_2+tetra-n-butyl ammonium bromide aqueous solution, *Chem. Eng. Sci.*, **81**, 319–328.

(152) Babaee S., Hashemi H., Mohammadi A.H., Naidoo P., Ramjugernath D., 2014, Experimental Measurement and Thermodynamic Modeling of Hydrate Dissociation Conditions for the Argon + TBAB + Water System, *J. Chem. Eng. Data*, **59**, 3900−3906.

(153) Chen G.J., Sun C.Y., Guo T.M., 2003, Modelling of the formation conditions of structure-H hydrates, *Fluid Phase Equilib.*, **204**, 107–117.

(154) Mohammadi A.H., Belandria V., Richon D., 2012, Use of an artificial neural network algorithm to predict hydrate dissociation conditions for hydrogen + water and hydrogen + tetra-n-butyl ammonium bromide + water systems, *Chem. Eng. Sci.*, **65**, 4302–4305.

(155) Fukumoto A., Paricaud P., Dalmazzone D., Bouchafaa W., Ho T., Fürst W., 2014, Modeling the Dissociation Conditions of Carbon Dioxide + TBAB, TBAC, TBAF, and TBPB Semiclathrate Hydrates, *J. Chem. Eng. Data*, **59**, 3193−3204.

(156) Fukumoto A., Dalmazzone D., Paricaud P., Fürst W., 2015, Experimental Measurements and Modeling of the Dissociation Conditions of Tetrabutylammonium Chloride Semiclathrate Hydrates in the Presence of Hydrogen, *J. Chem. Eng. Data*, **60**, 343−350.

(157) Fukumoto A., Silva L., Paricaud P., Dalmazzone D., Fürst W., 2015, Modeling of the dissociation conditions of H_2 + CO_2 semiclathrate hydrate formed with TBAB, TBAC, TBAF, TBPB and $TBANO_3$ salts. Application to CO_2 capture from syngas, *Int. J. Hydrogen Energy*, **40**, 9254−9266.

(158) Babaee S., Hashemi H., Javanmardi J., Eslamimanesh A., Mohammadi A.H., 2012, Thermodynamic model for prediction of phase equilibria of clathrate hydrates of hydrogen with different alkanes, alkenes, alkynes, cycloalkanes or cycloalkane, *Fluid Phase Equilib*., **336**, 71–78.

(159) Eslamimanesh A., Mohammadi A.H., Richon D., 2012, Thermodynamic modeling of phase equilibria of semi-clathrate hydrates of CO_2, CH_4 or N_2+tetra-n-butylammonium bromide aqueous solution, *Chem. Eng. Sci.*, **81**, 319–328.

(160) Illbeigi M., Fazlali A., Mohammadi A.H., 2011, Thermodynamic model for the pre-diction of equilibrium conditions of clathrate hydrates of methane + water-soluble or -insoluble hydrate former, *Ind. Eng. Chem. Res.*, **50**, 9437–9450.

(161) Sfaxi I.B.A., Belandria V., Mohammadi A.H., Lugo R., Richon D., 2012, Phase equilibria of CO_2+ N_2 and CO_2+CH_4 clathrate hydrates: experimental measurements and thermodynamic modelling, *Chem. Eng. Sci*., **84**, 602–611.

(162) Seo Y.T, Lee H., 2001, Multiple-Phase Hydrate Equilibria of the Ternary Carbon Dioxide, Methane, and Water Mixtures, *J. Phys. Chem. B*, **105**, 10084–10090.

(163) Seo Y., Lee H., Uchida T., 2002, Methane and carbon dioxide hydrate phase behavior in small porous silica gels: three-phase equilibrium determination and thermodynamic modeling, *Langmuir*, **18**, 9164–9170.

(164) Seo Y.T., Kang S.P., Lee H., 2001, Experimental determination and thermodynamic modeling of methane and nitrogen hydrates in the presence of THF, propylene oxide, 1,4-dioxane and acetone, *Fluid Phase Equilib.*, **189**, 99–110.

(165) Yoon J.-H., Chun M.-K., Lee H., 2002, Generalized model for predicting phase behavior of clathrate hydrate, *AIChE J.*, **48**, 1317–1330.

(166) Parrish W.R., Prausnitz J.M., 1972, Dissociation Pressures of Gas Hydrates Formed by Gas Mixtures, *Ind. Eng. Chem. Proc. Des & Dev.*, **11**, 26–35.

(167) Kontogeorgis G.M., Voutsas E.C., Yakoumis I.V., Tassios D.P., 1996, An Equation of State for Associating Fluids, *Ind. Eng. Chem. Res.*, **35**, 4310–4318.

(168) Kontogeorgis G.M., Yakoumis I.V., Meijer H., Hendriks H., Moorwood, T., 1999, Multicomponent phase equilibrium calculations for water–methanol–alkane mixtures, *Fluid Phase Equil.*, **158-160**, 201–209.

(169) Kontogeorgis G.M., Folas G.K., Muro-Suñé N., Roca Leon F., Michelsen M.L., 2008, Solvation Phenomena in Association Theories with Applications to Oil & Gas and Chemical Industries, *Oil Gas Sci. Technol. – Rev. IFP*, **63**, 305–319.

(170) McKoy V., Sinanoglu O., 1963, Theory of Dissociation Pressures of Some Gas Hydrates*, J. Chem. Phys.,* **38**, 2946-2956.

(171) Munck J., Skjold-Jorgensen S., Rasmussen P., 1988, Computations of the formation of gas hydrates, *Chem. Eng. Sci.*, **43**, 2661–2672.

(172) Holder G.D., Corbin G., Papadopoulos K. D., 1980, Thermodynamic and Molecular Properties of Gas Hydrates from Mixtures Containing Methane, Argon, and Krypton, *Ind. Eng. Chem. Fundam.*, **19**, 282–286.

(173) Takeuchi F., Ohmura R., Yasuoka K., 2009, Statistical-Thermodynamics Modeling of Clathrate-Hydrate-Forming Systems Suitable as Working Media of a Hydrate-Based Refrigeration System*, Int. J. Thermophys.*, **30**, 1838–1852.

(174) Sloan E.D., 1998, *Clathrate Hydrates of Natural Gases*, 2nd Ed., Marcel Decker, New York.

(175) Folas G.K., Kontogeorgis G.M., Michelsen M.L., Stenby E.H., 2006, Application of the Cubic-Plus-Association (CPA) Equation of State to Complex Mixtures with Aromatic Hydrocarbons, *Ind. Eng. Chem. Res.*, **45**, 1527–1538.

(176) Huang S.H., Radosz M., 1990, Equation of State for Small, Large, Polydisperse and Associating Molecules, *Ind. Eng. Chem. Res.*, **29**, 2284–2294.

(177) Herri J.-M., Bouchemoua A., Kwaterski M., Fezoua A., Ouabbas Y., Cameirao A., 2011, Gas hydrate equilibria for CO_2-N_2 and CO_2-CH_4 gas mixtures – Experimental studies and thermodynamic modeling, *Fluid Phase Equil.*, **301**, 171–190.

(178) Dharmawardhana P.B., Parrish W.R., Sloan E.D., 1980, Experimental Thermodynamic Parameters for the Prediction of Natural Gas Hydrate Dissociation Conditions, *Ind. Eng. Chem. Fundam.*, **19**, 410–414.

(179) Mehta A.P., Sloan E.D., 1996, Improved Thermodynamic Parameters for Prediction of Structure H Hydrate Equilibria, *AIChE J.*, **42**, 2036–2046.

(180) Tohidi B., Ostergaard K., Danesh A., Todd A., 1996, Equilibrium data and thermodynamic modelling of cyclohexane gas hydrates, *Chem. Eng. Sci.*, **51**, 259–263.

(181) Strobel T.A., Koh C.A., Sloan E.D., 2009, Thermodynamic predictions of various tetrahydrofuran and hydrogen clathrate hydrates, *Fluid Phase Equil.*, **280**, 61–67.

(182) Kontogeorgis G.M., Michelsen M.L., Folas G.K., Derawi S., von Solms N., Stenby E.H., 2006, Ten Years with the CPA (Cubic-Plus-Association) Equation of State. Part 1. Pure Compounds and Self-Associating Systems, *Ind. Eng. Chem. Res.*, **45**, 4855–4868.

(183) Tsivintzelis I., Kontogeorgis G.M., Michelsen M.L., Stenby E.H., 2011, Modeling phase equilibria for acid gas mixtures using the CPA equation of state. Part II: Binary mixtures with CO_2, *Fluid Phase Equil.*, **306**, 38–56.

(184) Graboski M.S., Daubert T.E., 1979, A modified Soave equation of state for phase equilibrium calculations. 2. Systems containing hydrogen, *Ind. & Eng. Chem. Proc. Des. Dev.*, **18**, 300–306.

(185) CERE ThermoSystem, *Center for Energy Resources Engineering*, 2014.

(186) Arya A., von Solms N., Kontogeorgis G.M., 2015, Determination of asphaltene onset conditions using the cubic plus association equation of state, *Fluid Phase Equil.*, **400**, 8–19.

(187) Bjørner G.M., Kontogeorgis G.M., 2016, Modeling derivative properties and binary mixtures with CO_2 using the CPA and the quadrupolar CPA equations of state, *Fluid Phase Equilib.*, **408**, 151–169.

(188) Stell G., Rasaiah J., Narang H., 1972, Thermodynamic perturbation theory for simple polar fluids. I, *Mol. Phys.*, **23**, 393-406.

(189) Rushbrooke G., Stell G., Høye J., 1973, Theory of polar liquids, *Mol. Phys.*, **26**, 1199–1215.

(190) Stell G., Rasaiah J., Narang H., 1974, Thermodynamic perturbation theory for simple polar fluids. II, *Mol. Phys.*, **27**, 1393–1414.

(191) Larsen B., Rasaiah J., Stell G., 1977, Thermodynamic perturbation theory for multipolar and ionic liquids, *Mol. Phys.*, **33**, 987–1027.

(192) Karakatsani E., Kontogeorgis G., Economou I., 2006, Evaluation of the truncated perturbed chain-polar statistical associating fluid theory for complex mixture fluid phase equilibria, *Ind. Eng. Chem. Res.*, **45**, 6063–6074.

(193) Karakatsani E.K., Economou I.G., 2006, Perturbed chain-statistical associating fluid theory extended to dipolar and quadrupolar molecular fluids, *J. Phys. Chem. B*, **110**, 9252–9261.

(194) Mohammadi A.H., Richon D., 2010, Clathrate hydrate dissociation conditions for the methane+cycloheptane/ cyclooctane+water and carbon dioxide+cycloheptane/cyclooctane+ water systems, *Chem. Eng. Sci.*, **65**, 3356–3361.

(195) Carpenter A., *CO_2 abatement in the iron and steel industry*, CCC/193, 2012, EA Clean Coal Centre.

(196) Babu P., Linga P., Kumar R., Englezos P., 2015, A review of the hydrate based gas separation (HBGS) process for carbon dioxide pre-combustion capture, *Energy*, **85**, 261–279.

(197) Kenarsari S.D., Yang D., Jiang G., Zhang S., Wang J., Russell A.G., Wie Q., Fan M., 2013, Review of recent advances in carbon dioxide separation and capture, *RSC Adv.*, **3**, 22739–22773.

(198) Xu C.G., Li X.S., 2014, Research progress of hydrate-based CO_2 separation and capture from gas mixtures, *RSC Adv.*, **4**,18301–18316.

(199) Seo Y., Kang S.-P., 2010, Enhancing CO_2 separation for pre-combustion capture with hydrate formation in silica gel pore structure, *J. Chem. Eng.*, **161**, 308–312.

(200) Seo Y., Lee H., Uchida T., 2002, Methane and carbon dioxide hydrate phase behavior in small porous silica gels: three-phase equilibrium determination and thermodynamic modeling, *Langmuir*, **18**, 9164–9170.

(201) Spencer D.F., *Methods and systems for selectively separating CO_2 from a multicomponent gaseous stream to produce a high pressure CO_2 product*, U.S. Patent No. 7,128,777; 31 Oct. 2006.

(202) Belandria V., Mohammadi A.H., Richon D., 2010, Phase equilibria of clathrate hydrates of methane+carbon dioxide: New experimental data and predictions, *Fluid Phase Equilib.*, **296**, 60–65.

(203) Ohgaki K., Takano K., Sangawa H., Matsubara T., Nakano S., 1996, Methane Exploitation by Carbon Dioxide from Gas Hydrates - Phase Equilibria for CO_2-CH_4 Mixed Hydrate System*, J. Chem. Eng. Jpn.*, **29**, 478–483.

(204) Seo Y.T., Kang S.-P., Lee H., Lee C.S., Sung W.M., 2000, Hydrate phase equilibria and the predictive curve for Gas Mixtures Containing Carbon Dioxide: A Proof-of-Concept to Carbon Dioxide Recovery from Multicomponent Gas Stream, *Korean J. Chem. Eng.*, **17**, 659–667.

(205) Unruh C.H., Katz D.L., 1949, Gas hydrates of carbon dioxide-methane mixtures, *Petrol. Trans. AIME*, **186**, 83–86.

(206) Bruusgaard H., Beltran J.G., Servio P., 2008, Vapor−Liquid Water−Hydrate Equilibrium Data for the System N_2 + CO_2 + H_2O, *J. Chem. Eng. Data*, **53**, 2594–2597.

(207) Belandria V., Eslamimanesh A., Mohammadi A.H., Richon D., 2011, Study of Gas Hydrate Formation in the Carbon Dioxide+Hydrogen+ Water Systems: Compositional Analysis of the Gas Phase, *Ind. Eng. Chem. Res.*, **50**, 6455–6459.

(208) Kim D.Y., Lee H., 2005, Spectroscopic identification of the mixed hydrogen and carbon dioxide clathrate hydrate, *J. Am. Chem. Soc.*, **127**, 9996–9997.

(209) Seo Y., Kang S.-P., 2010, Enhancing CO_2 separation for pre-combustion capture with hydrate formation in silica gel pore structure, *J. Chem. Eng.*, **161**, 308–312.

(210) Sugahara T., Murayama S., Hashimoto S., Ohgaki K., 2005, Phase equilibria for H_2+CO_2 + H_2O system containing gas hydrates, *Fluid Phase Equil.*, **233**, 190–193.

(211) Ma Q.L., Chen G.J., Ma C.F., Zhang L.W., 2008, Study of vapor–hydrate two-phase equilibria, *Fluid Phase Equilib.*, **265**, 84–93.

(212) Surovtseva D., Amin R., Barifcani A., 2011, Design and Operation of Pilot Plant for CO_2 Capture from IGCC Flue Gases by Combined Cryogenic and Hydrate Method, *Chem. Eng. Res. Des.*, **89**, 1752–1757.

(213) Beltran J.G., Servio P., 2010, Morphological investigations of methane-hydrate films formed on a glass surface, *Cryst. Growth Des.*, **10**, 4339–4347.

(214) Arjmandi M., Chapoy A., Tohidi B., 2007, Equilibrium Data of Hydrogen, Methane, Nitrogen, Carbon Dioxide, and Natural Gas in Semi-Clathrate Hydrates of Tetrabutyl Ammonium Bromide, *J. Chem. Eng. Data*, **52**, 2153–2158.

(215) Du J., Wang L., 2014, Equilibrium Conditions for Semiclathrate Hydrates Formed with CO_2, N_2, or CH_4 in the Presence of Tri-n-butylphosphine Oxide, *Ind. Eng. Chem. Res.*, **53**, 1234−1241.

(216) Li X.-S., Xu C.-G., Chen Z.-Y., Cai J., 2012, Synergic effect of cyclopentane and tetra-n-butyl ammonium bromide on hydrate-based carbon dioxide separation from fuel gas mixture by measurements of gas uptake and X-ray diffraction patterns, *Int. J. Hydrogen Energy*, **37**, 720–727.

(217) Li X.-S., Xia Z.-M., Chen Z.-Y., Wu H.-J., 2011, Precombustion Capture of Carbon Dioxide and Hydrogen with a One-Stage Hydrate/Membrane in the Presence of Tetra-butylammonium Bromide (TBAB), *Energy Fuels*, **25**, 1302–1309.

(218) Li X.-S., Xia Z.-M., Chen Z.-Y., Yan K.-F., Li G., Wu H.-J., 2010, Gas Hydrate Formation Process for Capture of Carbon Dioxide from Fuel Gas Mixture, *Ind. Eng. Chem. Res.*, **49**, 11614–11619.

(219) Li S., Fan S., Wang J., Lang X., Liang D., 2009, CO_2 capture from binary mixture *via* forming hydrate with the help of tetra-*n*-butyl ammonium bromide, *J. Nat. Gas Chem.*, **18**, 15–20.

(220) Xu C.-G., Li X.-S., Lv Q.-N., Chen Z.-Y., Cai J., 2012, Hydrate-based CO_2 (carbon dioxide) capture from IGCC (integrated gasification combined cycle) synthesis gas using bubble method with a set of visual equipment, *Energy*, **44**, 358–366.

(221) Xu C.-G., Zhang S.-H., Cai J., Chen Z.-Y., Li X.-S., 2013, CO_2 (carbon dioxide) separation from CO_2–H_2 (hydrogen) gas mixtures by gas hydrates in TBAB (tetra-n-butyl ammonium bromide) solution and Raman spectroscopic analysis, *Energy*, **59**, 719–725.

(222) Sabil K.M., Witkamp G.-J., Peters C.J., 2009, Phase equilibria of mixed carbon dioxide and tetrahydrofuran hydrates in sodium chloride aqueous solutions, *Fluid Phase Equil.*, **284**, 38–43.

(223) Yang M., Liu W., Song Y., Ruan X., Wang X., Zhao J., Jiang L., Li Q., 2013, Effects of Additive Mixture (THF/SDS) on the Thermodynamic and Kinetic Properties of CO_2/H_2 Hydrate in Porous Media, *Ind. Eng. Chem. Res.*, **52**, 4911−4918.

(224) Servio P., Lagers F., Peters C., Englezos P., 1999, Gas hydrate phase equilibrium in the system methane–carbon dioxide–neohexane and water, *Fluid Phase Equil.*, **158–160**, 795–800.

(225) Abolala M., Karamoddin M., Varaminian F., 2014, Thermodynamic modeling of phase equilibrium for gas hydrate in single and mixed refrigerants by using sPC-SAFT equation of state, *Fluid Phase Equilib.*, **370**, 69–74.

(226) Clarke M.A., Bishnoi P.R., 2004, Development of a new equation of state for mixedsalt and mixed solvent systems and application to vapour–liquid and solid(hydrate)–vapour–liquid equilibrium calculations, *Fluid Phase Equilib.*, **220**, 21–35.

(227) Eslamimanesh A., Mohammadi A.H., Richon D., 2011, An improved Clapeyron model for predicting liquid water–hydrate–liquid hydrate former phase equilibria, *Chem. Eng. Sci.*, **66**, 1759–1764.

(228) Eslamimanesh A., Gharagheizi F., Mohammadi A.H., Richon D., 2012, A statistical method for evaluation of the experimental phase equilibrium data of simple clathrate hydrates, *J. Chem. Eng. Sci.*, **80**, 402–408.

(229) Fan S.S., Chen G.J., Ma Q.L., Guo T.M., 2000, Experimental and modeling studies on the hydrate formation of CO_2 and CO_2-rich gas mixtures, *J. Chem. Eng.*, **78**, 173–178.

(230) Herri J.M., Bouchemoua A., Kwaterski M., Fezoua A., Ouabbas Y., Cameirao A., 2011, Gas hydrate equilibria for CO_2–N_2 and CO_2–CH_4 gas mixtures—experimental studies and thermodynamic modelling, *Fluid Phase Equilib.*, **301**, 171–190.

(231) Handa Y.P., Tse J.S., 1986, Thermodynamic Properties of Empty Lattices of structure I and Structure II Clathrate Hydrate, *J. Phys. Chem.*, **23**, 5917–5921.

(232) Javanmardi J., Moshfeghian M., Maddox R.N., 2001, An accurate model for predic-tion of gas hydrate formation conditions in mixtures of aqueous electrolytesolutions and alcohol, *Can. J. Chem. Eng.*, **79**, 367–373.

(233) Aasberg-Petersen K., Stenby E., Fredenslund A., 1991, Prediction of High-pressure Gas Solubility in Aqueous Mixture of Electrolytes, *Ind. Eng. Chem. Res.*, **30**, 2180–2185.

(234) Jager M.D., Sloan E.D., 2001, The effect of pressure on methane hydration in pure water and sodium chloride solutions, *Fluid Phase Equilib.*, **185**, 89–99.

(235) Kim S.H., Seo M.D., Kang J.W., Lee C.S., 2011, Hydrate-containing phase equilibria for mixed guests of carbon dioxide and nitrogen, *Fluid Phase Equilib.*, **306**, 229–233.

(236) Klauda J.B., Sandler S.I., 2003, Phase behavior of clathrate hydrates: a model for single and multiple gas component hydrates, *Chem. Eng. Sci.*, **58**, 27–41.

(237) Li X.S., Englezos P., 2004, Vapor–liquid equilibrium of systems containing alcohols, water, carbon dioxide and hydrocarbons using SAFT, *Fluid Phase Equilib.*, **224**, 111–118.

(238) Mei D.-H., Liao J., Yang J.-T., Guo T.-M., 1996, Experimental and modeling studies on the hydrate formation of a methane + nitrogen gas mixture in the presence ofaqueous electrolyte solutions, *Ind. Eng. Chem. Res.*, **35**, 4342–4347.

(239) Moradi G., Khosravani E., 2012, Application of PRSV2 equation of state to predict hydrate formation temperature in the presence of inhibitors, *Fluid Phase Equilib.*, **333**, 18–26.

(240) Moradi G., Khosravani E., 2013, Modeling of hydrate formation conditions for CH_4,C_2H_6, C_3H_8, N_2, CO_2 and their mixtures using the PRSV2 equation of state and obtaining the Kihara potential parameters for these components, *Fluid Phase Equilib.*, **338**, 179–187.

(241) Osfouri S., Azin R., Gholami R., Izadpanah A.A., 2015, Modeling hydrate formation conditions in the presence of electrolytes and polar inhibitor solutions, *J. Chem. Thermodyn.*, **89**, 251–263.

(242) Ramana Avula V., Gardas R.L., Sangwai J.S., 2014, An improved model for the phase equilibrium of methane hydrate inhibition in the presence of ionic liquids, *Fluid Phase Equilib.*, **382**, 187–196.

(243) Renault-Crispo J.-S., Lang F., Servio P., 2014, The importance of liquid phase compositions in gas hydrate modeling: carbon dioxide–methane–water case study, *J. Chem. Thermodyn.*, **68**, 153–160.

(244) Seo Y.T., Lee H., Yoon J.H., 2001, Hydrate Phase Equilibria of the Carbon Dioxide, Methane, and Water System, *J. Chem. Eng. Data*, **46**, 381–384.

(245) Sun C.-Y., Chen G.-J., 2005, Modelling the hydrate formation condition for sour gas and mixtures, *Chem. Eng. Sci.*, **60**, 4879–4885.

(246) Sun R., Duan Z.H., 2005, Prediction of CH_4 and CO_2 hydrate phase equilibrium and cage occupancy from ab initio intermolecular potentials, *Geochim. Cosmochim. Acta*, **69**, 4411–4424.

(247) Duan Z. H., Sun R., 2006, A model to predict phase equilibrium of CH_4 and CO_2 clathrate hydrate in aqueous electrolyte solutions, *Am. Mineral.*, **91**, 1346–1354.

(248) Tavasoli H., Feyzi F., Dehghani M.R., Alavi F., 2011, Prediction of gas hydrate formation condition in the presence of thermodynamic inhibitors with the Elliott–Suresh–Donohue equation of state, *J. Petrol. Sci. Eng.*, **77**, 93–103.

(249) Tsimpanogiannis I.N., Papadimitriou N.I., Stubos A.K., 2012, On the limitation of the van der Waals–Platteeuw-based thermodynamic models for hydrates with multiple occupancy of cavities, Mol. Phys., **110**, 1213–1221.

(250) Valavi M., Dehghani M.R., 2012, Application of PHSC equation of state in prediction of gas hydrate formation condition, *Fluid Phase Equilib.*, **333**, 27–37.

(251) Yang S.O., Cho S.H., Lee H., Lee C.S., 2001, Measurement and prediction of phase equilibria for water + methane in hydrate forming conditions, *Fluid Phase Equilib.*, **185**, 53–63.

(252) Ameripour S., Barrufet M., 2009, Improved correlations predict hydrate formation pressures or temperatures for systems with or without inhibitors, *J. Can. Petrol. Technol.,* **48**, 45–50.

(253) Bahadori A., Vuthaluru H.B., 2009, Prediction of hydrate formation temperature for natural gas using artificial neural network, *J. Nat. Gas Chem.*, **18**, 453–457.

(254) Eslamimanesh A., Mohammadi A.H., Richon D., 2011, Thermodynamic model for predicting phase equilibria of simple clathrate hydrates of refrigerants, *Chem.Eng. Sci.*, **66**, 5439–5445.

(255) Hosseini-Nasab S.M., Sefti M.V., Mohammadi A., 2012, The development of a new empirical correlation for predicting hydrate formation conditions, *Petrol. Sci.Technol*, **30**, 1755–1767.

(256) Omole O., Falode O.A., Arinkoola A.O., 2009, Development of empirical correlations for predicting formation of gas hydrate, *Int. J. Oil Gas Coal Technol.*, **2**, 24–43.

(257) Rashidabad V.N., Hatami A., Ebrahimi A., 2013, The thermodynamics effect of sodium chloride and sodium sulfate on the prevention of methane hydrate formation and offering its thermodynamics model by using neural networks, *J. Am. Sci.*, **9**, 116–124.

(258) Sloan E.D., Koh C.A., 2007, *Clathrate Hydrates of Natural Gases*, 3rd Ed., CRC Press, Boca Raton, USA.

(259) Avlonitis D., Danesh A., Todd A.C., 1994, Prediction of VL and VLL equilibria of mixtures containing petroleum reservoir fluids and methanol with a cubic EoS, *Fluid Phase Equil.*, **94**, 181–216.

(260) Ma Q., Chen G., Guo T., Zhang K., Zuo J. Y., Dan Z., Ng H.-J., 2005, Prediction of Structure-H Gas Hydrate Formation Conditions for Reservoir Fluids, *Chin. J. Chem. Eng*., **13**, 484–490.

Appendix A

The next Tables A.1 and A.2 present CO_2 hydrate experiments without and with promoter, respectively.

Table A.1 Experimental studies for gas hydrates of CO_2 + gas/gas mixture systems+ H_2O

Author(s)	Gas system (water is omitted)	Conditions		Study
		Temperature (K)	Pressure (Mpa)	
Adisasmito *et al.*[117]	CO_2 + CH_4	273.7– 287.6	2.52–10.95	PVT studies on dissociation conditions of gas hydrates
Belandria *et al.*[202]	CO_2 + CH_4	279.1– 289.9	2.96–13.06	PVT studies on dissociation conditions of gas hydrates
Belandria *et al.*[63]	CO_2 + CH_4	277.9– 285.5	1.51–8.27	PVT studies on dissociation conditions + compositions of vapor, liquid, and hydrate phases through measurements by a new designed apparatus and a mass balance approach
Ohgaki *et al.*[203]	CO_2 + CH_4	280.3	3.04–5.46	PVT studies on dissociation conditions + compositions of vapor and hydrate phases
Seo *et al.*[204]	CO_2 + CH_4	274.36–283.56	1.5–5.0	PVT studies on dissociation conditions of gas hydrates
	CO_2 + N_2	272.66–283.56	1.5–5	PVT studies on dissociation conditions + compositions of vapor and hydrate phases
Uchida *et al.*[43]	CO_2 + CH_4	258– 274.1 and 190	0.5–3 and 0.1	Kinetic study: investigation of the change of vapor-phase composition and cage occupancies using gas

				chromatography and Raman spectroscopy
Unruh and Katz[205]	$CO_2 + CH_4$	275.5– 285.7	1.99–7.0	PVT studies on dissociation conditions of gas hydrates
Belandria *et al.*[52]	$CO_2 + N_2$	273.6– 281.7	2.032–17.623	PVT studies on dissociation conditions + compositions of vapor, liquid, and hydrate phases through measurements by a new designed apparatus and a mass balance approach
Bruusgaard *et al.*[206]	$CO_2 + N_2$	274.3– 283.0	1.6–22.4	PVT studies on dissociation conditions + compositions of vapor in equilibrium with gas hydrate
Kang *et al.*[80]	$CO_2 + N_2$	274.95–282.00	1.39–32.3	PVT studies on dissociation conditions + compositions of vapor and hydrate phases
	$CO_2 + N_2$+THF	274.95–295.45	0.2 – 12.8	
Kang *et al.*[81]	$CO_2 + N_2$+THF	273.65	0.1	dissociation enthalpy by an isothermal microcalorimeter
Seo and Lee[26]	$CO_2 + N_2$	272.1	3.2– 14.5	PVT studies on dissociation conditions + compositions of vapor and hydrate phases
Belandria *et al.*[207]	$CO_2 + H_2$	273.6– 281.7	1.888–8.570	PVT studies on dissociation conditions + compositions of vapor phase through measurements by a new designed apparatus
Kim and Lee[208]	$CO_2 + H_2$	123.15	0.1	1H MAS NMR on cage occupancy by hydrogen molecules, gas chromatography of released gas from hydrate on cage

				occupancy by hydrogen molecules
Seo and Kang[209]	CO_2 + H_2	274.15	6.0– 9.2	PVT studies on dissociation conditions + ^{13}C NMR on cage occupancy by hydrogen molecules in hydrate formed in silica gel particles
Sugahara *et al.*[210]	CO_2 + H_2	274.3– 281.9	1.42– 9.13	Raman spectroscopy using quartz windows on cage occupancy by hydrogen molecules and direct gas release method
Ma *et al.*[211]	CO_2+H_2 +CH_4, CO_2+H_2 +N_2 +CH_4 and CO_2+CH_4 +C_2H_4	277.7– 288.2	0.28– 2.05	PVT studies on equilibrium conditions of semi-clathrate hydrate
Surovtseva *et al.*[212]	CO_2 + H_2 + N_2 + CH_4 + Ar+ para-toluene sulphonic acid (PTSA)	222	2.8, 5.3, 5.7	Combination of a gas hydrate formation process with a low temperature cryogenic one for capturing CO_2 from a coal gas stream. The operational conditions and the amount of captured CO_2 have been reported.

Table A.2 Experimental studies on clathrate/semi-clathrate hydrate for CO_2 + gas/gases systems + H_2O + promoters.

Author(s)	Gas system (water is omitted)	Conditions		Study
		Temperature (K)	Pressure (MPa)	

Beltran and Servio[213]	CO_2 + CH_4 + water/ neohexane emulsion	275.14–285.34	2.36–7.47	PVT studies on dissociation conditions + composition of vapor phase in equilibrium with hydrate phase
Acosta *et al.*[129]	CO_2 + CH_4 + TBAB	286– 293	3– 6.5	PVT studies
Arjmandi *et al.*[214]	CO_2 + N_2 + TBAB	285.15–292.95	4.688–33.503	PVT studies on dissociation conditions
	CO_2 + H_2 + TBAB	280.15–288.00	3.600–23.07	
	CO_2 + CH_4 + TBAB	287.15–298.15	4.688–41.369	
	CO_2 + TBAB	285.55–291.15	1.400–4.090	
	Natural Gas (NG) + TBAB	280.35–292.45	0.979–9.515	
Deschamps and Dalmazzone[130]	N_2 + TBAB	284.8–291.6	0.1– 20.5	Measurement of dissociation conditions, heat flow and phase diagram
	CO_2 + TBAB	284.8–288.6	0.1– 2.25	
	CO_2 + N_2 + TBAB	284.8–293.3	0.1– 9.18	
	CO_2 + CH_4 + TBAB	284.8–292.4	0.1–3.2	
Deschamps and Dalmazzone[44]	CO_2 + N_2 + TBAB and CO_2 + CH_4 + TBAB	284.8–293.3	0.1– 9.18	Measurements of dissociation enthalpy via differential scanning calorimetry (DSC) under pressure
Du and Wang[215]	N_2 + TBAB CH_4 + TBAB N_2 + Tri-n-butylphosphine Oxide (TBPO) CO_2 + TBPO CH_4 + TBPO	283.94 – 300.34	0.35 – 19.43	PVT studies
Duc *et al.*[9]	CO_2 (+TBAB)	279.3–285	3.5–24.3 (0.273–0.986)	PVT studies on dissociation conditions + composition of vapor
	N_2 (+TBAB)	279.3–284	30.3–50.0 (0.664–2.9)	

	CO_2 + N_2 (+ TBAB)	282.25–295.25	3.63–5.32	phase in equilibrium with hydrate phase
Fan *et al.*[116]	CO_2 + N_2 + TBAB	277.65	3.36–7.31	Measurements of semi-clathrate hydrate formation conditions and the effects of different additives through using equilibrium cell
	CO_2 + N_2 + TBAF	277.65	2.19–6.79	
Kim *et al.*[57]	CO_2 + H_2 + TBAB	283–290	2.5–5.0	PVT and kinetic studies on hydrate formation conditions, gas consumption, induction time of semi-clathrate gas hydrates of a flue gas containing CO_2+H_2 in a hydrate formation reactor. Enclathration of CO_2 molecules observed by Raman Spectroscopy
Li *et al.*[102]	CO_2 +H_2O	275.4–281.2	1.55–2.29	PVT measurements on formation and dissociation hydrate condition
	CO_2 + TBAB	280.2–288.8	0.4– 2.42	
	CO_2 + TBAC	280.1–289.2	0.47–3.77	
	CO_2 + TBAF	285.7–293.5	0.53–3.00	
	CO_2 +H_2O	275.4– 281.2	1.55–2.29	
Li *et al.*[70]	CO_2 + N_2 + TBAB + dodecyl trimethyl ammonium chloride (DTAC)	274.95–277.15	0.66–2.66	Measurement of induction time, pressure drop, split fraction via a crystallizer cell
Lin *et al.*[118]	CO_2 + TBAB	282.59–288.09	0.344–2.274	Measurements of dissociation enthalpy via

				differential thermal analysis (DTA) under pressure
Li *et al.*[134]	CO_2 + H_2 + CP + TBAB	274.65− 276.65	2.5− 4.5	Induction time, gas and hydrate phase composition, hydrate formation rate
Li *et al.*[216]	CO_2 + H_2 + CP + TBAB	274.65	4.0	Gas uptake and separation efficiency, Residual gas compositions at equilibrium, powder XRD analysis
Li *et al.*[217]	CO_2 + H_2 + TBAB	275.15− 285.15	1.00− 4.50	Induction time, gas consumed, vapor phase and residual gas compositions at equilibrium
Li *et al.*[218]	CO_2 + H_2 + TBAB	275.15− 282.45	1.00− 4.50	Induction time, gas consumed, residual gas compositions, Gas/Liquid Phase Volume Ratio
Li *et al.*[219]	CO_2 + TBAB	277.65	4.01	Kinetic studies
Li *et al.*[108]	CO_2 + N_2 +TBAB	275.15− 277.15	2.0− 2.3	PVT studies, induction time, gas consumption, hydrate and residual gas compositions at equilibrium
	CO_2 + N_2 + TBPB	275.15− 277.15	2.0− 2.3	
	CO_2 + N_2 + $TBANO_3$	274.15− 275.15	2.0− 4.0	
Lu *et al.*[84]	CO_2 + N_2 + TBAB/THF	278.05– 287.85	1.17–5.84	PVT studies on dissociation conditions of gas hydrates
Meysel *et al.*[139]	CO_2 + N_2 + TBAB	278.05– 293.3	1.956– 5.901	PVT studies on equilibrium conditions of semi-clathrate hydrate in a jacketed isochoric cell reactor

Mohammadi *et al.*[137]	$CO_2 + N_2 + TBAB$	277.1–293.2	1.12–16.21	PVT studies and compositional data of the gas phase in equilibrium with hydrate and aqueous solution
Park *et al.*[103]	$CO_2 + H_2 + TBAB$ $CO_2 + H_2 + TBAF$	282–290 293–302	0.5– 8	studies, Raman and NMR studies, gas composition and consumption
Xia *et al.*[91]	$CO_2 + CH_4 + TBAB$	284.45−291.55	0.00−2.83	PVT studies
	$CO_2 + CH_4 + THF$	277.85−294.95	0.00−2.08	
	$CO_2 + CH_4$ + Dimethyl sulfoxide (DMSO)	274.25−279.55	1.83−4.30	
	$CO_2 + CH_4 + TBAB$ + DMSO	274.25−291.55	0.00−6.40	
	$CO_2 + CH_4 + THF + DMSO$	274.25−294.95	0.00−6.40	
Xu *et al.*[220]	$CO_2 + TBAB$	274.15	3.0	Vapor phase and residual gas compositions, Effect of bubble size
Xu *et al.*[221]	$CO_2 + H_2 + TBAB$	274.15–284.5	0.08–6.00	PVT studies, Raman studies, gas consumption, hydrate compositions at equilibrium
Linga *et al.* [82]	$CO_2 + N_2 + THF$	273.75–275.95	0.92–3.2	PVT and kinetic studies on CO_2 capture from its mixture with N_2 via clathrate hydrate structures. Induction times, hydrate formation rates, CO_2 uptake amount accompanied with molar compositions of hydrate and vapor phases have also been measured

Delahaye *et al.*[87]	CO_2 + THF	278.3–290.7	0.19–2.52	Measurements of dissociation enthalpy via DTA and DSC under pressure
Hashimoto *et al.*[94]	CO_2 + H_2 + THF	280.1	0.23–2.46	PVT studies, Raman spectroscopy
Herslund *et al.*[22]	CO_2 + THF	283.3–285.2	0.61–0.91	PVT and kinetic studies on hydrate formation conditions, water consumption + compositions of promoters in equilibrium with gas hydrate
	CO_2 + CP + THF	275.1–286.6	0.3– 0.8	
Kang and Lee[95]	CO_2 + N_2 + THF	272–295	0.5– 13	PVT studies
Lee *et al.*[85]	CO_2 + H_2 + THF	279.2–283.6	.51–3.69	PVT and kinetic studies on hydrate formation conditions, gas consumption, induction time of gas hydrates of a flue gas containing CO_2+H_2 in a hydrate formation reactor
Lee *et al.*[111]	CO_2 + THF	279.7−291.1	0.18−2.17	PVT studies, gas and hydrate phase composition, Raman and XRD spectroscopy
	CO_2 + CH_4 + THF	283	0.50−0.52	
		290	1.37−2.36	
Linga *et al.*[83]	CO_2 + N_2 + THF	273.7	1.5	Induction time, gas consumed, vapor phase composition
Martinez *et al.*[86]	CO_2 + THF	275–303	0.21–2.01	Measurements of dissociation enthalpy via

				differential scanning calorimetry (DSC) under pressure
Ricaurte *et al.*[78]	CO_2 + CH_4 + THF + SDS	275−283	1.82−2.35	PVT studies, gas consumption and composition at equilibrium
Sabil *et al.*[98]	CO_2 + THF	286.21–295.47	0.90–7.05	PVT studies on hydrate formation conditions
Sabil *et al.* [97]	CO_2 + THF	275.12−291.51	1.05−2.60	PVT studies, dissociation enthalpy, compressibility factor
Sabil *et al.*[96]	CO_2 + THF	284.4– 290.5	1.53 – 2.47	PVT studies, induction time, gas consumption
Sabil *et al.*[222]	CO_2 + THF + NaCl	267.55–289.82	0.80–7.05	PVT studies
Sabil *et al.*[96]	CO_2 + THF	284.4– 290.5	1.53 – 2.47	PVT studies, induction time, gas consumption
	CO_2 + THF + NaCl	283.9– 288.3	1.73 – 2.03	
Yang *et al.*[223]	CO_2 + H_2 + THF	278.55−290.95	3.00−8.23	PVT studies, induction time
Makino *et al.*[105]	CO_2 + TBAC	289.27 – 293.33	0.36 – 4.42	PVT studies on hydrate formation conditions
Mayoufi *et al.*[121]	CO_2 + TBAC	287.6 –291.7	0– 2.0	Measurements of dissociation enthalpy via DSC under pressure
	CO_2 + $TBANO_3$	278.4 –282.3		
	CO_2 + TBPB	281.1 – 289.0		
Mohammadi and Richon[72]	CO_2 + methyl-CP	276.7–279.4	1.81–2.56	PVT studies on hydrate formation conditions
	CO_2 + methyl-cyclohexane (mCH)	276.4–280.4	1.69–2.91	
	CO_2 + CP	284.3–291.8	0.35–2.52	
	CO_2 + CH	275.2–278.1	0.95–1.81	
Cha and Seol[15]	CO_2 + CP	280.0– 289.0	3.1	Kinetic studies on hydrate formation conditions, gas
	CO_2 + CH	275.5– 282.0		

				consumption, induction time
Mooijer-van den Heuvel *et al.*[74]	CO_2 + tetrahydropyran (THP)	280.43–291.47	0.42–4.2	PVT studies on hydrate formation conditions + hydrate compositions at equilibrium
	CO_2 + cyclobutanone (CB)	279.12–315.91	0.38–11.90	
	CO_2 + CH	274.97–288.50	0.90–10.40	
	CO_2 + mCH	277.06–280.99	1.86–10.89	
Zhang and Lee[133]	CO_2 + CP	286.65–292.61	0.89–2.51	PVT on hydrate dissociation conditions, dissociation enthalpy via μDSC
Li *et al.*[71]	CO_2 + N_2 + CP	281.1	2.49–3.95	The kinetics of hydrate formation in a flue gas sample containing CO_2 + N_2 have been studied in a reactor along with measurements of vapor and hydrate compositions at equilibrium
	CO_2 + N_2 + CP	281.1	2.60–3.66	
Zhang *et al*.[88]	CO_2 + H_2 + CP	284– 291	1.5 –4.5	Measurements of dissociation enthalpy via DSC under pressure
	CO_2 + H_2 + THF	284– 289.5	3.5–15	
Shin *et al.*[92]	CO_2 + 3-methyl-1-butanol (3M1B)	272.6 − 282.8	1.14− 4.35	PVT studies, Raman spectroscopy, XRD
	CO_2 + 1,4-dioxane (DXN)	281.7− 292	1.15− 4.25	
Seo *et al.*[79]	CO_2 + THF	279.75− 290.05	0.35− 2.08	PVT studies
	CO_2 + Propylene Oxide (PO)	271.95− 281.45	0.38− 2.00	
	CO_2 + DXN	274.65− 280.95	1.08− 2.76	
	CO_2 + acetone	270.05− 279.15	0.81− 2.54	
	CO_2 + DXN	274.65− 280.95	1.08− 2.76	

Shin *et al.*[92]	CO_2 + acetone	270.05−279.15	0.81−2.54	
Van Denderen *et al.*[93]	CO_2 + CH_4 + THF	275.15	1.5−8	PVT studies, Raman spectroscopy, XRD, Kinetic studies
	CO_2 + CH_4 + Cetyl trimethyl ammonium bromide (CTAB)	275.15	6− 8	
	CO_2 + CH_4 + fluorosurfactant	275.15	6− 8	
Servio *et al.*[224]	CO_2 + CH_4 + neohexane	273.9– 283.2	1.3– 5.10	PVT studies

Appendix B

Experimental uncertainties of temperature and pressure are shown in Tables B.1, B.2, and B.3.

Table B.1 Hydrate equilibrium points for CP and TBAB+CP solutions with temperature and pressure uncertainties.

Temperature		Pressure		CP	CO_2 in CO_2 +N_2 gas mixture	*U (T)*	*U(P)*
K	°C	bar	MPa	wt% (mol%)	mol%	(°C)	(bar)
286.73	13.58	19.97	2.00	20 (6.03)	6.87	0.036	0.070
290.36	17.21	38.61	3.86	20 (6.03)	6.87	0.026	0.034
291.32	18.17	49.64	4.96	20 (6.03)	6.87	0.023	0.018
293.13	19.98	65.25	6.53	20 (6.03)	6.87	0.023	0.020
286.41	13.26	18.91	1.89	52.57 (22.15)	6.87	0.023	0.018
289.27	16.12	34.54	3.45	52.57 (22.15)	6.87	0.023	0.028
291.14	17.99	49.37	4.94	52.57 (22.15)	6.87	0.023	0.017
293.04	19.89	65.09	6.51	52.57 (22.15)	6.87	0.023	0.022
				TBAB - wt% (mol%) + CP (5 vol%)			
280.20	7.05	22.10	2.21	5 (0.29)	6.87	0.037	0.023
281.45	8.30	32.66	3.27	5 (0.29)	6.87	0.039	0.031
282.82	9.67	49.64	4.96	5 (0.29)	6.87	0.025	0.019
283.59	10.44	62.16	6.22	5 (0.29)	6.87	0.039	0.037
282.75	9.60	19.51	1.95	10 (0.62)	6.87	0.023	0.018
284.25	11.10	33.76	3.38	10 (0.62)	6.87	0.024	0.019
285.41	12.26	49.35	4.94	10 (0.62)	6.87	0.027	0.028
286.34	13.19	65.50	6.55	10 (0.62)	6.87	0.024	0.020
285.38	12.23	18.59	1.86	20 (1.38)	6.87	0.023	0.017

286.48	13.33	32.84	3.28	20 (1.38)	6.87	0.026	0.092
287.96	14.81	44.57	4.46	20 (1.38)	6.87	0.025	0.061
290.32	17.17	57.10	5.71	20 (1.38)	6.87	0.040	0.122

Table B.2 Hydrate equilibrium points for TBAB solution with temperature and pressure uncertainties.

Temperature		Pressure		TBAB	CO_2 in CO_2 +N_2 gas mixture	*U (T)*	*U(P)*
K	°C	bar	MPa	wt% (mol%)	mol%	(°C)	(bar)
279.83	6.68	18.26	1.83	5 (0.29)	11.24	0.037	0.018
281.47	8.32	37.68	3.77	5 (0.29)	11.24	0.058	0.028
281.48	8.33	23.07	2.31	5 (0.29)	14.92	0.032	0.019
283.15	10.00	42.13	4.21	5 (0.29)	14.92	0.041	0.023
284.21	11.06	52.98	5.30	5 (0.29)	14.92	0.023	0.017
284.74	11.59	62.14	6.21	5 (0.29)	14.92	0.032	0.020
282.51	9.36	18.87	1.89	10 (0.62)	6.87	0.026	0.019
284.3	11.15	34.23	3.42	10 (0.62)	6.87	0.039	0.021
285.17	12.02	48.44	4.84	10 (0.62)	6.87	0.026	0.021
286.56	13.41	64.47	6.45	10 (0.62)	6.87	0.025	0.020
283.83	10.68	23.06	2.31	10 (0.62)	14.92	0.026	0.020
285.37	12.22	36.13	3.61	10 (0.62)	14.92	0.024	0.019
286.91	13.76	53.76	5.38	10 (0.62)	14.92	0.024	0.028
287.97	14.82	72.06	7.21	10 (0.62)	14.92	0.023	0.017
285.06	11.91	19.81	1.98	20 (1.38)	6.87	0.024	0.018
286.09	12.94	32.85	3.28	20 (1.38)	6.87	0.023	0.017
287.18	14.03	47.7	4.77	20 (1.38)	6.87	0.025	0.050
288.04	14.89	61.58	6.16	20 (1.38)	6.87	0.023	0.028

Table B.3 Hydrate equilibrium points for TBAF solution with temperature and pressure uncertainties.

Temperature		Pressure		TBAF	CO_2 in CO_2 +N_2 gas mixture	*U(T)*	*U(P)*
K	°C	bar	MPa	wt% (mol%)	mol%	(°C)	(bar)
293.18	20.03	20.32	2.03	10 (0.76%)	0.48	0.057	0.021
293.61	20.46	35.50	3.55	10 (0.76%)	0.48	0.035	0.019
293.91	20.76	50.13	5.01	10 (0.76%)	0.48	0.030	0.019
294.14	20.99	64.17	6.42	10 (0.76%)	0.48	0.025	0.018
294.30	21.15	79.13	7.91	10 (0.76%)	0.48	0.049	0.029
287.05	13.90	9.68	0.97	5 (0.36%)	0.48	0.023	0.017

287.55	14.40	25.55	2.55	5 (0.36%)	0.48	0.023	0.017
288.20	15.05	47.58	4.76	5 (0.36%)	0.48	0.033	0.018
288.93	15.78	72.48	7.25	5 (0.36%)	0.48	0.028	0.019
280.99	7.84	10.19	1.02	3.2 (0.23%)	0.48	0.023	0.017
281.61	8.46	24.75	2.48	3.2 (0.23%)	0.48	0.023	0.017
282.23	9.08	40.51	4.05	3.2 (0.23%)	0.48	0.023	0.017
282.88	9.73	66.92	6.69	3.2 (0.23%)	0.48	0.023	0.017
283.35	10.20	82.84	8.28	3.2 (0.23%)	0.48	0.023	0.017
				TBAF – wt% (mol%) +5 vol%CP			
292.64	19.49	9.69	0.97	10 (0.76%)	0.48	0.023	0.017
293.34	20.19	25.65	2.57	10 (0.76%)	0.48	0.023	0.017
293.91	20.76	47.68	4.77	10 (0.76%)	0.48	0.023	0.017
294.05	20.90	71.42	7.14	10 (0.76%)	0.48	0.023	0.017
286.29	13.14	12.84	1.28	5 (0.36%)	0.48	0.023	0.017
287.78	14.63	29.89	2.99	5 (0.36%)	0.48	0.023	0.017
288.44	15.29	47.31	4.73	5 (0.36%)	0.48	0.023	0.017
289.62	16.47	69.10	6.91	5 (0.36%)	0.48	0.023	0.017

Molar concentration uncertainties of inserted gas are shown in Tables B.4.

Table B.4 Gas molar composition and gas inserted uncertainty U(n_{gas}) for every hydrate equilibrium point.

CO_2 inserted (mol)	**N_2 inserted** (mol)	**H_2O inserted** (mol)	**Promoter inserted** (mol)	**U(n_{gas})**	**CO_2 in CO_2 +N_2 gas mixture** (mol%)	**Promoter concentration** (wt%)	
0.00773	0.0692	1.31	0.00403	**1.89%**	14.92%	5%	TBAB
0.00698	0.0626	1.31	0.00403	**2.02%**	14.92%	5%	TBAB
0.01673	0.1499	1.31	0.00403	**1.75%**	14.92%	5%	TBAB
0.00861	0.0771	1.31	0.00403	**1.91%**	14.92%	5%	TBAB
0.00873	0.0782	1.24	0.00806	**1.94%**	14.92%	10%	TBAB
0.00778	0.0697	1.24	0.00806	**1.95%**	14.92%	10%	TBAB
0.01095	0.0981	1.24	0.00806	**1.98%**	14.92%	10%	TBAB
0.00660	0.0591	1.24	0.00806	**2.00%**	14.92%	10%	TBAB
0.00604	0.0749	1.31	0.00403	**1.91%**	11.24%	5%	TBAB
0.00942	0.1169	1.31	0.00403	**1.90%**	11.24%	5%	TBAB
0.00484	0.1031	1.24	0.00806	**1.75%**	6.87%	10%	TBAB
0.00589	0.1255	1.24	0.00806	**1.75%**	6.87%	10%	TBAB
0.00509	0.1084	1.24	0.00806	**1.79%**	6.87%	10%	TBAB

0.00523	0.1114	1.24	0.00806	**1.78%**	6.87%	10%	TBAB
0.00643	0.1371	0.51	0.06507	**1.72%**	6.87%	40%	CP
0.00451	0.0960	0.51	0.06507	**1.94%**	6.87%	40%	CP
0.00434	0.0926	0.51	0.06507	**1.79%**	6.87%	40%	CP
0.00447	0.0954	0.51	0.06507	**1.87%**	6.87%	40%	CP
0.00757	0.1613	1.19	0.05667	**2.33%**	6.87%	20%	CP
0.00431	0.0918	1.19	0.05667	**2.17%**	6.87%	20%	CP
0.00330	0.0703	1.19	0.05667	**1.91%**	6.87%	20%	CP
0.00492	0.1048	1.19	0.05667	**1.81%**	6.87%	20%	CP
0.00482	0.1028	1.64	0.03002	**1.77%**	6.87%	10%	TBAB+CP (5 vol%)
0.00457	0.0973	1.64	0.03002	**1.81%**	6.87%	10%	TBAB+CP (5 vol%)
0.00338	0.0721	1.64	0.03002	**2.22%**	6.87%	10%	TBAB+CP (5 vol%)
0.00467	0.0996	1.64	0.03002	**1.83%**	6.87%	10%	TBAB+CP (5 vol%)
0.00445	0.0948	2.19	0.03065	**1.89%**	6.87%	5%	TBAB+CP (5 vol%)
0.00221	0.0471	2.19	0.03065	**2.97%**	6.87%	5%	TBAB+CP (5 vol%)
0.00384	0.0819	2.19	0.03065	**1.86%**	6.87%	5%	TBAB+CP (5 vol%)
0.00332	0.0707	2.19	0.03065	**2.55%**	6.87%	5%	TBAB+CP (5 vol%)
0.00265	0.0565	1.77	0.02578	**2.06%**	6.87%	20%	TBAB
0.00351	0.0747	1.77	0.02578	**1.88%**	6.87%	20%	TBAB
0.00419	0.0894	1.77	0.02578	**2.68%**	6.87%	20%	TBAB
0.00392	0.0834	1.77	0.02578	**2.07%**	6.87%	20%	TBAB
0.00246	0.0525	1.24	0.03540	**2.07%**	6.87%	20%	TBAB+CP (5 vol%)
0.00280	0.0596	1.24	0.03540	**5.99%**	6.87%	20%	TBAB+CP (5 vol%)
0.00297	0.0633	1.24	0.03540	**3.99%**	6.87%	20%	TBAB+CP (5 vol%)
0.00353	0.0752	1.24	0.03540	**6.07%**	6.87%	20%	TBAB+CP (5 vol%)
0.000199	0.0647	1.74	0.01276	**1.94%**	0.48%	10%	TBAF
0.000218	0.0711	1.74	0.01276	**1.85%**	0.48%	10%	TBAF
0.000225	0.0732	1.74	0.01276	**1.83%**	0.48%	10%	TBAF
0.000231	0.0753	1.74	0.01276	**1.80%**	0.48%	10%	TBAF
0.000397	0.1293	1.74	0.01276	**1.78%**	0.48%	10%	TBAF
0.000419	0.1364	1.94	0.00674	**1.67%**	0.48%	5%	TBAF
0.000227	0.0739	1.94	0.00674	**2.02%**	0.48%	5%	TBAF
0.000316	0.1030	1.94	0.00674	**1.72%**	0.48%	5%	TBAF
0.000318	0.1037	1.94	0.00674	**1.72%**	0.48%	5%	TBAF

0.000212	0.0689	1.26	0.02430	**1.82%**	0.48%	10%	TBAF+CP (5 vol%)
0.000216	0.0703	1.26	0.02430	**1.81%**	0.48%	10%	TBAF+CP (5 vol%)
0.000382	0.1243	1.26	0.02430	**1.77%**	0.48%	10%	TBAF+CP (5 vol%)
0.000456	0.1485	1.26	0.02430	**1.73%**	0.48%	10%	TBAF+CP (5 vol%)
0.000157	0.0512	1.31	0.01902	**1.96%**	0.48%	5%	TBAF+CP (5 vol%)
0.000297	0.0966	1.31	0.01902	**1.72%**	0.48%	5%	TBAF+CP (5 vol%)
0.000268	0.0874	1.31	0.01902	**1.74%**	0.48%	5%	TBAF+CP (5 vol%)
0.000395	0.1286	1.31	0.01902	**1.68%**	0.48%	5%	TBAF+CP (5 vol%)
0.000111	0.0362	2.03	0.03318	**2.25%**	0.48%	3.2%	TBAF
0.000181	0.0590	2.03	0.03318	**1.76%**	0.48%	3.2%	TBAF
0.000177	0.0576	2.03	0.03318	**2.72%**	0.48%	3.2%	TBAF
0.000384	0.1251	2.03	0.03318	**1.99%**	0.48%	3.2%	TBAF
0.000161	0.0526	2.03	0.03318	**2.90%**	0.48%	3.2%	TBAF

Appendix C

The Table C.1 summarises recent works in hydrate phase equilibria modeling. The systems examined for many of these works are shown in Table C.2.

Table C.1 Most recent modeling approaches in hydrate phase equilibria.

Authors	Temperature (K)	Pressure (MPa)	Study
EoS and Clapeyron eq. based models			
Abolala *et al.*[225]	273.15–292.65	0.56–40.2	The gas hydrate formation conditions of various refrigerants were predicted via the simplified PC-SAFT theory in combination with the Vdw-P model.
Babaee *et al.*[158]	268–280	60.1–100.1	The van der Waals–Platteeuw solid solution theory is used for determination of the fugacity of water in hydrate phase. Phase behavior of the hydrogen + water system is modeled using the Valerama–Patel–Teja equation of state (VPT-EoS) with non-density dependent mixing rules. Due to the lack of experimental solubility data of hydrogen in the investigated promoters, the

			phase equilibria of the hydrogen + promoter system is treated using the VPT-EoS-GE method consisting the UNIFAC activity model and the modified Huron–Vidal (MHV1) mixing rules.
Clarke and Bishnoi[226]	264–285.5	0.33–10	The proposed equation of state is based upon contributions to the Helmholtz free energy from a non-electrolyte term and three electrolyte terms. The equation of state is used in conjunction with the Vdw-P model to predict the SVLE conditions.
Eslamimanesh *et al.*[159]	279–295	0–120	A thermodynamic model is proposed for representation/prediction of phase equilibria of semi-clathrate hydrates. The vdW–P solid solution theory is used, revised with two modifications for evaluations of Langmuir constants and vapor pressure of water in the empty hydrate lattice, in which these values are supposed to be a function of TBAB concentration in aqueous solution. The Peng–Robinson (PR-EoS) equation of state along with retuned parameters of Mathias–Copeman alpha function is applied for calculation of the fugacity of gaseous hydrate former. For determination of the activity coefficient of the non- electrolyte species in the aqueous phase, the non random two liquid (NRTL) activity model is used.
Eslamimanesh *et al.*[227]	276–294	2–500	The model based on conventional Clapeyron model. Considering that the effect of pressure on molar volume of gas hydrate could not ignored, the “Clausius–Clapeyron” equation was improved from $\frac{dP}{dT} = \frac{\Delta H_H}{T\,\Delta V}$ to $\frac{dP}{dT} = \frac{\Delta H_H + nx\Delta H_S}{T\,\Delta V}$.
Eslamimanesh *et al.*[151]	273.2–292	1.35–101	The PR EoS and NRTL activity model are applied for modeling the fluid phases. The vdW–P theory along with two modifications is used for hydrate phase.
Eslamimanesh *et al.*[228]	248.15–298.15	0.008–439	A statistical method for diagnostics of the outliers in phase equilibrium data (dissociation data) of simple clathrate hydrates is presented. The applied algorithm is performed on the basis of the Leverage mathematical approach, in which the statistical Hat matrix, Williams Plot, and the residuals of a selected correlation results lead to define the probable outliers.

Fan *et al.*[229]	267.2–279.7	0.8–3.5	The hydrate models recently developed by this group (Chen–Guo and Zuo–Guo model) and a typical literature reported Vdw-P type model were tested.
Fukumoto et al.[155]	275–300	0–5	The model proposed by Paricaud[112] is applied. The SAFT-VRE equation of state is used to describe the properties of fluid phases. Group contribution methods are proposed to predict the fusion enthalpies and the congruent melting points of semiclathrate hydrates. The vdw-P theory is combined with the model to calculate the dissociation conditions of carbon dioxide semiclathrate hydrates.
Fukumoto et al.[156]	282.31–289.75	0–16	The model proposed by Paricaud[112] is applied to predict the dissociation condition of the H_2 semiclathrate hydrate with TBAC. The parameters in the model have been determined by describing the liquid−vapor−hydrate three phase lines measured in this work and from the literature.
Fukumoto et al.[157]	273–303	0–30	The model proposed by Paricaud[112] is applied to predict the dissociation condition of the H_2+CO_2 semiclathrates hydrates with TBA salts and TBPB.
Illbeigi *et al.*[160]	274.2–296.48	1.06–14.05	The thermodynamic model is based on the Vdw-P solid solution theory combined with an equation of state and activity model. The Peng-Robinson (PR) and Soave-Redlich-Kwong (SRK) equations of state with random mixing rules are used to model the gas phase, while the UNIFAC method is used to model the liquid phase(s).
Herri *et al.*[230]	273.2–280	1.39–32.31	The data have been described by means of the vdW-P model in which the Kihara parameters had been recalculated for an optimized set of macroscopic parameters taken from Handa and Tse[231].
Javanmardi *et al.*[232]	263−279	0.9−3.0	This method uses a generalization of the Aasberg-Petersen model[233] for water activity. Calculated values of the hydrate formation temperature in the presence of alcohols and electrolytes are compared with those obtained by other existing models.
Jager and Sloan[234]	267–302	6.6–72.26	Calculations have been done on literature data for methane hydrate and new data. Both the Clapeyron relation and Vdw-P hydrate theory has been used.

Kim *et al.*[235]	272–286	1.2–24.1	Complex phase behaviors composed of two-, three- and four- phases were observed and they were analyzed by comparing with calculations using GSMGem program developed by Sloan and Koh[24].
Klauda and Sandler[236]	273.1–304.9	1–100	A fugacity-based model is developed for the prediction of equilibrium pressures and cage occupancies of pure and mixed component hydrates.
Larson[122]	257–283	0.5–4.5	Predicted the equilibrium hydrate formation conditions of CO_2 hydrates.
Li and Englezos[237]	298–313	5.0–11.0	SAFT equation of state was employed for the correlation and prediction of vapor–liquid equilibrium of eighteen binary mixtures. The predicted values agreed with the experimental data except for the H_2O–CH_3OH–CH_4 at low CH_3OH concentration in liquid phase of 60 wt%.
Mei *et al.*[238]	268.1−285.8	2.05−12.68	The generalized hydrate model proposed recently by this group was used to predict the hydrate formation conditions.
Moradi and Khosravani[239]	232.6– 398.15	0.185–20.51	The model is based on equality of water fugacity in the liquid water and hydrate phases. The Vdw-P model is applied for calculating the fugacity of water in the hydrate phase. The Stryjek and Vera modification of Peng–Robinson (PRSV2) equation of state is used to evaluate the fugacity of water in the vapor and liquid phases.
Moradi and Khosravani[240]	274.14–398.15	0.0053–827	The vdW-P model is applied for calculating the fugacity of water in the hydrate phase. The Stryjek and Vera modification of Peng–Robinson (PRSV2) equation of state is used to evaluate the fugacity of water in the vapor and liquid phases.
Osfouri *et al.*[241]	259.0–285.2	1.1–23	The proposed model is based on the γ–φ approach, which uses modified Patel–Teja equation of state (VPT EoS) for characterizing the vapor phase, the solid solution theory by vdW-P for modeling the hydrate phase, the non-electrolyte NRTL-NRF local composition model and Pitzer–Debye–Huckel equation as short-range and long-range contributions to calculate water activity in single electrolyte solutions. Also, the Margules equation was used to determine the activity of water in solutions containing polar inhibitor (glycols).

Pahlavanzadeh *et al.*[99]	271.5–305	1–55	The solid solution theory of Vdw-P is used for calculating the fugacity of water in the hydrate phase. The UNIFAC group contribution model is used to calculate the water and THF, 1,4-dioxane or acetone fugacities in the aqueous phase.
Paricaud[112]	223–315	0–30	A thermodynamic approach is proposed to determine the dissociation conditions of salt hydrates and semiclathrate hydrates. The thermodynamic properties of the liquid phase are described with the SAFT-VR equation of state, and the solid-liquid equilibria are solved by applying the Gibbs energy minimization criterion under stoichiometric constraints. The vdW-P theory combined with the new model for salt hydrates is used to determine the dissociation temperatures of semiclathrate hydrates.
Ramana Avula *et al.*[242]	272.9–291.59	2.48–20.78	The hydrate phase is computed from modified vdW–P model. The Peng–Robinson equation of state (PR-EoS) and developed activity model as a combination of Pitzer–Mayorga–Zavitsas-hydration model is used to evaluate the fugacities of gas and liquid phases, respectively. The hydrate phase stability prediction is also computed using the liquid phase activity predicted by NRTL and Pitzer–Mayogra models, separately, and is compared with the results predicted from the developed model.
Renault-Crispo *et al.*[243]	274.19–444.26	0.6–68.9	This work demonstrates the sensitivity and importance of the liquid phase compositions on selected models and parameters. The equations of state used to model two-phase systems are the Soave–Redlich–Kwong, the Valderrama–Patel–Teja and the Trebble–Bishnoi equations of state. The modeling analysis for three-phase systems is based on the Trebble–Bishnoi equation of state along with the model by Vdw-P.
Robinson and Mehta[76]	274–283	1.3–4.5	The conditions for initial hydrate formation in the system of CO_2–C_3H_8–H_2O over a wide concentration range for the hydrate-water-rich liquid–gas phase region were measured and predicted in terms of solid–vapor K-factor.
Seo and Lee[162], Seo *et al.*[244]	272–284	1.5–5.0	The three phase equilbria for aqueous phase containing CO_2 and CH_4 were predicted. The vapor and liquid phases were treated with SRK-EoS incorporated with the second-order modified Huron–Vidal (MHV2) mixed

			rule and hydrate phase with the Vdw-P model.
Seo et al.[163]	255–284.53	0.807–10.5	Hydrate phase equilibria data modeled based on Vdw-P model[23]. The fugacities of supercooled water and all components in the vapor phase were calculated using the Soave-Redlich-Kwong (SRK) equation of state incorporated with the modified Huron-Vidal second order mixing rule.
Seo *et al.*[164]	280.56–302.46	1.74–11.84	A new thermodynamic model was developed to describe the phase equilibria of mixed hydrates containing two guest molecules. The Soave–Redlich–Kwong equation of state (SRK EoS) was used with the modified Huron–Vidal (MHV2) mixing rule incorporated with the modified UNIFAC.
Sfaxi *et al.*[161]	278.1–285.3	3.24–29.92	A thermodynamic model based on the CPA equation of state for fluid phases combined with the Vdw-P solid solution theory for the hydrate phase is presented. The dissociation data generated in this work along with the experimental data reported in the literature are compared with the results of this model and also with the predictions of two other thermodynamic models, namely HWHYD and CSMGem.
Sun and Chen[245]	273.5–299.7	0.5–8.5	By introducing Debye–Huckel electrostatic contribution term, their method coupled with Chen–Guo model was successfully used to predict the thermodynamics property of hydrates.
Sun and Duan[246], Duan and Sun[247]	253–293	0.5–200	Ab initio potential model predicting initial hydrate formation conditions for CH_4 and CO_2. Compared to the models employing the Kihara potential or Lennard-Jones potential, atomic site–site potentials were more accurate either under low pressure or under high pressure.
Tavasoli *et al.*[248]	273.2–310.3	0.2–100	Elliott–Suresh–Donohue (ESD) equation of state (EoS) which is based on thermodynamic perturbation theory and uses the Wertheim association contribution to account for association interactions, is applied to predict hydrate formation conditions in the presence and absence of thermodynamic inhibitors. The ESD EoS is coupled with the Vdw-P model.
Tsimpanogiannis *et al.*[249]	270–310	20–500	Novel Grand Canonical Monte Carlo molecular simulations are applied for the case of pure s(II) N_2 hydrate. The simulation

			compares the calculated cavity occupancies with experimental data and observes reasonable agreement.
Tumba *et al.*[64]	275–285	1.52–16.23	A thermodynamic model, developed based on Vdw-P solid solution theory accompanied with the Peng-Robinson equation of state (PR-EoS) and the non random two-liquid (NRTL) activity model, was successfully applied to represent/predict the obtained experimental data.
Valavi and Dehghani[250]	263.3–300.9	0.1–9	The modified PHSC (Perturbed hard sphere chain) EoS has been employed to predict the hydrate formation conditions of pure gases as well as their gas mixtures in the presence and absence of thermodynamic inhibitors, electrolytes, mixed electrolytes and mixture of inhibitor–electrolytes.
Yang *et al.*[251]	240–298.2	1.1–19.4	Applicability of the lattice fluid equation of state by the present authors was also investigated for the unified description of various phase equilibria with Langmuir constants in the Vdw-P model for hydrates and hydrogen-bonding free energy of water fitted to data, the model was found to consistently describe various two- and three-phase equilibria.
Yoon *et al.*[165]	205–295	0.01–69	A generalized hydrate equilibrium model was developed for accurately predicting the complete phase behavior of simple and mixed hydrate systems. The fugacities of all components in the vapor and liquid phases coexisting with hydrates were calculated by using the SRK-EoS incorporated with the MHV2 mixing rule. The UNIFAC group contribution model was also used as the excess Gibbs energy for the MHV2 model.
Gas gravity methods and correlation based methods			
Ameripour and Barrufet[252]	<305.38	<82.7	Two correlations calculate the hydrate formation pressure or temperature for single components or gas mixtures, with or without inhibitors.
Bahadori and Vuthaluru[253]	265–298	1.2–40.0	A novel correlation based on the extracted data from Katz gas-gravity charts was proposed to predict the hydrate formation conditions for gases.
Eslamimanesh *et al.*[254]	265.31–283.49	0.007–1.489	A thermodynamic model is presented for the study of the phase equilibria of clathrate hydrates of simple refrigerants. The Vdw-P

			solid solution theory is used to model the hydrate phase.
Holder *et al.*[172]	-	-	Empirical correlations developed in different forms and with various numbers of parameters.
Hosseini-Nasab *et al.*[255]	270.9–300	3–31	The authors employed SAS (SAS Institute, Cary, North Carolina) to develop a correlation for predicting the hydrate-formation temperatures for both pure and mixture of hydrocarbon systems using the gravity method. The method correlates the hydrate-formation pressure against specific gravity, pressure, and water-vapor pressure.
Omole *et al.*[256]	-	-	This study employed Statistical Analysis Software (SAS) to develop a new correlation for predicting the hydrate formation temperatures for both pure and mixture of hydrocarbon systems using gravity method. The method correlates the hydrate-formation pressure against specific gravity, pressure and water-vapour pressure.
Rashidabad *et al.*[257]	263.2–281.7	2.5–9.5	A 10 variable linear regression model was offered for thermodynamic model of hydrate formation of methane in the presence of electrolytes and the obtained data was compared with the model calculations numerical results.

Table C.2 Average standard pressure/temperature deviations of modeling results from literature.

Authors	Systems	Average standard pressure deviation (AAPD) (%)		Average standard temperature deviation (AATD) (%)
Abolala *et al.*[216]	Refrigerants	1.15		–
Babaee *et al.*[217]	Derivatives of butane, pentane, cyclopentane and cyclohexane	–		0.06
Eslamimanesh *et al.*[219]	CO_2	1.8		–
	CH_4	2.3		–
	N_2	4		–
Eslamimanesh *et al.*[222]	R-134a	4.9*	5.3**	–
	R-141b	0.1*	10**	–
	R-152b	16* [s(II)]	30** [s(II)]	–
		1.5* [s(I)]	2.4** [s(I)]	–
	R-32	1.8*	0.6**	–

Fan *et al.*[223]	CO_2 +(N_2/CH_4/C_2H_6/MEG/MeOH)	4.82[=]	7.92[~]	5.91[×]	0.14[=]	0.25[~]	0.28[×]
Fukumoto et al.[155,^]	TBAB + CO_2		–			0.35	
	TBAC + CO_2		–			0.42	
	TBAF + CO_2		–			0.60	
	TBPB + CO_2		–			0.41	
Fukumoto et al.[156,^]	TBAC		–			0.47	
Illbeigi *et al.*[224]	CH_4 + (CC6 or derivatives)/CP/acetone/1,4-dioxane	3.99[z]	4.35[ɵ]	7.95[ϕ]		–	
Herri *et al.*[225,^]	CO_2/ CH_4 /CO_2 + CH_4		976.7			–	
	CO_2/N_2/CO_2 + N_2		393.2			–	
	N_2		16.64			–	
	N_2/CH_4/ N_2 + CH_4		123.7			–	
Javanmardi *et al.*[227,^]	CO_2 +CH_4/H_2S/C_2H_6/CH_4+C_3H_8/ + MeOH		–			1.19	
Kim *et al.*[230]	CO_2 + N_2	11.9 (CSMGem)		19.4 (HYSYS)		–	
Klauda and Sandler[231]	NG single components		20.4			–	
	NG binary and ternary systems		11.6			–	
Mei *et al.*[233,^]	CO_2 + CH_4 (+salts)		13.96			–	
Moradi and Khosravani[235,^]			7.62			0.729	
	NG single components						
	NG ternary and quaternary systems with MeOH/MEG		–			0.401	
Moradi and Khosravani[236,^]			11.15			–	
	NG single components						
	NG binary, ternary and quaternary systems		13.25			–	
Osfouri *et al.*[237]	NG single and binary components + salts		5.86			–	
	NG single and binary components + mixture of salts		5.23			–	
	NG single components +MEG+NaCl/$CaCl_2$/(NaCl+$CaCl_2$)		14.13			–	
Paricaud[112,^]	CO_2+HI/LiBr/TBAB		10.5			–	
Sun and Chen[244]	NG ternary and quaternary systems		5.89			–	
Tavasoli *et al.*[247,^]	NG ternary, quaternary and multicomponent systems		9.75			–	

	NG ternary systems with MEG/MeOH/EtOH	6.98	–
Valavi and Dehghani[249]	NG ternary systems	4.62	–
	NG ternary systems with MEG/MeOH/EtOH	6.15	–
	NG ternary systems with salt	5.82	–
	NG quaternary systems with mixture of salts	6.80	–
	NG single components + MeOH + salt	7.56	–
Yang *et al.*[250]	$CH_4 + H_2O$	25.50	–
Yoon *et al.*[251]	NG single components	3.41	–

*Absolute average deviations of the calculated hydrate dissociation pressures.
**Absolute average deviations of the predicted hydrate dissociation pressures.
¯AAD based on Chen and Guo model[223, 233,234].
˜AAD based on Zuo and Guo model[223, 233,234].
ˣAAD based on CSMHYD model[24,166,223].
^Maximum AAD % values are mentioned.
ᶻFluid phase is modeled by SRK.
ᵉFluid phase is modeled by PR.
ΦFluid phase model is taken from literature.

Appendix D

The different Kihara parameters in literature and the EoS used to calculate them are presented in Table D.1.

Table D.1 Kihara parameters for the compounds examined in this work.

Component	$a \cdot 10^{10}$ (m)	$\sigma \cdot 10^{10}$ (m)	ε/k_B (K)	EoS used for fugacity calculation	Reference
Carbon dioxide	0.6805	2.9643	171.70	*a* parameter is obtained from Sloan and Koh[258] and σ, ε are correlated	Herslund[20]
	0.6805	2.97638	175.405	CSMHYD/CSMGem	Sloan and Koh[24]
	0.7530	2.349	420.300	Valderrama-Patel-Teja (VPT EoS) with non-density-dependent mixing rules	Avlonitis[259]
	0.6805	2.9818	168.77	CSMHYD	Sloan[174]
	0.7200	2.9681	169.09	modified Redlich-Kwong	Parrish and Prausnitz[166]
Nitrogen	0.3526	3.1723	128.07	Soave-Redlich-Kwong	Strobel *et al.*[181]
	0.3526	3.13512	127.426	CSMHYD/CSMGem	Sloan and Koh[24]

	0.3350	2.84500	136.700	Valderrama-Patel-Teja with non-density-dependent mixing rules	Avlonitis[259]
	0.3350	3.25980	133.080	Valderrama-Patel-Teja with non-density-dependent mixing rules	Tohidi *et al.*[174]
	0.3526	3.0124	125.15	CSMHYD	Mehta and Sloan[179]; Sloan[174]
	0.700	3.6142	127.95	modified Redlich-Kwong	Parrish and Prausnitz[166]
Cyclopentane	0.8968	3.1480	250.89	CSMHYD	Sloan[174]
Methyl-Cyclopentane (mCP)	1.0054	4.5420	353.66	CSMHYD	Mehta and Sloan[179]
	1.0054	3.56878	229.928	CSMHYD/CSMGem	Sloan and Koh[24]
	1.0054	4.5380	353.66	Peng-Robinson	Ma *et al.*[260]
Ethyl-cyclopentane (eCP)	1.1401	3.60425	219.083	CSMHYD/CSMGem	Sloan and Koh[24]
Ethyl-cyclopentane (eCP)	1.1401	3.4045	304.71	CSMHYD	Mehta and Sloan[179]
Cyclohexane (CC6)	0.9750	4.2675	253.00	modified PVT with non-density-dependent mixing rules	Tohidi *et al.*[174]
Methyl-Cyclohexane (mCC6)	1.0693	3.1931	407.29	CSMHYD	Mehta and Sloan[179]
	1.0693	3.2148	407.29	Peng-Robinson	Ma *et al.*[260]
	1.0693	3.58776	237.989	CSMHYD/CSMGem	Sloan and Koh[24]
Cycloheptane (CC7)	1.0576	3.5902	250.19	CSMGem	Sloan and Koh[24]
	1.0575	3.5199	312.44	Peng-Robinson	Ma *et al.*[260]
Cyclooctane (CC8)	1.1048	3.6550	277.80	CSMGem	Sloan and Koh[24]; Ma *et al.*[260]
	1.1048	3.6337	277.80	CSMHYD	Mehta and Sloan[179]
Methyl-Cyclooctane (mCC8)	1.0693	3.58776	237.989	CSMGem	Sloan and Koh[24]

Appendix E

E.1 Contributions to Conferences

International Conferences

Tzirakis F., von Solms N., Kontogeorgis G., Coquelet C., Stringari P., *Experimental data for CO_2+N_2+TBAB+H_2O*, oral presentation, ESAT Conference, TU Eindhoven, July 6th-9th, 2014.

Tzirakis F., von Solms N., Kontogeorgis G., Coquelet C., Stringari P., *Experimental Data For CO_2 Hydrate Promotion*, International Conference on Gas Hydrates (ICGH8-2014), poster presentation, Beijing, China, 28th July – 1st August, 2014.

Tzirakis F., von Solms N., Kontogeorgis G., Coquelet C., Stringari P., *Experimental data for CO_2+N_2+TBAB/F(+CP)+H_2O*, oral presentation, ESAT Conference, NTUA, Athens, July 11th-14th, 2015.

Tzirakis F., von Solms N., Kontogeorgis G., Coquelet C., Stringari P., *Experimental data for CO_2+N_2+TBAB/F(+CP)+H_2O*, oral presentation, ICCDU Conference, National University of Singapore, Singapore, July 5th-9th, 2015.

Internal Meetings

Tzirakis F., von Solms N., Kontogeorgis G., Coquelet C., Stringari P., Hydrate equilibrium data for CO_2+N_2 system with the use of TBAB, TBAF, CP, TBAB+CP, TBAF+CP (**Oral**), CERE Annual Discussion Meeting, Snekkersten, Denmark, June 25th-27th, 2014.

Tzirakis F., von Solms N., Kontogeorgis G., Coquelet C., Stringari P., Hydrate equilibrium data for CO_2+N_2 system with the use of pressure reduction chemicals (promoters) (**Oral**), CERE Annual Discussion Meeting, Snekkersten, Denmark, June 17th-19th, 2015.

Tzirakis F., von Solms N., Kontogeorgis G., Coquelet C., Stringari P., Hydrate equilibrium data and modeling of CO_2+cyclo-alkane hydrates (**Oral**), CERE Annual Discussion Meeting, Helsingør, Denmark, June 15th-17th, 2016.

Tzirakis F., von Solms N., Kontogeorgis G., Coquelet C., Stringari P., Experiments for CO_2 hydrates – promoters (**Poster**), CERE Annual Discussion Meeting, Snekkersten, Denmark, June 19th-21th, 2013.

Tzirakis F., von Solms N., Kontogeorgis G., Coquelet C., Stringari P., Experimental hydrate promotion data for CO_2+N_2+TBAB+H_2O system (**Poster**), CERE Annual Discussion Meeting, Snekkersten, Denmark, June 25th-27th, 2014.

Tzirakis F., von Solms N., Kontogeorgis G., Coquelet C., Stringari P., Hydrate equilibrium data for CO_2+N_2 system with the use of pressure reduction chemicals (promoters) (**Poster**), CERE Annual Discussion Meeting, Snekkersten, Denmark, June 17th-19th, 2015.

Tzirakis F., von Solms N., Kontogeorgis G., Coquelet C., Stringari P., Experimental uncertainties of hydrate equilibrium data (**Poster**), CERE Annual Discussion Meeting, Snekkersten, Denmark, June 17th-19th, 2015.

D.2 List of Publications

Tzirakis F., Stringari P., von Solms N., Coquelet C., Kontogeorgis G., Hydrate equilibrium data for the CO_2+N_2 system with the use of Tetra-n-butylammonium bromide (TBAB), cyclopentane (CP) and their mixture, *Fluid Phase Equilib.*, **2016**, *408*, 240-247.

Tzirakis F., Stringari P., von Solms N., Coquelet C., Kontogeorgis G., Hydrate Equilibrium Data for CO_2+N_2 System in the Presence of Tetra-n-butylammonium Fluoride (TBAF) and Mixture of TBAF and Cyclopentane (CP), *J. Chem. Eng. Data*, **2016**, *61*, 1007–1011.

Tzirakis F., Karakatsani E., Kontogeorgis G., Evaluation of CPA EoS (cubic-plus-association equation of state) for ternary, quaternary and multicomponent systems in the presence of mono-ethylene glycol (MEG), *Ind. Eng. Chem. Res.*, **2016**, *55*, 11371–11382.

D.3 Distinction

Otto Mønsteds Foundation grant for ESAT and ICCDU conferences (2015)

D.4 Attended Courses

- Advanced Raman Spectroscopy (10 ECTS)
- Thermodynamic Models, Fundamentals and Computational Aspects (7.5 ECTS)
- Advances in Chemical and Biochemical Engineering (2.5 ECTS)
- Phase Equilibria for Separation Processes (5 ECTS)

- Environmental Economics (5 ECTS)

Ἀληθῶς, Κύριε, ἐάν μὴ ταπεινωθῶμεν, οὐ παύῃ ταπεινῶν ἡμᾶς.